Technische Universität München

Lehrstuhl für Technische Chemie II

Hydrogenation of tetralin on bimetallic Pt-Pd catalysts

Yanzhe Yu

Vollständiger Abdruck der von der Fakultät für Chemie der Technischen Universität München zur Erlangung des akademischen Grades eines

Doktors der Naturwissenschaften (Dr. rer. nat.)

genehmigten Dissertation.

Vorsitzender: Univ.-Prof. Dr. Ing. Kai-Olaf Hinrichsen

Prüfer der Dissertation:

1. Univ.-Prof. Dr. Johannes A. Lercher

2. Univ.-Prof. Moniek Tromp, Ph.D.

Die Dissertation wurde am 29.11.2011 bei der Technischen Universität München eingereicht und durch die Fakultät für Chemie am 16.01.2012 angenommen.

Acknowledgements

As my PhD study at Technische Universität München is approaching the end, I would like to thank all the people who have contributed to my work; this thesis wouldn't have been possible without their help and supports.

My deepest gratitude goes first and foremost to Prof. J. A. Lercher, who has provided me with the opportunity of doing my master thesis, and later the PhD studies in TC II; I am grateful for his continuous guidance throughout my PhD work, for all the enlightening discussions with him, and also for his ideas which always lead to solutions to puzzles that I encountered in my PhD pursuit. His open mind towards research and enthusiasm for science has helped create a free and delightful research environment in our group, which I really appreciate.

Besides, I would like to thank Dr. Oliver Y. Gutiérrez, for his unconditional support, especially for discussion on the experimental results and for reading and correcting all my publications and this dissertation with patience and attention; and Andy (Prof. A. Jentys), for sharing his expert knowledge in EXAFS and XANES with me, and for the enlightening discussions on kinetics and modeling of the nanoclusters. I would also like to express my sincere gratitude to Prof. G.L. Haller (Yale University, US), our conversations reagarding hydrogenation reactions and XAS analysis are really helpful.

I am indebted to Xaver, who is always ready to help in case of technical problems; and Matin, who performed AAS measurements for my samples. People at Hasylab, Desy Hamburg are also thankfully acknowledged for their supports during the XAS experiments.

It is my pleasure to also acknowledge two past group members that I've had the pleasure to work alongside: Benjamin, for the great help during my master thesis and at the beginning of my PhD. His hydrogenation set-up is still working very well and producing numerous data. And Ana, who has been a great friend and office mate, it was a pleasure to work with her together in the "clean" sulfur lab and our discussion on the hydrogenation part was inspiring.

I would also like to extend my thanks to all the colleagues and friends in TC II, who have made my time at TC II enjoyable and enriched.
Last but not least, I want to dedicate this work to my family and friends who are always supportive.
Thank you.

Yanzhe Yu
Nov. 2011

Table of Contents

Abbreviations

Å	Angstrom
AAS	Atomic absorption spectroscopy
AGO	Atmosphere gas oil
ASA	Amorphous silica-alumina
BAS	Brønsted acid site
BPR	Back pressure regulator
℃	Celsius
CN	Coordination number
CO	Carbon monoxide
DBT	Dibenzothiophene
eV	Electron volt
EXAFS	Extended X-ray absorption fine structure
FCC	Fluid catalytic cracking
HAD	Hydrodearomatization
HC	Hydrocarbon
HCO	Heavy crude oil
HDN	Hydrodenitrogenation
HDO	Hydrodeoxygenation
HDS	Hydrodesulfurization
HYD	Hydrogenation
IR	Infrared
K	Kelvin
kPa	Kilopascals
LCO	Light cycle oil
LAS	Lewis acid site
mA	Milli ampere
mbar	Milli bar
MFC	Mass flow controller
nm	Nanometer

NMR	Nuclear magnetic resonance spectroscopy
PM	Particulate matter
ppm	Parts per million
SiC	Silicon carbide
SR	Solvent recycler
TBR	Trickle bed reactor
TEM	Transmission electron microscopy
TMS	Transition metal sulfides
TOS	Time on stream
TPR	Temperature programmed reduction
VGO	Vacuum gas oil
WHSV	Weight hourly space velocity
XANES	X-ray absorption near edge structure
XAS	X-ray absorption spectroscopy

Chapter 1

General introduction

Diesel powered vehicles become increasingly more common in the world market, especially in Europe. For environmental protection, many efforts have been paid to limit the emission from diesel fuel and to reduce diesel engine exhausted gases. The improvement of diesel fuel quality by lowering the concentration of aromatic and nitrogen/sulfur compounds enhances the efficiency of fuel combustion and thus decreases diesel exhaust emissions such as NO_x, SO_x and particulate matter. Supported noble metal catalysts reveal excellent activity in aromatics hydrogenation; unfortunately those catalysts can be easily poisoned by nitrogen or sulfur containing molecules. Acidic supports and alloying of different noble metals (e.g. Pt and Pd) enhances the resistance ability of noble metal catalysts towards poisons. In the end of this chapter, the scope of this doctoral thesis is highlighted.

1. Motivation

1.1. Background

The segment of diesel powered vehicles is growing fast worldwide (Figure 1). Due to better fuel efficiency, more power, and more durability than gasoline powered vehicles, diesel cars become more common in the market. Now over 50% of new passenger cars in Europe have diesel engines compared with less than 25% in early 1990s.

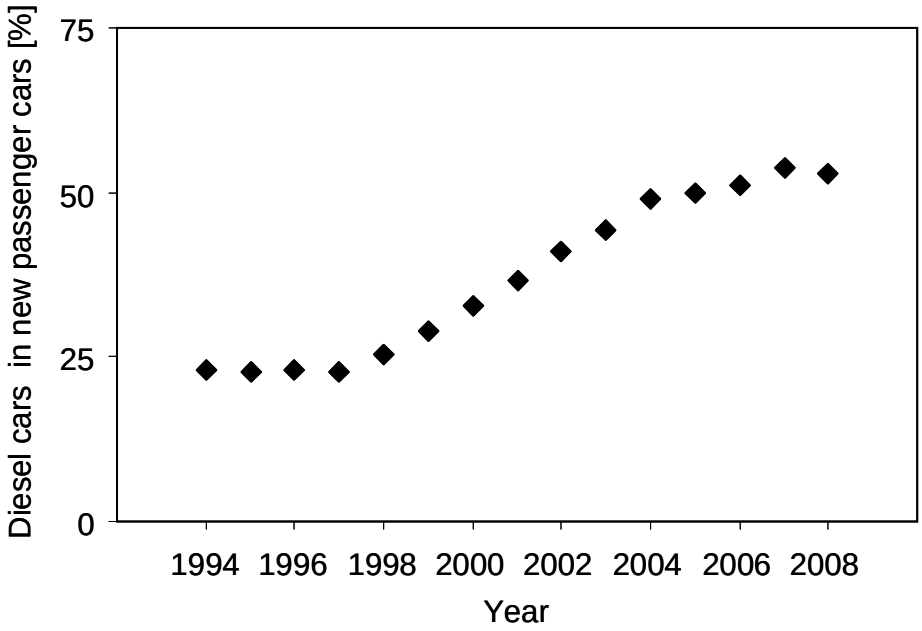

Figure 1. Diesel penetration in new passenger cars in Europe [1].

With the increasing amount of diesel vehicles, the demand of diesel fuel has grown up steadily in the past decades, making diesel the fastest growing segment of the refined products. Figure 2 shows the distillates share of oil consumption in EU in the passed 20 years [2]. The middle distillate, which contains diesel fuel, has the fastest growth compared to other products.

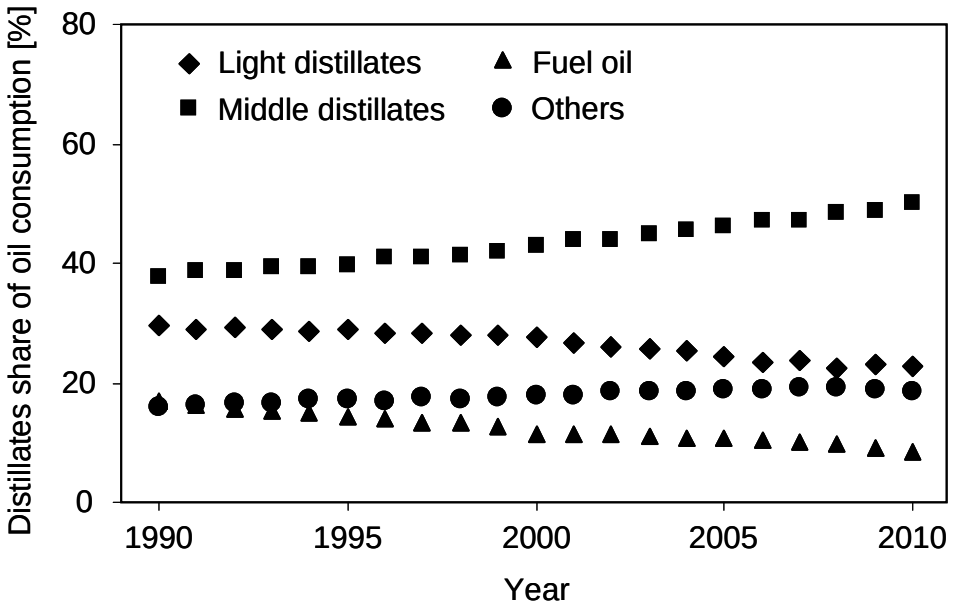

Figure 2. Distillates share of oil consumption in European Union (Source: BP Statistical review of world energy, 2011)

1.2. Emission from diesel fuel

Diesel fuel is a complex mixture of alkanes (C9 to C30 of normal, branched, and cyclic homologues, 60 to 90 vol. %), aromatics (e.g., alkylbenzenes; 5 to 40 vol. %), and small amounts of alkenes (0 to 10 vol. %) obtained from the middle distillates of refinery [3]. Ideally when fuel is burned with the correct amount of air in a diesel engine, only water vapor, carbon dioxide and nitrogen are released. All the gases are environmentally benign except carbon dioxide, which is the main cause of greenhouse-effect. However, this ideal combustion of diesel can not be achieved in reality. In respect to the excess oxygen design of diesel engines, they do not emit much CO or unburned hydrocarbon, but the high emissions of particulate matter (PM) and NO_x is the main problem [4,5].

PM emission is mainly the result of incomplete diesel combustion. Most diesel exhaust particles have aerodynamic diameters with a size of 0.1 to 0.25 μm [6-8]. The particle size distribution of diesel exhaust is bimodal, with a nuclei mode of 0.0075 to 0.042 μm (particles formed by nucleation) and an accumulation mode of 0.042 to 1.0 μm (particles formed by agglomeration of nuclei particles). Most of

the particles emitted from diesel engines are less than 1.0 μm in diameter. Due to the small size of those fine particles, they can easily penetrate into the lungs and cause health problems. SO_x, produced by combustion of S-containing molecules in the fuel, is the main reason for acid rain. Another major emission component, NO_x, is a key ingredient in the formation of urban smog, and also can contribute to the formation of acid rain.

1.3. Relation of diesel properties and emission

The emission of diesel engines can be minimized from mainly two sides: (1) improve the diesel engine and apply exhaust after-treatment system, such as catalytic converter for exhaust gases and particle filter; (2) improve the quality of diesel fuel. The main variables to evaluate diesel fuel quality are cetane number, aromatic, nitrogen and sulfur content.

- Cetane number and aromatic content

Cetane number is a measure of a fuel's ignition delay, namely the time period between the start of injection and the first identifiable pressure increase during combustion of the fuel. In a particular diesel engine, higher cetane number fuels will have shorter ignition delay periods than lower cetane number fuels. Thus, high cetane-number diesel provides more time for the fuel combustion process to be completed, thus produces less PM and NO_x emission than low cetane number fuels. Several studies have been conducted to establish a link between diesel fuel properties and the emission of PM [9,10]. It was found that the amount of PM produced in a diesel engine can be reduced by increasing the cetane number (Figure 3). Increasing the cetane number can also result in a reduction of NO_x in exhaust gases [11].

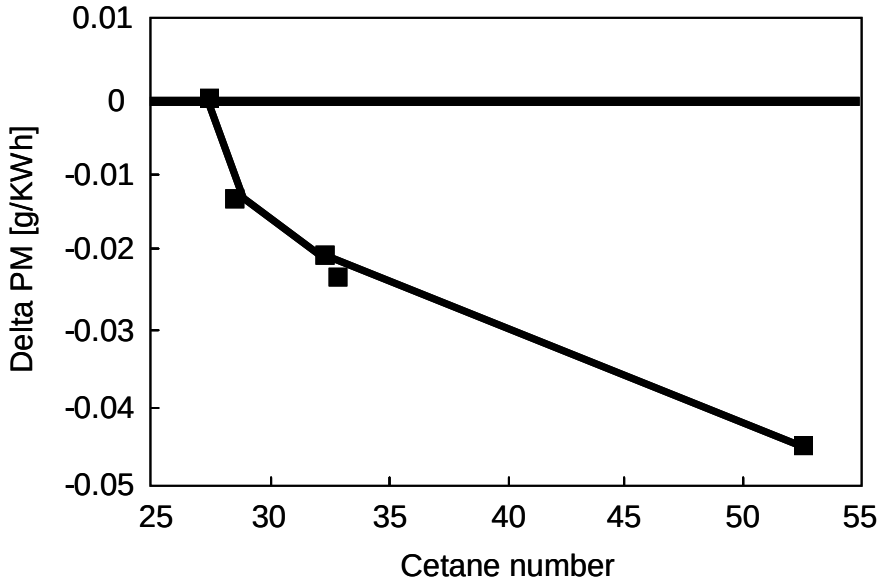

Figure 3. Cetane number and emission of particulate matter (without sulfates) [10]. Delta PM is the amount of particular matter emission (g/KWh) at different cetane number compared to the particular matter from the standard.

Aromatic compounds in diesel fuel are precursors of PM in the diesel engine exhaust, which is also related to cetane number of diesel fuel. Figure 4 shows that reducing the aromatic content of diesel can drastically increase the cetane number.

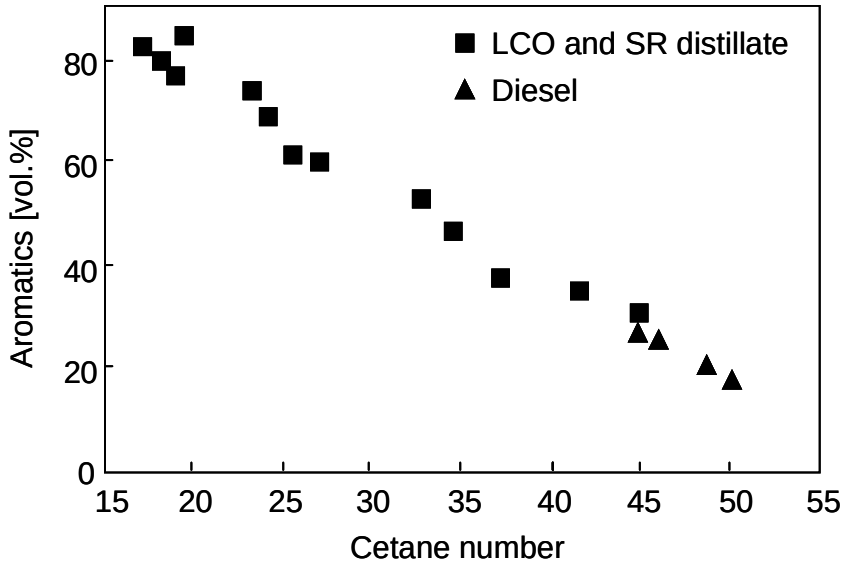

Figure 4. Relation between aromatic content and cetane number (data: [12]).

- Nitrogen content

Nitrogen-containing molecules (Figure 5) in the feedstocks are normally heterocyclic and difficult to remove. Those nitrogen-containing heterocycles are further divided into basic and nonbasic compounds. Basic compounds include six-membered ring heterocycles such as pyridine, quinoline and acridine. Nonbasic nitrogen compounds include five-membered ring heterocycles such as pyrrole, indole and carbazole. After the N-containing compounds are combusted in the engines, the environmental deleterious gas NO_x is produced.

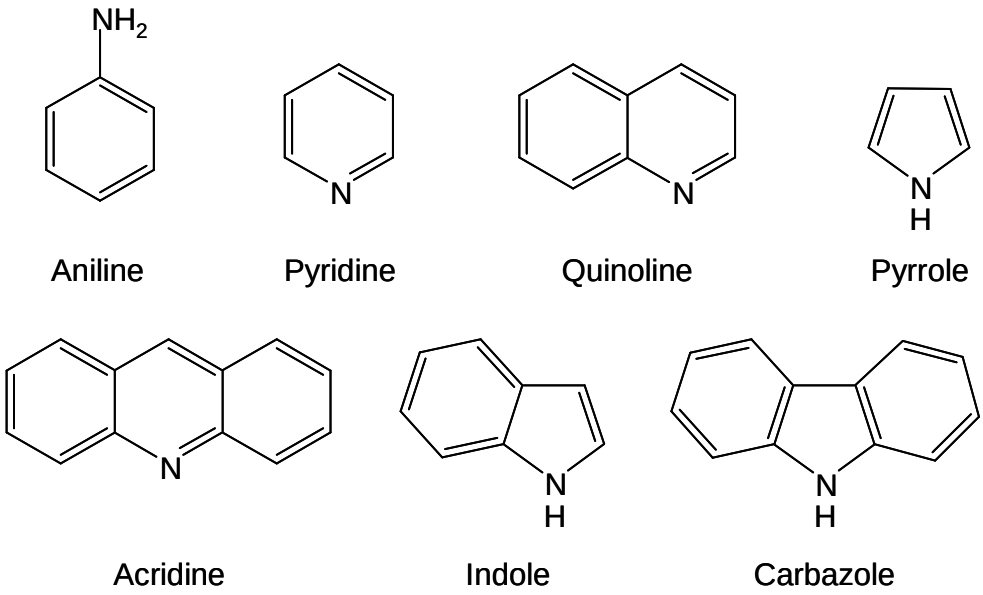

Figure 5. Nitrogen-containing compounds in diesel fuel.

- Sulfur content

Sulfur-containing molecules (Figure 6) present in diesel fuel are non-heterocyclic or heterocyclic. The former group comprises thiols, sulfides and disulfides; the latter group is mainly composed of thiophenes with one to several aromatic rings and their alkyl or aryl substituents.

The sulfur-containing compounds are converted into SO_x during combustion, which is the main cause of acid rain. On the other hand, the sulfur-containing compounds also affect PM emissions because some of the sulfur in the fuel is converted to sulfate particles in the exhaust.

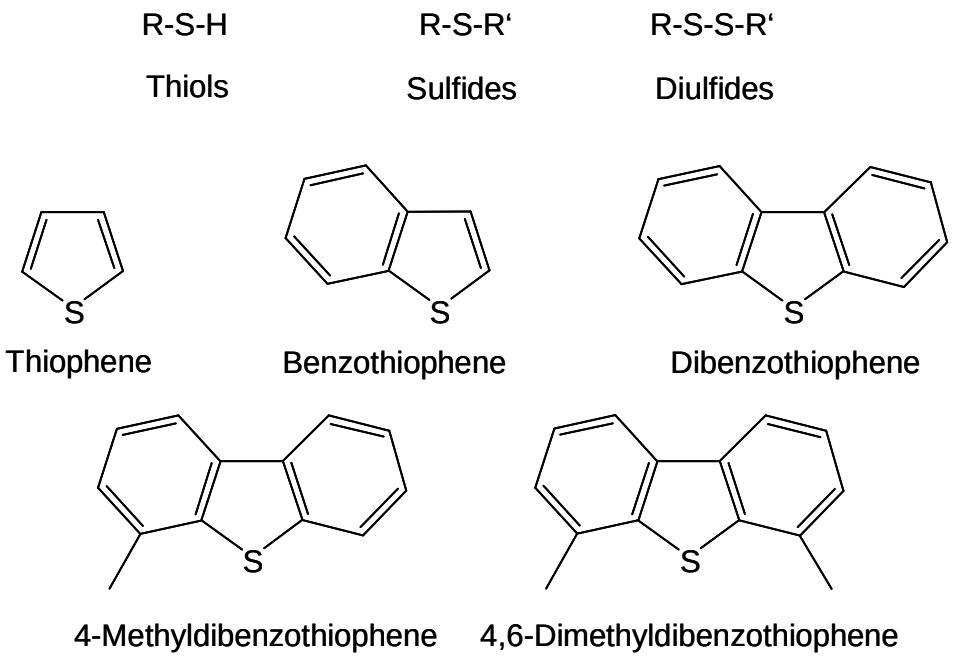

Figure 6. Sulfur-containing compounds in diesel fuel.

1.4. Legislation of diesel fuel

Emission from passenger cars (Table 1) becomes stricter limited in order to reduce the impact of exhaust gases on the environment.

Table 1. European emission standards for passenger cars (Source data from [13])

Emission standard	Year	Emission (g/km)			
		CO	NO_x	HC+ NO_x	PM
Euro 1	1992	2.72	-	0.97	0.14
Euro 2	1996	1.00	-	0.70	0.08
Euro 3	2000	0.64	0.50	0.56	0.05
Euro 4	2005	0.50	0.25	0.30	0.025
Euro 5	2009	0.50	0.18	0.23	0.005
Euro 6 (future)	2014	0.50	0.08	0.17	0.005

Therefore, stricter regulations are required in diesel production. In 1994 a maximum sulfur level of 2000 ppm was introduced in Europe for all gas oils. The minimum cetane number was assigned to 49. The maximum sulfur content in diesel fuel was further decreased in 1996 and 2000 to 500 ppm and 350 ppm, respectively. Furthermore, in the year 2000 the maximum polyaromatics level of 11 % and a minimum cetane number of 51 started to become effective. Since 2005 the maximum sulfur level in diesel fuel in the EU is 50 ppm for highway vehicles. 2009 is the starting year for ultra clean diesel (10 ppm S, 8 % polyaromatics) for highway and nonroad vehicles.

2. Diesel production and hydrotreating

2.1. Diesel production

Typically, crude oil is initially separated into different fractions by atmospheric distillation, including straight-run diesel and atmosphere gas oil (AGO). The AGO is hydrocracked to obtain hydrocracked gas oil. The atmospheric residue is then further separated by vacuum distillation into vacuum gas oil (VGO) and vacuum residue. The VGO is hydrotreated to reduce sulfur and nitrogen contents before fluid catalytic cracking (FCC) to get light cycle oil (LCO) [14]. Diesel fuel produced by a refinery is a blend of all the appropriate available streams: straight-run diesel, FCC light cycle oil and hydrocracked gas oil.

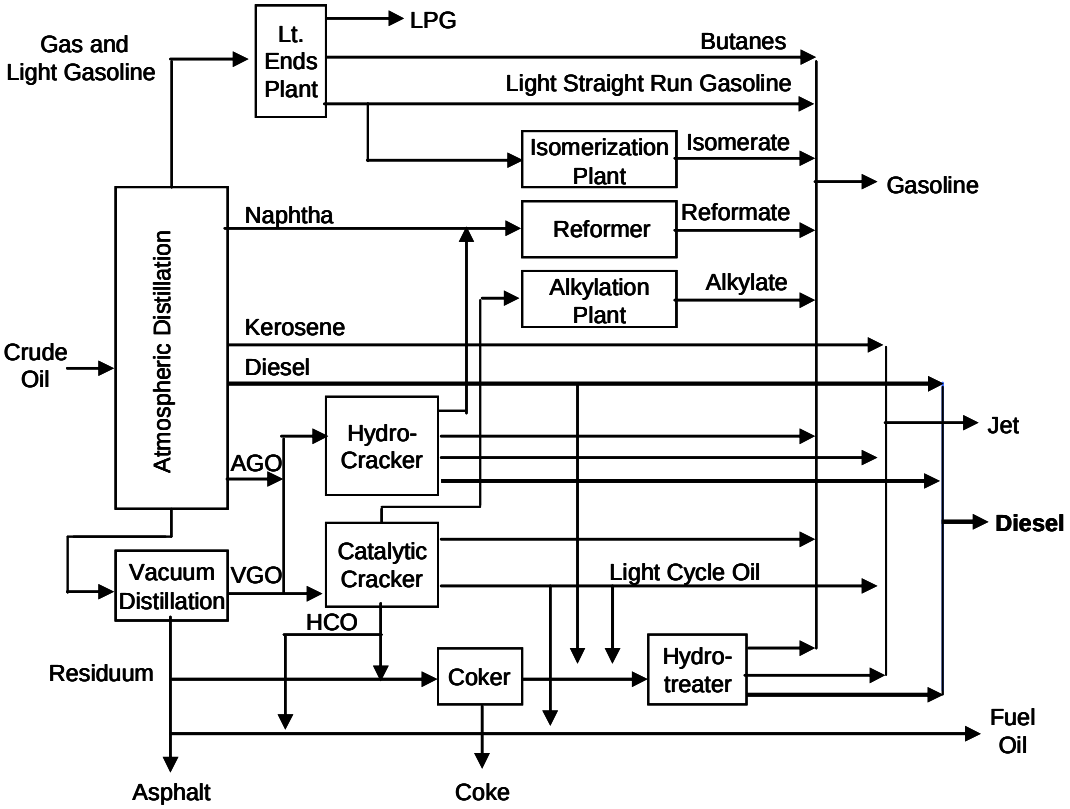

Figure 7. Diesel productions in modern refinery.

2.2. Deep hydrotreating

Deep hydrotreating process must be involved in diesel production in order to meet the strict requirements. Hydrotreating is defined as using hydrogen to remove heteroatoms in gas-oil upgrading. It is normally classified into hydrodearomatization (HDA), hydrodeoxygenation (HDO), hydrodesulfurization (HDS), and hydrodenitrogenation (HDN) processes. A two-stage hydrotreating process is widely used in industry [15,16]. As shown in Figure 8, in the first stage, transition metal sulfides such as CoMoS or NiMoS are used for HDS and HDN to minimize the sulfur and nitrogen contents to an acceptable level for the second step, where deep hydrogenation of aromatics is conducted on noble metal catalysts, such as Pt or Pd on different supports.

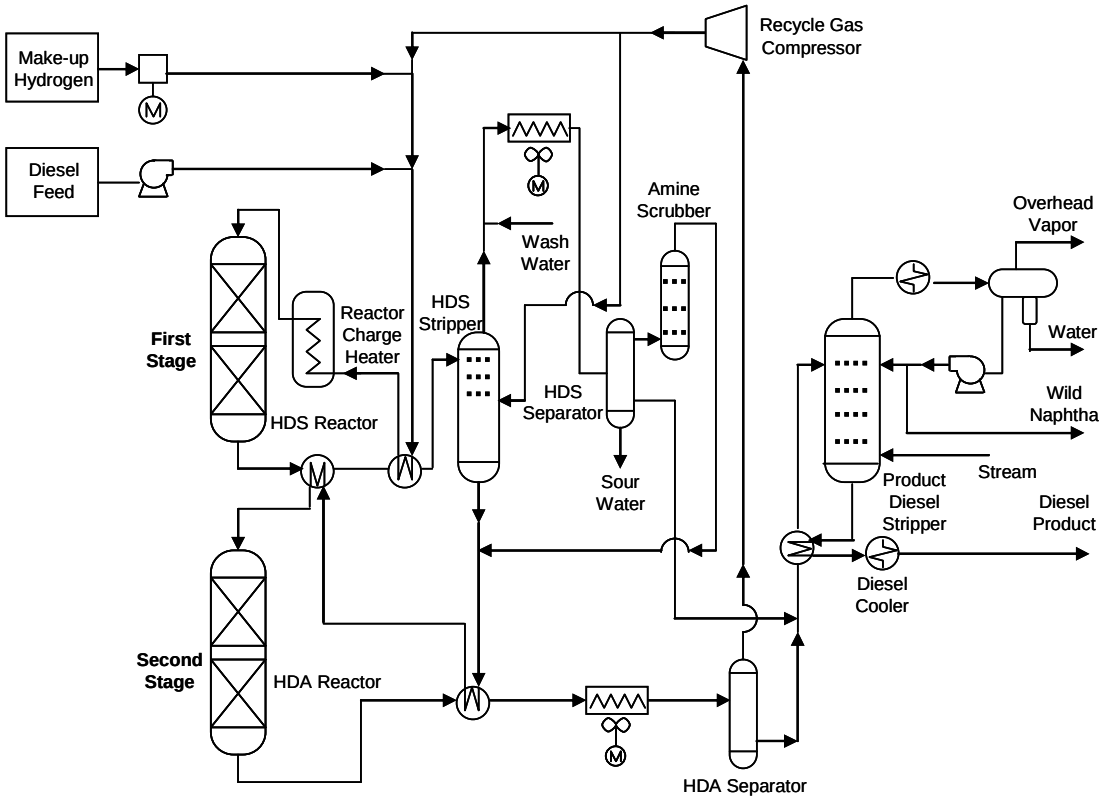

Figure 8. Topsøe's two-stage hydrotreating process [17].

3. Conventional hydrotreating catalysts

Transition metal sulfides (TMS) supported on γ-Al_2O_3 and promoted with Ni or Co are conventional hydrotreating catalysts [18]. On those catalysts, only moderate levels of aromatic saturation can be achieved under typical hydrotreating conditions. Further increase of operation conditions (higher temperature or H_2 pressure) can not help in a deeper level of aromatic saturation due to the thermodynamic limitations in hydrogenation (see Figure 9).

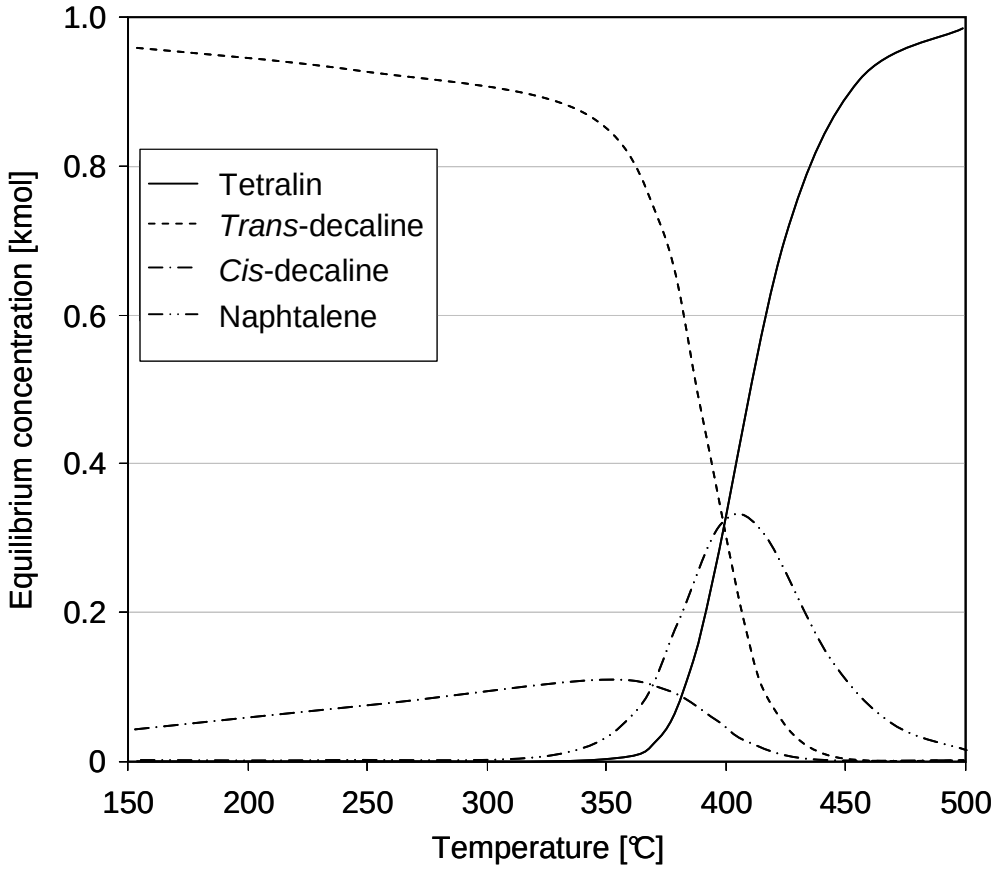

Figure 9. Thermodynamic equilibrium between tetralin, *cis*- and *trans*-decalin, naphthalene in temperature of 150 to 500℃ at 50 ba r hydrogen pressure [19].

4. Noble metal hydrotreating catalysts

Noble metal catalysts have excellent hydrogenation activity at relative low temperatures, making them a good choice for deep hydrogenation reactions. However, noble metals can be easily poisoned by sulfur and nitrogen compounds which are present in industrial feeds [20]. Therefore, developing a noble metal catalyst with high hydrogenation activity and good resistance towards poisoning is required.

4.1. Effect of supports

Numerous studies have been done to improve the sulfur resistance of noble metal catalysts, and it has been found than the catalytic activity and sulfur tolerance can be improved by using acid support, such as HY[21-23] and Beta [24] zeolites. This observation can be explained by the partial electron transfer from noble metal nanoparticles to the acid sites of the support [25]. The electron deficient metal nanoparticles are more resistant towards sulfur poisoning due to a weaker metal-sulfur bond [16]. Another explanation is the alternative hydrogenation pathway on the acid sites in the perimeter of noble metal nanoclusters. The aromatic molecules adsorb on the acid sites and hydrogenate by the spillovered hydrogen disassociated in the sulfur-covered metal sites [26,27]. Besides zeolites, amorphous silica-alumina is also applied as acid carrier for supported noble metal catalysts. Vannice et al. [28-30] reported that Pt or Pd supported on amorphous silica-alumina is much active than the catalysts supported on alumina in benzene and toluene hydrogenation. Moreover, due to its mesoporous property, ASA allows bulky molecules pass through the pores without diffusion limitations.

4.2. Effect of alloying noble metals

It is also reported that the sulfur resistance is improved by alloying two different noble metals, e.g. Pt and Pd [31-33]. However, the sulfur tolerance of the bimetallic Pt-Pd catalysts is influenced by many factors, such as the preparation procedures, degree of Pt-Pd alloy formation, morphology and surface composition of Pt-Pd particles, Pt-Pd nanocluster sizes and interactions between the bimetallic particles and support [16].

The two highly dispersed active metals, Pt and Pd, are thought to exist as an alloy, which contributes to the high sulfur tolerance because of its structural and electronic effects rather than the degree of metal dispersion in bimetallic Pt-Pd catalysts [34]. The Pt-Pd bimetallic interaction leads to the increase in the amount of electron deficient metal sites, which improves the sulfur tolerance by reducing the electrophilic sulfur adsorption [35]. On the other hand, the structure

changes in Pt-Pd bimetallic catalysts give rise to different active sites that make the adsorption of H_2 more competitive [32].

5. Scope of thesis

In our previous study [27,36,37] on amorphous silica-alumina (ASA) supported Pt catalysts, the effect of the supports (with different silica/alumina ratios) and the important role of Brønsted acid sites is stated: when sulfur-containing compounds are present in the feed, the cleaved S from sulfur-containing molecules absorbs strongly on Pt particle surfaces and blocked the active metal sites, thus the hydrogenation of aromatic molecules on the metal surfaces is hindered. However, hydrogen molecules are still able to penetrate into the S-poisoned metal surfaces and disassociate. On the other hand, aromatic molecules can adsorb on the Brønsted acid sites at the perimeter of the poisoned metal clusters and hydrogenated by the spillovered hydrogen dissociated from poisoned metal clusters.

In this thesis, we focus on Pt-Pd systems. Bimetallic Pt-Pd catalysts (with a Pd:Pt molar ratio of 3) supported on amorphous silica-alumina with different Si/Al ratios and on silica were synthesized. In chapter 2, the characterization of the Pt-Pd catalysts is presented. The Pt-Pd nanoclusters in the catalysts were studied in detail using X-ray absorption spectroscopy and CO adsorption infrared spectroscopy. Chapter 3 summarizes the results of tetralin hydrogenation on the bimetallic Pt-Pd catalysts in the absence and presence of quinoline and dibenzothiophene, and the hydrogenation activity and resistance towards poisons are further correlated with the structure of the Pt-Pd nanoclusters.

From the study in chapter 2 and 3, it is found that the morphology and surface composition of the Pt-Pd nanoparticles are very important in tetralin hydrogenation activity and resistance towards poisoning. Therefore, in chapter 4 Pt-Pd nanoparticles with different structure and morphology are prepared using different metal precursors and changing the pH value of precursor solutions. The different Pt-Pd nanoclusters are physicochemically and kinetically characterized. The correlation between the Pt-Pd nanocluster morphology, hydrogenation

activity and poison resistance is described.

In chapter 5, all main results and conclusions are summarized and a schematic representation of hydrogenation pathways on supported Pt-Pd catalysts is proposed.

6. Reference

[1] EU Economic Report, March 2009 (http://www.acea.be/images/uploads/files/20090309_ER_0902_2009_I_Q1-4_public_web.pdf)

[2] BP Statistical review of world energy, 2011 (http://www.bp.com/assets/bp_internet/globalbp/globalbp_uk_english/reports_and_publications/statistical_energy_review_2011/STAGING/local_assets/spreadsheets/statistical_review_of_world_energy_full_report_2011.xls)

[3] Diesel fuel and exhaust emissions, United Nations environment Programme, International labour organization, World health organization (http://www.inchem.org/documents/ehc/ehc/ehc171.htm)

[4] R.W Westerholm, K.E. Egebäck, Environ. Health Perspect. 102 (1994) 13.

[5] J.L. Mauderly, Environ. Health Perspect. 102 (1994) 165.

[6] D.F. Dolan, D.B. Kittelson, D.Y.H. Pui, SAE Technical Paper Series (1980), No. 800187.

[7] R.L. Williams, Dev. Toxicol. Environ. Sci. 10 (1982) 15.

[8] K.J Baumgard, J.H. Johnson, SAE Technical Paper Series (1996) no. 960131.

[9] F. Anisits, O. Hiemesch, W. Dabelstein, J. Cooke, M. Mariott, Motortechnische Zeitschrift, 52 (1991) 242.

[10] M. Gairing, W. W. Lange, A. Le Jeune, D. Naber, A. Reglitzky, A. Schäfer, Motortechnische Zeitschrift, 55 (1994) 8.

[11] N. Ladommatos, M. Parsi, A. Knowles, Fuel, 75 (1996) 8.

[12] G.H. Unzelman, AM-87-33, NPRA Annual meeting, March 1987.

[13] European Parliament, Council, Official Journal L 242 , 30/08/1991 P. 0001 – 0106; Official Journal L 350 , 28/12/1998 P. 0001 – 0057; Official Journal L 252 ,

20/09/2002 P. 0020 – 0032 and Official Journal L 171 , 29/06/2007 P. 0001 - 0016

[14] J.H. Gary, G.E. Handwerk, Petroleum Refining Technology and Economics, 4th Edition, Marcel Dekker, Inc., New York. 2001

[15] A. Stanislaus, B.H. Cooper, Catal. Rev. Sci. Eng. 36 (1994) 75.

[16] B.H. Cooper, B B.L. Donnis, Appl. Catal. A 137 (1996) 203.

[17] F. E. Bingham, P. Christensen. Revamping HDS Units to Meet High Quality Diesel Specifications. in Asian Pacific Refining Technology Conference. 2000. Kuala Lumpur, Malaysia.

[18] H. Topsøe, B.S. Clausen, F.E. Massoth, Hydrotreating Catalysis, Springer Verlag, Berlin, 1996.

[19] Simulation with software: HSC Chemistry for Windows

[20] J. Barbier, E. Lamy-Pitara, P. Marecot, J.P. Boitiaux, J.P. Cosyns, F. Verna, Adv. Catal. 37 (1990) 279.

[21] C. Song, A.D. Schmitz, Energy Fuels 11 (1997) 656.

[22] H. Yasuda, N. Matsubayashi, T. Sato, Y. Yoshimura, Catal. Lett. 54 (1998) 23.

[23] H. Yasuda, T. Sato, Y. Yoshimura, Catal. Today 50 (1999) 63.

[24] B. Pawelec, R. Mariscal, R.M. Navarro, S. van Bokhorst, S. Rojas, J.L.G. Fierro, Appl. Catal. A: Gen. 225 (2002) 223.

[25] W.M.H. Sachtler, A.Y. Stakheev, Catal. Today 12 (1992) 283.

[26] J. Wang, L.M. Huang, Q.Z. Li, Appl. Catal. A: Gen. 175 (1998) 191.

[27] M.F. Williams, B. Fonfé, A. Jentys, C. Breitkopf, J.A.R. van Veen, J.A. Lercher, J. Phys. Chem. C 114 (2010) 14532.

[28] S. D. Lin and M. A. Vannice, Journal Of Catalysis, 1993. 143(2) 563.

[29] S. D. Lin and M. A. Vannice, J. Catal., 1993. 143 539.

[30] D. Poondi and M. A. Vannice, J. Catal., 1996. 161 742.

[31] T.B. Lin, C.A. Jan, J.R. Chang, Ind. Eng. Chem. Res. 34 (1995) 4284.

[32] H. Jiang, H. Yang, R. Hawkins, Z. Ring, Catal. Today 125 (2007) 282.

[33] R.M. Navarro, B. Pawelec, J.M. Trejo, R. Mariscal, J.L.G. Fierro, J. Catal. 189 (2000) 184.

[34] H. Yosuda, Y. Yoshimura, Catal. Lett. 46 (1997) 43.

[35] J.K. Lee, H.K. Rhee, J. Catal. 177 (1998) 208.

[36] M.F. Williams, B. Fonfé, C. Sievers, A. Abraham, J.A. van Bokhoven, A. Jentys, J.A.R. van Veen, J.A. Lercher, J. Catal. 251 (2007) 485.

[37] M.F. Williams, B. Fonfé, C. Woltz, A. Jentys, J.A.R. van Veen, J.A. Lercher, J. Catal. 251 (2007) 497.

Chapter 2

Bimetallic Pt-Pd catalysts: Physicochemical characterization

Bimetallic Pt-Pd catalysts (with a Pd:Pt molar ratio of 3) supported on amorphous silica-alumina with different Al_2O_3/SiO_2 ratios and on silica were synthesized and characterized. The concentration of Lewis acid sites increased with the alumina content of support, whereas the concentration of Brønsted acid sites reached a maximum at 20 wt.% of alumina. The impregnation with Pt and Pd led to the formation of bimetallic particles of 1.4 - 1.8 nm diameter. Infrared spectroscopy of adsorbed CO and the analysis of the extended X-ray absorption fine structure indicated the formation of core-shell Pt-Pd bimetallic particles with a Pd enriched surface and a Pt rich core. In addition a small fraction of monometallic Pd clusters was formed regardless of the support composition. The morphology and composition of the bimetallic clusters strongly depended on the support composition. The molar Pd/Pt ratio in the bimetallic clusters decreased, while the proportion of surface Pt increased with increasing alumina content in the support. The varying surface metal composition is attributed to different interaction strengths between the metal precursors and supports during the preparation steps. X-ray absorption near edge structure provided evidence of electron deficiency of Pt atoms in the bimetallic Pt-Pd particles.

1. Introduction

Bimetallic Pt-Pd catalysts have received considerable attention, because they show high activity in a variety of catalytic applications [1]. The interest in studying Pt-Pd catalysts originates from its superior activity, selectivity and stability compared with monometallic Pt or Pd catalysts. For instance, the bimetallic Pt-Pd catalysts have been shown to have higher resistance towards poisons compared to Pt catalysts [2-4]. From a fundamental point of view, exploring bimetallic catalysts also allows a better understanding of mechanisms and variables involved in the catalyzed reactions. Therefore, extensive efforts has been undertaken to elucidate the morphology of metallic clusters and to draw structure-activity relationships [5-7].

For supported bimetallic clusters, the surface and bulk composition strongly depend on a series of parameters, e.g., preparation procedures, metal-metal and metal-support interactions. Thus, it is not surprising that diverse and apparently contradictory studies on the genesis and structure of Pt-Pd catalyst are found in the literature. The formation of homogenous Pt-Pd particles on silica and NaY zeolite has been reported [8,9]. However, experimental and theoretical evidence for the segregation of Pd to the surface of bimetallic Pt-Pd clusters is more abundant [10-15]. Pd is claimed to segregate to the surface during thermal treatment, probably because of the different surface energy of Pt and Pd [16]. Many other factors, however, may also affect Pd migration. For example, studies of alumina- and carbon-supported Pt-Pd catalysts show that the migration of Pd atoms to the surface is enhanced by thermal treatment in H_2 or O_2, but suppressed by high metal dispersion [17]. Furthermore, not only the variables involved in the reduction step can influence the characteristics of Pt-Pd catalysts. For instance, the particle size and composition of bimetallic clusters on alumina are notably affected by replacing nitrate precursors with acetylacetonate during the preparation procedure [18]. The thermal treatment applied to the catalyst precursor may also affect the oxidation state of the metal before the reduction step as shown in ref. [8].

The large number of variables determining the nature of supported bimetallic particles makes it difficult to deduce general models for the metal phase in the Pt-Pd catalysts without characterizing a sizable number of different bimetallic catalysts to deduce structure-activity correlations. In this study, we aim to investigate the characteristics of Pt-Pd clusters supported on amorphous silica alumina (ASA) as a function of the silica to alumina ratio, which induces a change in the concentration of Brønsted and Lewis acid sites of the support. Nuclear magnetic resonance spectroscopy (NMR), infrared spectroscopy using CO and pyridine as probe molecules, transmission electron microscopy (TEM), and X-ray absorption spectroscopy using EXAFS analysis are utilized to derive a structural model for the Pt-Pd catalysts.

The features of the catalysts here studied, are going to be correlated to their catalytic performance in the hydrogenation of tetralin in the absence and presence of dibenzothiophene and quinoline in the second part of this work [19]. The final goal is to propose a mechanistic model of the tetralin hydrogenation on the Pt-Pd/ASA catalysts that includes the metal phase and Brønsted acid sites in the support. To better address the effect of acidity, a monometallic Pt catalyst and its Cs-exchanged form were also prepared and characterized.

2. Experimental

2.1. Preparation of supported Pt-Pd catalysts

A series of Pt-Pd based catalysts (with a molar ratio of Pd:Pt = 3) supported on amorphous silica-alumina (ASA) with Al_2O_3/SiO_2 ratios of 5/95, 20/80 and 55/45 and pure silica were prepared by incipient wetness impregnation. The ASA supports were synthesized by mixing aqueous solutions of $AlCl_3 \cdot 6H_2O$ in acetic acid (pH = 1.5) and sodium silicate in NH_4OH (pH = 12). The pH of the mixture was 7.5. The resulting gel was washed with a diluted solution of ammonium acetate to eliminate sodium cations. Subsequently, the gel was dried at 400 K and treated in air at 783 K for 2 h and at 949 K for 2 h. The pure silica support

was provided by Shell and thermally treated in air at 783 K for 2 h and at 949 K for 2 h.

The supports were impregnated with an aqueous solution of $[Pt(NH_3)_4](NO_3)_2$ and $[Pd(NH_3)_4](NO_3)_2$ using the incipient wetness impregnation technique. The pH of the solution was 7.7. Subsequently, the catalysts were equilibrated for 0.5 h on a mini rolling-road, and dried (453 K, 10 min) and calcined (563 K, 10 min) in a rotating-tube oven. Finally, the catalysts were reduced at 623 K in hydrogen for 2 h.

Two additional monometallic Pt catalysts were synthesized to study the role of the Brønsted acidity in tetralin hydrogenation in the absence and presence of poisons. One of the catalysts was 0.8 wt.% Pt supported on ASA with an alumina to silica mass ratio of 38/62 (Pt/ASA(38/62)). In the other catalyst (Cs-Pt/ASA(38/62)) the Brønsted acid sites were ion-exchanged by cesium ions, to suppress the support acidity. The parent Pt/ASA(38/62) catalyst was prepared by the same method as described for Pt/ASA samples in ref [20]. In order to exchange this catalyst with Cs the sample was first reduced in flowing H_2 at 623 K and then cooled to room temperature in He. After passivation at room temperature (1 vol.% O_2 in He) the sample was impregnated with an aqueous solution of $CsNO_3$ in excess (30 mg Cs per gram of catalyst) followed by equilibration on a mini rolling road for 1 h. Subsequently, the catalyst was dried for 2 h at 393 K, treated in synthetic air for 2 h at 573 K and finally reduced in H_2 for 2 h at 623 K.

2.2. Elemental analysis, specific surface area and porosity

The chemical compositions of the supported catalysts were determined by atomic absorption spectroscopy (AAS) using an UNICAM 939 spectrometer. The specific surface area and average pore diameter of the catalysts were derived from N_2 adsorption-desorption measurements carried out at liquid nitrogen temperature using a PMI automated BET sorptometer. Prior to the measurements, all samples were outgassed at 523 K for 20 h. The specific

surface areas and the micropore and mesopore distributions were calculated applying the BET and BJH models, respectively.

2.3. MAS-NMR spectroscopy

The catalyst samples were packed at ambient conditions into 4 mm ZrO_2 rotors for the ^{27}Al NMR experiments. The spectra were obtained with a Bruker Avance AMX 400 NMR spectrometer operating at 104.263 MHz for aluminium. Solid $(NH_4)Al(SO_4)_2$ (δ_{Al} = -0.59 ppm) was used as standard for the chemical shifts [20].

2.4. IR spectroscopy

IR spectra of adsorbed pyridine were used to characterize acid sites, while the spectra of adsorbed CO were used to characterize the properties of the metal surface. The adsorption of pyridine was studied with a Perkin Elmer 2000 spectrometer operating at a resolution of 4 cm^{-1}. Prior to the sorption experiments, the catalyst samples were activated in vacuum (p = 10^{-6} mbar) at 673 K for 1 h. The activated samples were exposed to pyridine ($p_{(Py)}$ = 10^{-2} mbar) at 423 K for 0.5 h and after outgassing at 423 K for 1 h the IR spectra were recorded. The concentration of Lewis (LAS) and Brønsted (BAS) acid sites were quantified using the molar extinction coefficients of 0.965 $cm \cdot \mu mol^{-1}$ for LAS and 0.726 $cm \cdot \mu mol^{-1}$ for BAS.

The CO adsorption experiments were performed using a Bruker ISF88 spectrometer using a resolution of 4 cm^{-1}. Samples of the catalysts were reduced in H_2 at 623 K for 1 h at a pressure 1 bar followed by outgassing in vacuum (p = 10^{-6} mbar) for 1 h to remove the adsorbed hydrogen. The samples were cooled to 313 K and CO was adsorbed at 0.5 mbar. Subsequently, the sample was evacuated for 15 minutes at 10^{-6} mbar and an additional spectrum was recorded.

2.5. Transmission electron microscopy

The catalyst samples treated in H_2 (623 K for 2 h) were ground, suspended in ethanol and ultrasonically dispersed. Drops of the dispersions were applied on a

copper grid-supported carbon film. A JEM-2010 Jeol transmission electron microscope operating at 120 kV was used to perform the measurements.

2.6. X-ray absorption spectroscopy

X-ray absorption spectra were collected at the beamlines X1 and C at HASYLAB, DESY, Hamburg, Germany. The storage ring was operated at 4.5 GeV at an average current of 100 mA. The Si (311) double crystal monochromator was detuned to 60% of the maximum intensity to minimize the intensity of higher harmonics in the X-ray beam. The samples were prepared as self-supporting wafers and reduced in situ with H_2 at 588 K for 1 h and then flushed with He at 588 K for 0.5 h to remove adsorbed H_2. The X-ray absorption spectra were collected at the Pt L_{III} edge (11564 eV) and the Pd K edge (24365 eV) at 77 K. The position of the edge was calibrated using the spectra of a simultaneously measured Pt or Pd foil. For the EXAFS and XANES analysis, the scattering background was subtracted using a polynomial function and all spectra were normalized to unity. The VIPER and XANDA programs were used for analyzing the datasets [21].

For EXAFS analysis the oscillations were weighted with k^2 and Fourier transformed within the limits k = 2.0 – 11.0 $Å^{-1}$. Using multiple-edge fitting with equal distances for Pt-Pd and Pd-Pt neighbors the local environments of the Pt and Pd atoms were determined from the oscillation (in k space) using phase-shift and amplitude function for Pt-Pt, Pd-Pd, Pt-Pd and Pd-Pt calculated assuming multiple scattering processes (FEFF Version 8.30) [22,23].

3. Results

3.1. Textural properties and chemical composition of the oxide supported Pt-Pd bimetallic catalysts

The chemical compositions of the Pt-Pd catalysts obtained from AAS are summarized in Table 1. The metal content was approximately 0.8 wt.% in all samples with a Pd/Pt molar ratio of 3. The overall metal loading of the samples

corresponds to the Pt content on the ASA supported monometallic catalysts studied in a previous work [20]. The specific surface areas were 313, 308 and 452 $m^2 \cdot g^{-1}$ for the Pt-Pd catalysts supported on ASA(55/45), ASA(20/80) and ASA(5/95), respectively. The catalyst supported on pure silica had a specific surface area of 167 $m^2 \cdot g^{-1}$. The average pore diameters did not exhibit any trend depending on the silica content.

Table 1. Textural properties, chemical composition and mean metal particle size of Pt-Pd catalysts.

Catalyst	Concentration (wt.%)				BET Surface area ($m^2 \cdot g^{-1}$)	Pore diameter (nm)	Particle size[1] (nm)
	Pt	Pd	Al_2O_3	SiO_2			
Pt-Pd/ASA(55/45)	0.30	0.55	55.2	44.0	313	4.0	1.4
Pt-Pd/ASA(20/80)	0.30	0.52	20.2	79.0	308	13.9	1.8
Pt-Pd/ASA(5/95)	0.29	0.50	5.4	93.8	452	6.1	1.6
Pt-Pd/SiO_2	0.30	0.52	0.0	99.2	167	24.8	1.4

[1] Mean metal particle size determined by TEM.

3.2. Acid properties of the Pt-Pd bimetallic catalysts

The acid properties of the catalysts were characterized by pyridine adsorption/desorption followed by IR spectroscopy. The concentrations of Brønsted (BAS) and Lewis (LAS) acid sites were estimated from the quantitative evaluation of the spectra and are summarized in Table 2. The catalysts supported on pure SiO_2 did not show any acidity, indicating that the presence of the metal does not induce Lewis acidity. The concentration of LAS increased with the alumina concentration in the samples, i.e., Pt-Pd/ASA(5/95) < Pt-Pd/ASA(20/80) < Pt-Pd/ASA(55/45). In contrast, the total concentration of Brønsted acid sites increased according in the following sequence: Pt-Pd/ASA(55/45) < Pt-Pd/ASA(5/95) < Pt-Pd/ASA(20/80).

Table 2. Brønsted acid sites (BAS) and Lewis acid sites (LAS) concentrations calculated from pyridine adsorption IR spectroscopy for Pt-Pd catalysts.

Catalyst	Acid site concentration (µmol·g^{-1})	
	BAS	LAS
Pt-Pd/ASA(55/45)	22	192
Pt-Pd/ASA(20/80)	58	183
Pt-Pd/ASA(5/95)	45	156
Pt-Pd/SiO_2	0	0

3.3. ^{27}Al NMR - Chemical environment of aluminum in Pt-Pd bimetallic catalysts

The chemical environment of the aluminum species was investigated for the two samples with the highest alumina contents, i.e., Pt-Pd/ASA(55/45) and Pt-Pd/ASA(20/80). The results are shown in Fig. 1 and compared to monometallic Pt/ASA samples [20]. The known spectrum of pure Al_2O_3 exhibited two signals at 67 and 9 ppm, corresponding to tetrahedral and octahedral aluminum, respectively [24]. With ASA(55/45), the position of the signals shifted to 57 and 4 ppm and a new resonance at approximately 29 ppm was observed. The upfield shifts of the signals at 4 and 57 are assigned to a significant dilution of aluminum in the neighborhood of a central Al-atom. The peak at 29 ppm has been assigned to strongly distorted tetrahedral [25,26] or pentavalent aluminum species [27-30]. The samples with less alumina, Pt/ASA(20/80) and Pt-Pd/ASA(20/80), showed a remarkable upfield shift of the peak attributed to tetragonal coordinated aluminum from 67 (pure Al_2O_3) to 51 ppm. Some geometric factors, e.g., disordered Al-O-Si angles [31] and the composition of the further coordination shells could also influence the resonance of tetrahedral Al [32]. The other aluminum species were found in six- and five-fold coordination states as can be seen from the resonance signals at 2 and 27 ppm, respectively. Generally, for both bimetallic samples the shifts in the NMR spectra were similar to the shifts observed for the Pt/ASA

samples [20]. As the supported Pt and Pd-Pt clusters influence the chemical environment of aluminum in a similar way, we would like to refer to ref. [20] for a detailed description of the surface properties of the ASA supports.

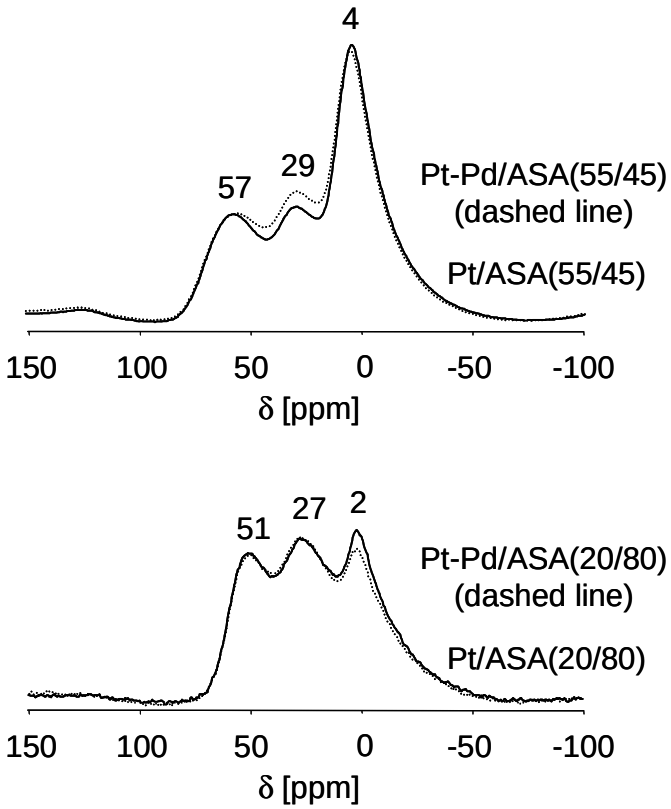

Figure 1. ^{27}Al NMR of Pt-Pd/ASA(55/45) and Pt-Pd/ASA(20/80) (data are compared to monometallic Pt samples [20]).

3.4. Characterization of the Pt-Pd nanoclusters

The supported Pt-Pd metal nanoparticles were characterized by TEM, EXAFS, XANES and CO adsorption IR spectroscopy. Representative TEM pictures are shown in Fig. 2, the grey areas represent the oxide supports and the small darker dots represent the noble metal particles. Particle size histograms (compiled in Fig. 3) were derived from the TEM images by analyzing about 300 metal particles per catalyst. The mean metal particle sizes for Pt-Pd/SiO_2, Pt-Pd/ASA(5/95), Pt-Pd/ASA(20/80) and Pt-Pd/ASA(55/45) were 1.4, 1.6, 1.8 and 1.4 nm, respectively (see Table 1). In comparison to the catalysts containing only Pt [20], the mean

metal particle sizes on the ASA supports increased from an average of 0.8 nm for the Pt/ASA catalysts to 1.4 - 1.8 nm for the Pt-Pd/ASA catalysts. The particle size distributions were also broader for the bimetallic catalysts (with sizes ranging from 0.8 to 3.0 nm) showing that the bimetallic Pt-Pd particles are not as uniformly dispersed on the ASA surface as monometallic Pt.

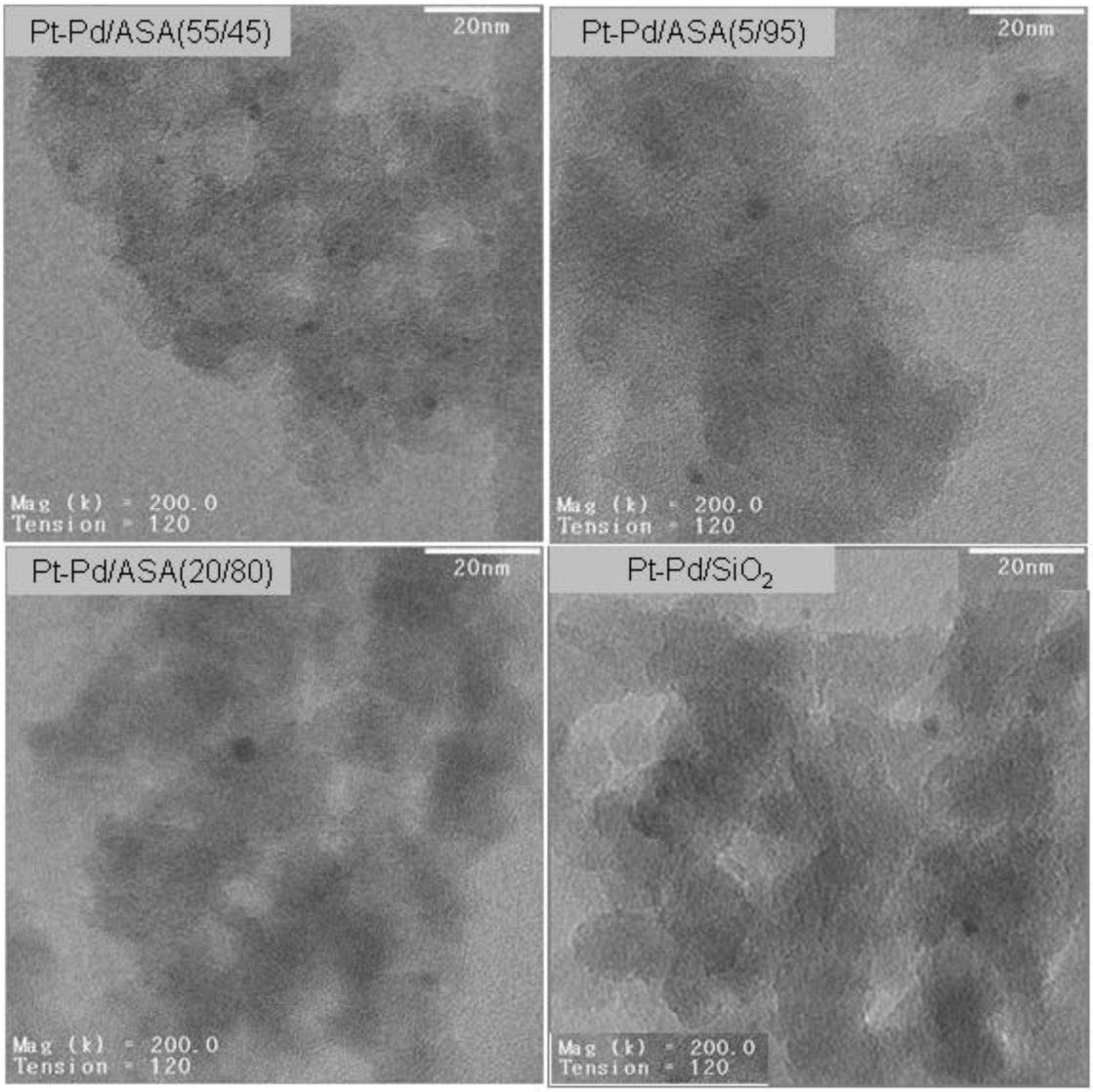

Figure 2. Representative TEM images of Pt-Pd/ASA(55/45), Pt-Pd/ASA(20/80), Pt-Pd/ASA(5/95) and Pt-Pd/SiO_2.

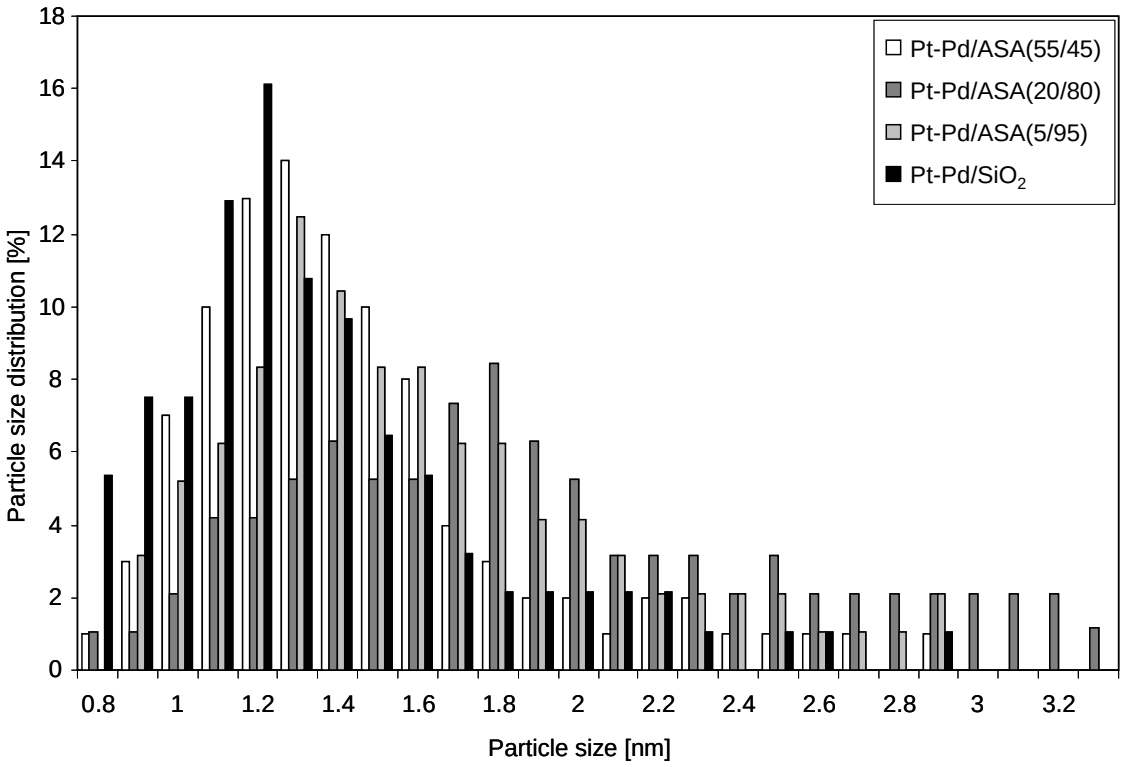

Figure 3. Size histograms derived from TEM for Pt-Pd/ASA(55/45), Pt-Pd/ASA(20/80), Pt-Pd/ASA(5/95) and Pt-Pd/SiO_2 catalysts.

EXAFS was used to further characterize the morphology of Pt-Pd clusters. The Fourier transforms of the EXAFS at the Pt L_{III} edge and at the Pd K edge for the reduced Pt-Pd materials are shown in Figs. 4 and 5. Table 3 summarizes the structural parameters, i.e., the coordination numbers (CN) and the interatomic distances (r) calculated from the analysis of the EXAFS oscillations in k space. The interatomic distances for the Pt-Pt, Pt-Pd, Pd-Pd and Pd-Pt bonds showed generally a slight contraction (max. 2.5%) typical for small metal particles [33]. Regardless of the composition of the support, the total coordination of Pt, i.e., sum of coordination numbers (CN_{Pt-Pt} + CN_{Pt-Pd}) is around 11, whereas the total coordination of Pd (CN_{Pd-Pd} + CN_{Pd-Pt}) is nearly 6. In cubooctahedral particles (both metals have face-centered cubic lattices) [34-36], the total coordination number for the atoms on the surface is around 6, whereas the coordination

numbers for the inner atoms is 12. Thus, the high values for the sum of the coordination numbers of Pt (CN_{Pt-Pt} + CN_{Pt-Pd}) suggest that the Pt atoms are preferably inside the core of the bimetallic particle, surrounded by Pd, for which the total coordination numbers (CN_{Pd-Pd} + CN_{Pd-Pt}) around 6 indicate that the main fraction of Pd is on the surface of the bimetallic particles. The similar coordination numbers for all catalysts indicate that the general structural features of the bimetallic Pt-Pd clusters do not depend on the support. It must be pointed out, that Pt-Pd/ASA(55/45) has the highest CN_{Pt-Pd}, CN_{Pd-Pt} and lowest CN_{Pt-Pt}, CN_{Pd-Pd}.

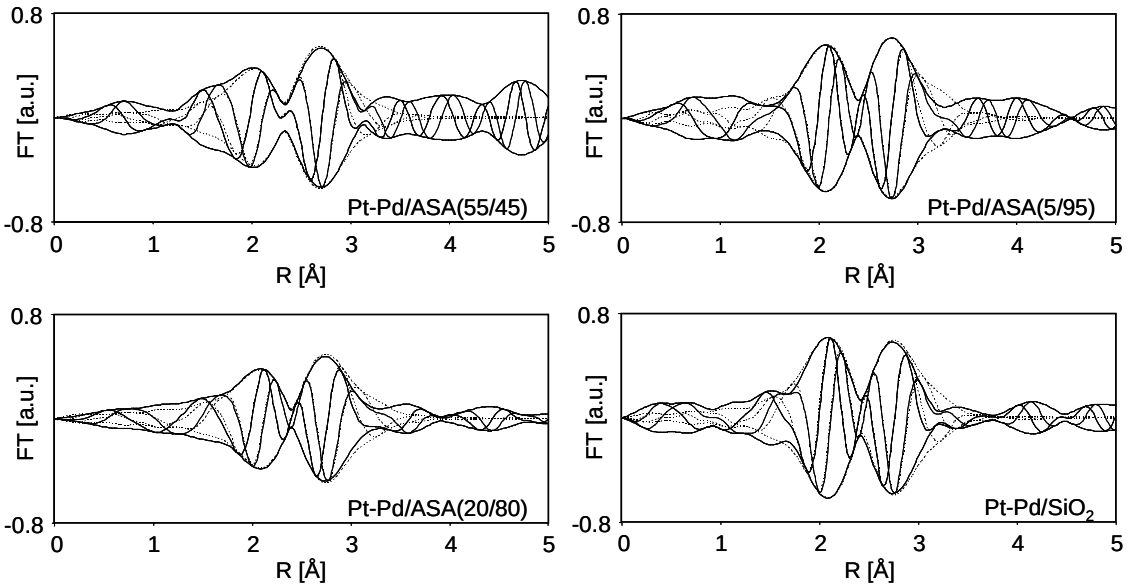

Figure 4. Fourier transforms (k^2 –weighted, Δk 2-11 $Å^{-1}$) of Pt-Pd/ASA(55/45), Pt-Pd/ASA(20/80), Pt-Pd/ASA(5/95) and Pt-Pd/SiO_2 (solid lines) at Pt L_{III} edge (11564 eV) and their Pt-Pt and Pt-Pd fitted contributions (dashed lines) after in situ treatment in H_2 at 588 K.

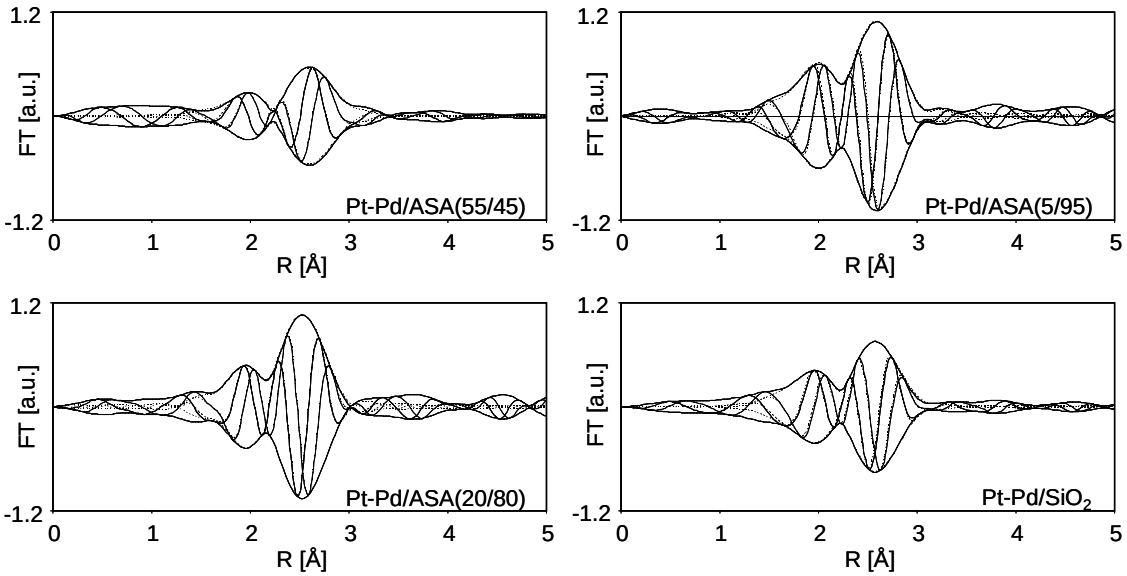

Figure 5. Fourier transforms (k^2 –weighted, Δk 2-11 $Å^{-1}$) of Pt-Pd/ASA(55/45), Pt-Pd/ASA(20/80), Pt-Pd/ASA(5/95) and Pt-Pd/SiO_2 (solid lines) at the Pd K edge (24365 eV) and their Pd-Pd and Pd-Pt fitted contributions (dashed lines) after in situ treatment in H_2 at 588K.

Table 3. Fitted values from the EXAFS spectra for Pt-Pd catalysts: coordination number (CN), radial distance (r) and Pd:Pt ratio in the bimetallic clusters[1].

Catalyst	Edge	Pt-Pt		Pt-Pd		Pd-Pt		Pd-Pd		Pd:Pt ratio[1]
		CN	r [Å]	CN	r [Å]	CN	r [Å]	CN	r [Å]	
Pt-Pd /ASA(55/45)	Pt L_{III}	7.38	2.75	3.74	2.71					1.17
	Pd K					3.21	2.71	3.05	2.72	
Pt-Pd /ASA(20/80)	Pt L_{III}	7.99	2.73	3.21	2.73					1.24
	Pd K					2.59	2.73	4.33	2.74	
Pt-Pd /ASA(5/95)	Pt L_{III}	8.02	2.75	3.30	2.71					1.41
	Pd K					2.34	2.71	4.22	2.76	
Pt-Pd /SiO_2	Pt L_{III}	8.02	2.71	3.60	2.72					1.69
	Pd K					2.13	2.72	3.95	2.76	

[1] Pd:Pt ratio determined as CN_{Pt-Pd}:CN_{Pd-Pt}. These values correspond to the composition of the bimetallic cluster not to the overall Pd:Pt ratio of 3 as determined by atomic absorption spectroscopy.

Since both, the $2p_{3/2}$ to $5d_{3/2}$ and the $2p_{3/2}$ to $5d_{5/2}$ electronic transitions, are observed at the Pt L_{III} edge, the hole density in the $5d_{5/2}$ and $5d_{3/2}$ state is reflected in the white line intensity of the Pt L_{III} edge. Thus, further electronic effects of intermixing Pt and Pd are evident in the X-ray absorption near edge structure (XANES) at the Pt L_{III} edge as shown in Fig. 6. The increase of the white line height in the XANES indicates a lower electron density of Pt in the bimetallic nanoclusters compared to metallic (bulk) Pt [37]. Moreover, the composition of the ASA supports did not affect the electronic states of Pt atoms in Pt-Pd clusters, since the white line intensities above Pt L_{III} edges for Pt-Pd catalysts seemed to be constant. A more in-depth analysis is given in the discussion section of this contribution.

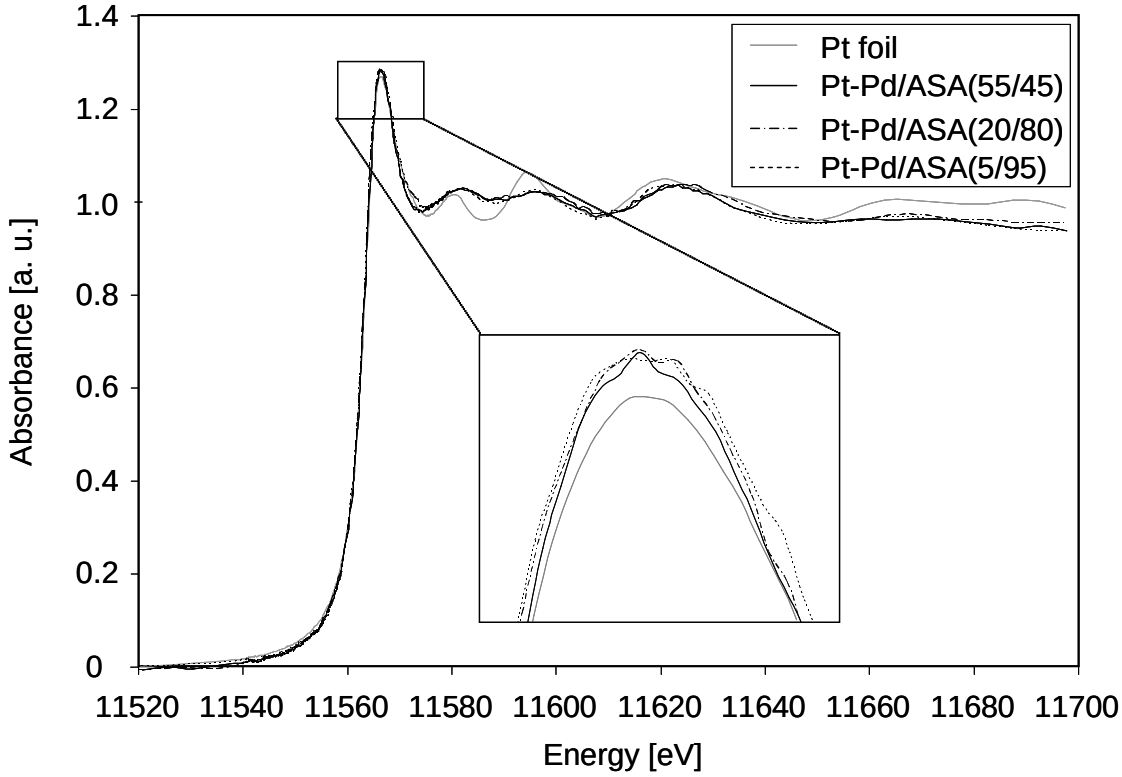

Figure 6. Normalized XANES at the Pt L_{III} edge in He at 588 K of Pt foil and Pt-Pd/ASAs after in situ reduced in H_2 at 588 K.

Metal nanoparticles were also characterized by CO adsorption on the reduced samples as presented in Fig. 7. Bands were observed at 2099, 2101, 2099 and 2095 for Pt-Pd/ASA(55/45), Pt-Pd/ASA(20/80), Pt-Pd/ASA(5/95) and Pt-Pd/SiO_2, respectively, corresponding to linearly adsorbed CO on Pt and Pd [10]. In these bands, the contributions of CO linearly bound to Pt and to Pd overlap. After evacuation, the intensity of the bands decreased and its position shifted to lower wavenumbers i.e., to 2078, 2084, 2083, and 2074 cm^{-1} for Pt-Pd/ASA(55/45), Pt-Pd/ASA(20/80), Pt-Pd/ASA(5/95) and Pt-Pd/SiO_2, respectively. Both observations are attributed to a decrease of the CO surface coverage due to desorption of CO from Pd [38]. To differentiate between Pd-CO and Pt-CO complexes, CO was adsorbed on monometallic Pd/ASA(30/70) and Pt/ASA(30/70) samples (not shown here) and the stepwise CO adsorption/desorption experiment described before led to the total removal of linearly adsorbed CO on Pd. In consequence, for the bimetallic materials (Figure 7, dashed lines), the decrease in intensity and position shift of the bands of CO linearly adsorbed after evacuation is assigned to the removal of CO from Pd. Even though the surface of bimetallic clusters is Pd enriched, the concentration of surface Pt is not negligible, because the intensity of bands corresponding to CO linearly adsorbed on Pt remains important in all cases.

Further broad bands in the spectra of the Pt-Pd materials were observed below 2000 cm^{-1}, which are assigned to CO adsorbed in a bridged form on Pd atoms (the exact band position is shown in Figure 7) [39]. The bands at 1860-1920 cm^{-1} were assigned to Pd_2-CO complexes or CO adsorbed on a defect-rich terraces [10,40], whereas bands at frequencies between 1950 and 1990 cm^{-1} are attributed to dimeric $[Pd_2\text{-}CO]_2$ species or CO adsorbed on the edges of aggregates [10,38]. The bands assigned to dimeric $[Pd_2\text{-}CO]_2$ species, decreased in intensity with increasing alumina concentrations in the supports and for Pt-Pd/ASA(55/45) the band almost completely disappeared upon evacuation. Note that dimeric $[Pd_2\text{-}CO]_2$ complexes can only be present, if there are at least four adjacent Pd atoms on the particle surface. Therefore, we conclude that the proportion of surface Pd is the lowest in Pt-Pd/ASA(55/45). The bands at 1860-

1920 cm^{-1} remained almost unchanged on evacuation, which was tentatively attributed to the conversion of $[Pd_2\text{-}CO]_2$ to monomeric Pd_2-CO during the CO desorption. While a further possibility could be that CO is adsorbed in a bridged form on Pt-Pd pairs, however, this structure cannot be identified unequivocally using the present results.

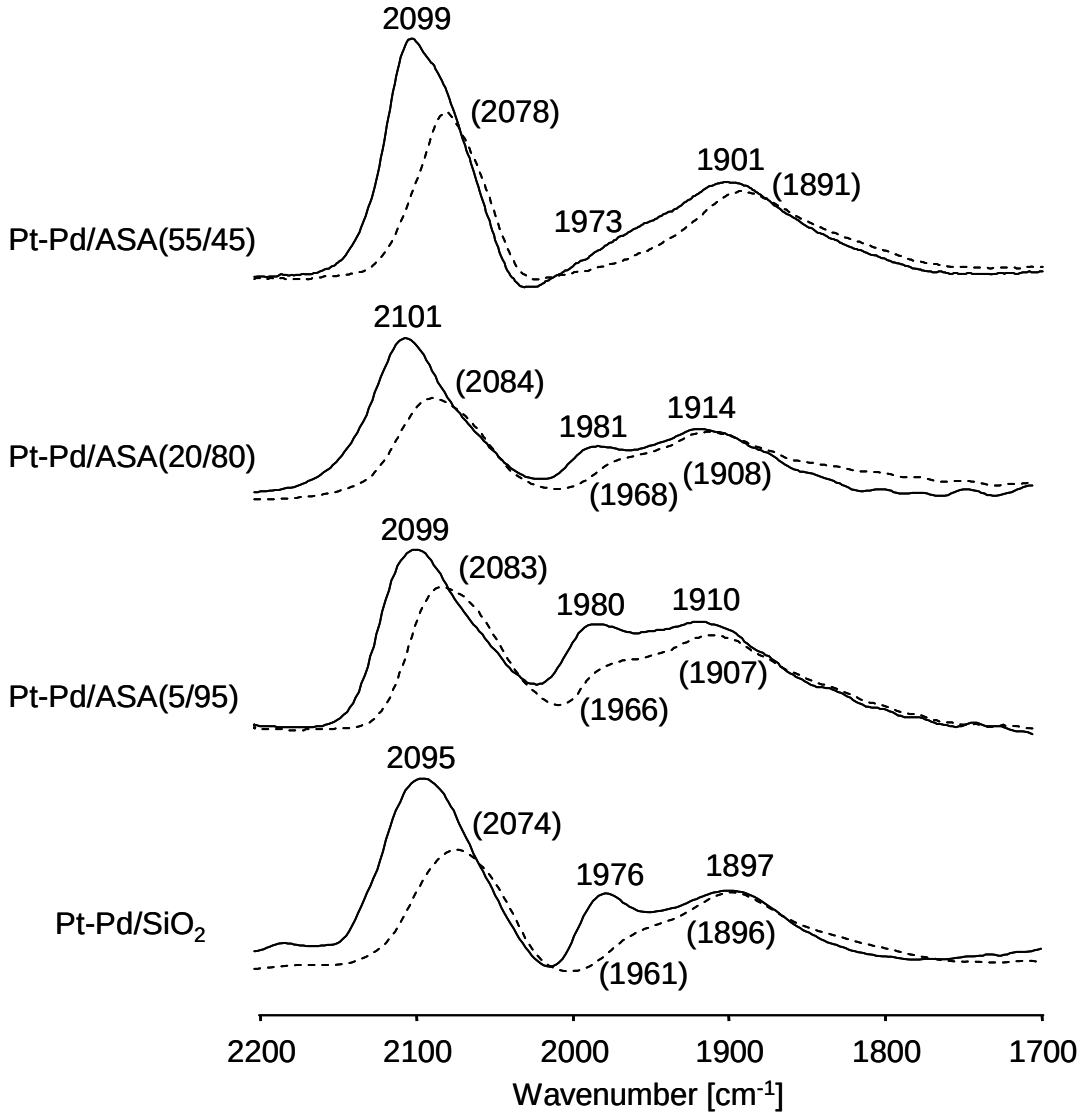

Figure 7. IR spectra of CO adsorbed on Pt-Pd/ASA(55/45), Pt-Pd/ASA(20/80), Pt-Pd/ASA(5/95), Pt-Pd/SiO_2 and Pd/ASA(20/80) catalysts at T = 40 ºC, $p_{(CO)}$ = $5 \cdot 10^{-1}$ mbar (continuous lines) and after evacuation for 15 min (dashed lines, band values in brackets).

The normalized integrated peak areas of linearly and bridged adsorbed CO at 0.5 mbar and after evacuation for 15 minutes are summarized in Table 4. The Pt-Pd/ASA(55/45) sample had the highest ratio of linear to bridged adsorbed CO (1.21 and 1.12 before and after evacuation, respectively) and the highest intensity of linearly adsorbed CO (2060-2110 cm^{-1}) before and after evacuation. Both observations indicate the lowest concentration of surface Pd atoms, and consequently the highest concentration of Pt atoms on the surface of this sample. The Pt-Pd/SiO_2, Pt-Pd/ASA(5/95) and Pt-Pd/ASA(20/80) catalysts had very similar values of linear to bridged adsorbed CO (1.02-1.08 after CO adsorption at 0.5 mbar and 0.86-0.91 after evacuation for 15 min), suggesting that the bimetallic clusters in these materials had a very similar surface composition. It is likely that the particular characteristics of the metallic clusters on ASA(55/45) originate from the fact that the surface of this material is the least homogenous, i.e., segregated alumina regions are formed as reported in ref. [20].

Table 4. Summary of weight normalized integrated peak areas of linearly and bridged adsorbed CO on the Pt and Pt-Pd catalysts at 0.5 mbar and after evacuation for 15 minutes at $5 \cdot 10^{-6}$ mbar (in brackets).

Catalyst	Linearly adsorbed CO (2060-2110 cm^{-1})	Bridged adsorbed CO (1840-1990 cm^{-1})	Ratio of linearly to bridged adsorbed CO
Pt-Pd/ASA(55/45)	865 (592)	714 (529)	1.21 (1.12)
Pt-Pd/ASA(20/80)	578 (416)	540 (485)	1.07 (0.86)
Pt-Pd/ASA(5/95)	642 (473)	628 (545)	1.02 (0.87)
Pt-Pd/SiO_2	710 (490)	658 (541)	1.08 (0.91)

3.5. Characterization of the Pt/ASA(38/62) and Cs-Pt/ASA(38/62) catalysts

The Pt/ASA(38/62) and Cs-Pt/ASA(38/62) catalysts were prepared to test the hypothesized role of Brønsted acidity in tetralin hydrogenation in the absence and presence of poisons. Impregnation of Pt/ASA(38/62) with Cs^+ did neither

influence the mean Pt cluster diameter (0.9 nm determined by TEM) nor the concentration and wavenumber of linearly adsorbed CO (2075 cm^{-1}) upon evacuation (Figure 8). On the other hand, pyridine adsorption showed that the Cs^+ treatment led to almost complete removal of Brønsted acid sites (from 54 to only 7 $\mu mol \cdot g^{-1}$), whereas the concentration of Lewis acid sites remained constant at 223 $\mu mol \cdot g^{-1}$ (see Table 5).

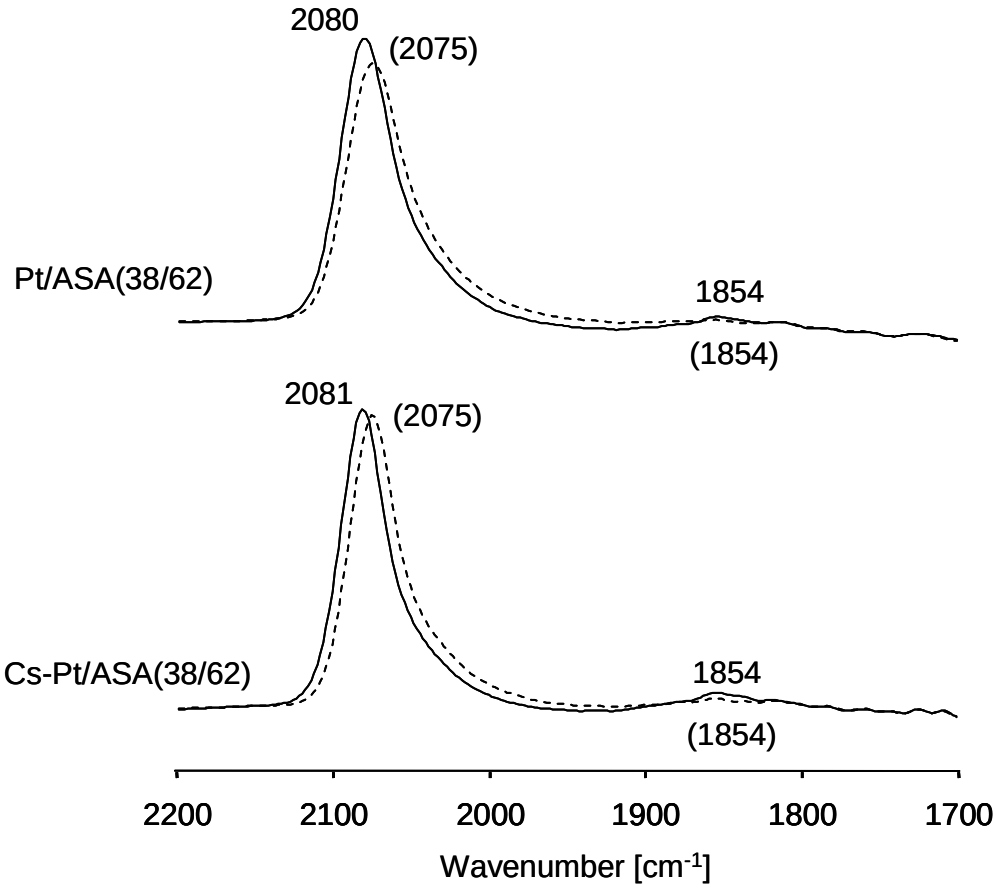

Figure 8. IR spectra of CO adsorbed on Pt/ASA(38/62) and Cs-Pt/ASA(38/62) catalysts at T = 40 ºC, $p_{(CO)} = 5 \cdot 10^{-1}$ mbar (continuous lines). Spectra recorded after evacuation for 15 min were also included (dashed lines, band values in brackets).

Table 5. Summary of TEM, pyridine adsorption IR and CO adsorption IR data of Pt/ASA(38/62) and Cs-Pt/ASA(38/62).

Catalyst	Particle size[1] (nm)	Acid site concentration (μmol·g^{-1})		Normalized peak area of linear adsorbed CO (2060-2110 cm^{-1})	Normalized peak area of bridge adsorbed CO (1840-1990 cm^{-1})
		BAS	LAS		
Pt/ASA(38/62)	0.9	54	223	1609.3	157.6
Cs-Pt/ASA(38/62)	0.9	7	221	1605.9	158.1

[1] Mean metal particle size determined by TEM.

4. Discussion

4.1. Characteristics of the ASA support

Let us compare briefly the characteristics of the supports in the Pt-Pd/ASA catalysts reported here with the characteristics of the support in Pt/ASA reported in ref. [20]. The results of ^{27}Al NMR indicated that the chemical environment of aluminum in the Pt-Pd/ASA catalysts is very similar to that observed for Pt/ASA. Thus, the synthesis of bimetallic catalysts did not affect the distribution of silica, alumina and aluminosilicate phases. Furthermore, the trends of the acidity were preserved regardless the composition of the metallic clusters, i.e., the concentration of LAS increased with the alumina concentration and the concentration of BAS reached a maximum at 20 wt.% alumina. This observation was in line with previously used material, for which it was found that the concentration of LAS correlated with the alumina regions, whereas the BAS were generated only on aluminosilicate domains [20].

4.2. Structure of the Pt-Pd clusters

The catalytic properties of bimetallic Pt-Pd/ASA depend not only on the nature of the Pt-Pd particles, it is also known that the sulfur tolerance of bimetallic catalysts is influenced by factors, such as particle size, there structure and the interactions between metal particles and supports. The preparation of ASA supported Pt-Pd

catalysts yielded particles with average diameters of 1.4 -1.8 nm (TEM), which were larger than the average diameters of the monometallic Pt clusters (0.8 nm) previously reported**.** Let us first analyze the local structure of Pd and Pt in ASA and silica-supported catalysts by their EXAFS.

In a homogeneously distributed bimetallic nanoparticle consisting of atoms A and B, (CN_{AA} + CN_{AB}) should be equal to (CN_{BB} + CN_{BA}), where CN_{AA}, CN_{AB}, CN_{BB} and CN_{BA} are partial coordination numbers. If atoms of element A segregate to the surface and those of element B to the core, (CN_{AA} + CN_{AB}) < (CN_{BB} + CN_{BA}) should be observed. Moreover, regardless of the structure of the particle containing atoms of type A and B, the simple conditions expressed in equations (1) and (2) must be satisfied [41].

$$CN_{AB} \cdot x_A = CN_{BA} \cdot x_B \quad (1)$$

$$r_{AB} = r_{BA} \quad (2)$$

In equation (1) and (2), x_A and x_B are the molar factions of element A and B, r_{AB} and r_{BA} are the interatomic distances between A-B and B-A, respectively. Thus, in the EXAFS analysis of all bimetallic Pt-Pd catalysts, $r_{Pt\text{-}Pd} = r_{Pd\text{-}Pt}$ was set as constraint in the fitting program. All calculated structure parameters are listed in Table 3. Substitution of $x_A = N_A/(N_A+N_B)$ and $x_B = N_B/(N_A+N_B)$ into Equation (1) leads to Equation (3) (making A=Pt and B=Pd) where N_{Pt} and N_{Pd} are the numbers of Pt and Pd atoms in the bimetallic Pt-Pd clusters. By eliminating (N_{Pt} + N_{Pd}) on both sides, Equation (4) is obtained.

$$CN_{Pt\text{-}Pd} \cdot N_{Pt}/(N_{Pt} + N_{Pd}) = CN_{Pd\text{-}Pt} \cdot N_{Pd}/(N_{Pt} + N_{Pd}) \quad (3)$$

$$CN_{Pt\text{-}Pd} \cdot N_{Pt} = CN_{Pd\text{-}Pt} \cdot N_{Pd} \quad (4)$$

Note that the relation given in Equation (4) was not used as a constraint when fitting the EXAFS data; therefore, it can be applied to identify the presence of additional monometallic particles.

Let us consider Pt-Pd/SiO_2 as example for this discussion. Since $CN_{Pt\text{-}Pd}$ = 3.60 and $CN_{Pd\text{-}Pt}$ = 2.13 for Pt-Pd/SiO_2 (Table 3), the molar ratio of Pd:Pt = N_{Pd}:N_{Pt} = 1.69 in the bimetallic Pt-Pd nanoclusters are determined according to Equation (4). However, the overall molar ratio of Pd:Pt is 3, so the difference to the calculated value of 1.69 suggests that besides the bimetallic Pt-Pd nanoclusters,

a fraction of monometallic Pd nanoparticles has to be also present in the Pt-Pd/SiO_2 catalyst. A schematic model of a Pt-Pd particle with a size of 1.4 nm and Pd:Pt ratio of 1.69 is shown in Figure 9. According to the results of the EXAFS analysis Pd is concluded to segregate to the surface and Pt atoms form the core. The coordination numbers of the model in Fig. 9 match the values of the EXAFS fitting in Table 3 except for $CN_{Pd\text{-}Pd}$. The Pd:Pt ratios for the other Pt-Pd/ASA catalysts were calculated in the same way and are also summarized in Table 3. In all cases, the Pd:Pt ratios were smaller than 3, indicating that monometallic Pd particles have to be additionally present in all bimetallic Pt-Pd catalysts.

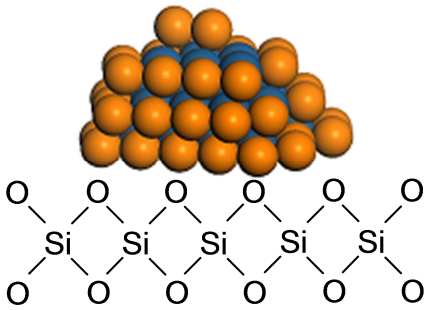

Figure 9. Model of a Pt-Pd cluster (1.4 nm) with a Pd (orange spheres) to Pt (blue spheres) ratio of 1.69.

The adsorption of CO followed by IR spectroscopy confirmed that the Pt-Pd clusters supported on ASA(55/45) have the highest fraction of Pt at the surface. The high intensity of the band of linearly bound CO allows concluding that all catalysts have a fraction of accessible Pt. Let us now analyze this in more quantitative terms. The total number of surface Pd or Pt atoms can be expressed by Equations (5) and (6). $(CO)_{Pd\text{-}B}$ and $(CO)_{Pd\text{-}L}$ are the concentrations of CO adsorbed on Pd in the bridging (each CO molecules binds to 2 metal atoms) and linear mode, respectively. $(CO)_{Pt\text{-}B}$ and $(CO)_{Pt\text{-}L}$ represent the CO adsorbed on Pt in the bridging and linear mode, respectively.

$$\mathrm{Pd} = 2(\mathrm{CO})_{\mathrm{Pd-B}} + (\mathrm{CO})_{\mathrm{Pd-L}} \quad (5)$$

$$\mathrm{Pt} = 2(\mathrm{CO})_{\mathrm{Pt\text{-}B}} + (\mathrm{CO})_{\mathrm{Pt\text{-}L}}\ ;\ \mathrm{Pd} = 2(\mathrm{CO})_{\mathrm{Pt\text{-}B}} + (\mathrm{CO})_{\mathrm{Pt\text{-}L}} \quad (6)$$

Given that the concentration of adsorbed CO can be calculated as A_i/k_i, being A_i and k_i the absorbance and molar extinction coefficient for a given CO species, respectively, Equations (5) and (6) become:

$$\mathrm{Pd} = \frac{2A_{\mathrm{Pd\text{-}B}}}{k_{\mathrm{Pd\text{-}B}}} + \frac{A_{\mathrm{Pd\text{-}L}}}{k_{\mathrm{Pd\text{-}L}}} \qquad (7)$$

$$\mathrm{Pt} = \frac{2A_{\mathrm{Pt\text{-}B}}}{k_{\mathrm{Pt\text{-}B}}} + \frac{A_{\mathrm{Pt\text{-}L}}}{k_{\mathrm{Pt\text{-}L}}} \qquad (8)$$

Defining the relation of the molar extinction coefficients on Pt and Pd as $k_{i\text{-}L}/k_{i\text{-}B}=K_i$, equations (9) and (10) are obtained.

$$\mathrm{Pd} = \frac{2A_{\mathrm{Pd\text{-}B}}K_{\mathrm{Pd}}}{k_{\mathrm{Pd\text{-}L}}} + \frac{A_{\mathrm{Pd\text{-}L}}}{k_{\mathrm{Pd\text{-}L}}} \qquad (9)$$

$$\mathrm{Pt} = \frac{2A_{\mathrm{Pt\text{-}B}}K_{\mathrm{Pt}}}{k_{\mathrm{Pt\text{-}L}}} + \frac{A_{\mathrm{Pt\text{-}L}}}{k_{\mathrm{Pt\text{-}L}}} \qquad (10)$$

Combining then Equations (5) and (6) to express the surface Pd/Pt ratio Equation (11) is obtained.

$$\frac{\mathrm{Pd}}{\mathrm{Pt}} = \frac{k_{\mathrm{Pt\text{-}L}}}{k_{\mathrm{Pd\text{-}L}}} \frac{2K_{\mathrm{Pd}}A_{\mathrm{Pd\text{-}B}}+A_{\mathrm{Pd\text{-}L}}}{2K_{\mathrm{Pt}}A_{\mathrm{Pt\text{-}B}}+A_{\mathrm{Pt\text{-}L}}} \qquad (11)$$

Equation (11) is a very general relation and can be simplified assuming that the value of K_i is (in agreement with [10]) around 2.5. Furthermore, the concentration of CO adsorbed on Pt in the bridging mode is negligible compared to the other adsorbed species. Hence, Equation (11) is reduced to Equation (12).

$$\frac{\mathrm{Pd}}{\mathrm{Pt}} = \frac{k_{\mathrm{Pt\text{-}L}}}{k_{\mathrm{Pd\text{-}L}}} \frac{5A_{\mathrm{Pd\text{-}B}}+A_{\mathrm{Pd\text{-}L}}}{A_{\mathrm{Pt\text{-}L}}} \qquad (12)$$

It is reasonable to assume that the absorbance of CO linearly adsorbed on Pt ($A_{Pt\text{-}L}$) corresponds to the integrated peak area determined in the range 2060-2110 cm^{-1} after evacuation. The absorbance of CO adsorbed in the bridge mode on Pd ($A_{Pt\text{-}B}$) corresponds to the area of the bands in the 1840-1990 cm^{-1} range. Finally, the absorbance of linearly adsorbed CO on Pd ($A_{Pd\text{-}L}$) is the difference of the peak areas in the 2060-2110 cm^{-1} range before and after evacuation. There are some indications in literature that the values for $k_{Pt\text{-}L}$ and $k_{Pd\text{-}L}$ are similar [42,43], so we can assume that the ($k_{Pt\text{-}L}/k_{Pd\text{-}L}$) ratio is close to 1, which allows estimation of the surface Pd/Pt ratios for the bimetallic catalysts. The resulting Pd/Pt surface ratios are 4.9, 6.2, 6.1 and 5.9 for Pt-Pd/ASA(55/45), Pt-

Pd/ASA(20/80), Pt-Pd/ASA(5/95) and Pt-Pd/ASA(SiO_2), respectively. Hence the IR characterization by CO adsorption suggests that (i) more than 80 % of the metal at the surface is Pd, (ii) the fraction of surface Pt atoms is minor (about 15 %) but not negligible and (iii) the catalyst supported on ASA(55/45) has the lowest concentration of surface Pd atoms, which is in good agreement with the results of the EXAFS analysis.

4.3. Electronic effects of alloying

The XANES analysis at the Pt L_{III} edge showed a lower electron density on the metal nanoclusters compared with the bulk Pt foil. A more rigorous analysis of the XANES can be done by comparing the relative intensity of empty states at the Fermi level of the materials. This relative intensity of the peaks is determined by subtracting the intensity of the absorption edge from the corresponding near-edge X-ray absorption fine structure fitted with a sigmoidal function [44]. The densities of empty states are plotted in Figure 10 as a function of the composition of the support. The data corresponding to the Pt catalysts reported in ref. [45] are also shown. The intensities for the Pt-Pd nanoparticles are larger than those of the corresponding monometallic Pt catalysts implying an increase of the electron deficiency in the Pt d-band by alloying with Pd. Moreover, in contrast to the Pt nanoparticles on various ASA supports, the support composition does not influence the electronic state of Pt. This suggests that the electron deficiency of Pt is mainly caused by the withdrawal of electrons by Pd. Thus, any electronic effect caused by the support is compensated by the effects of alloying. The electron deficiency of Pt after alloying with Pd has been documented by several groups [2,46,47] and in ref. [47] even the formation of $Pt^{x\delta+}$-$xPd^{\delta-}$ ionic bonds has been proposed.

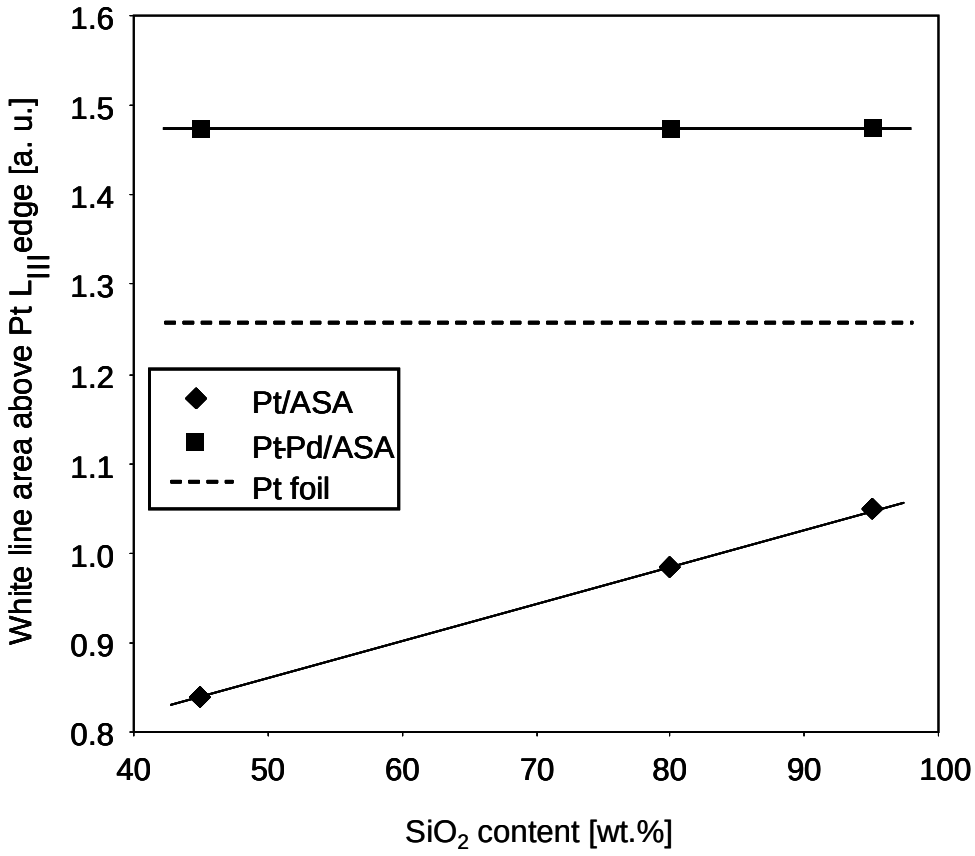

Figure 10. White line intensities above the Pt L_{III} edge as a function of the support silica content of the Pt/ASA and Pt-Pd/ASA catalysts.

The XANES at the Pd K edge were also measured (not shown here) and the corresponding white line intensities above the Pd K edge are shown in Fig. 11. In line with the proposed electron withdrawal from Pt to Pd, the white line intensities of the Pd K edge of the catalysts were smaller than that of Pd foil and as observed for the Pt L_{III} XANES. Also for Pd the composition of the supports did not affect the electronic states of Pd atoms.

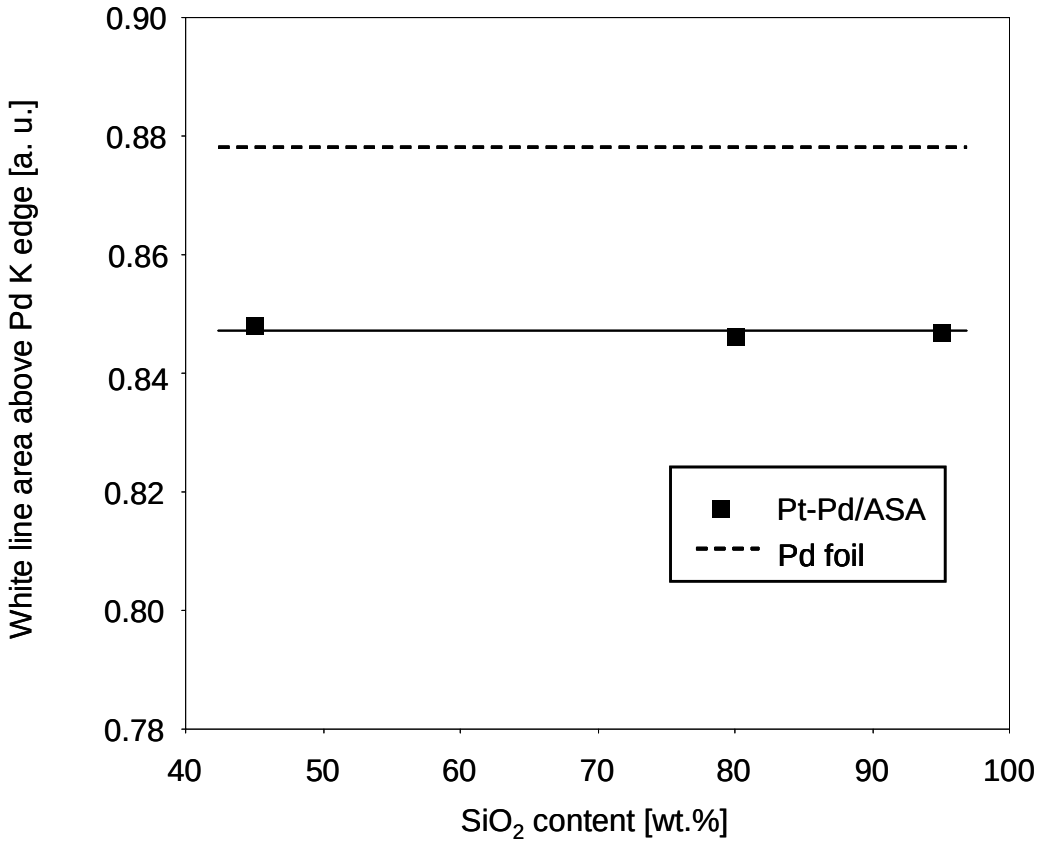

Figure 11. White line intensities above the Pd K edge as a function of the support silica content of the Pt-Pd/ASA catalysts.

4.4. On the synthesis of the Pt-Pd clusters and segregation of Pd to the surface

It is clear that the support composition determines the morphology of the Pt-Pd clusters. At the moment, the origin of this dependence is uncertain, but let us tentatively propose that the interactions between the precursor ions and the surface play a key role. On negatively charged surfaces, the adsorption of cations, $[Pt(NH_3)_4]^{2+}$ $[Pd(NH_3)_4]^{2+}$ in our case, is driven by electrostatic interactions [48]. On positively charged (protonated) surfaces, the cations are adsorbed by ion exchange [49]. At the impregnation conditions used in this study (pH=7.7), the silica surface is negative (PZC=2-3.5) [50]. Thus, the deposition of Pt and Pd cationic species on silica is driven by electrostatic interactions. The

picture is more complicated for the case of mixed oxides. The surface of ASA has three different domains, i.e., silica, alumina and aluminosilicate regions (Al_2O_3 and SiO_2 homogeneously mixed), the proportion of these domains depend on the alumina to silica ratio. As alumina is added aluminosilicate domains exist, whereas pure Al_2O_3 appears above a critical alumina concentration. These domains of the solid have very different point of zero charge (PZC), i.e., 2-3.5, 8-9 and intermediate values for SiO_2, Al_2O_3 and aluminosilicate, respectively [50, 51]. Thus, the surface charge of ASA is not homogenous during the impregnation of the metal precursor solution and it is likely that the both kinds of interactions, electrostatic and ion exchange compete. The alumina and probably also the aluminosilicate region are positively charged. Therefore, the contribution of the ion exchange mechanism has to increase with increasing alumina content in the support. Considering that the electrostatic interaction is weaker than the adsorption via ion exchange, we suggest that the mobility of metal-containing species decreases with the content of alumina. Following the same rationale, the interactions between carrier and supported species increase in strength with increasing alumina content. This agrees with the fact that alumina interacts stronger with supported species than silica.

The segregation of Pd to the surface of Pt-Pd clusters is thermodynamically favored because Pd has lower surface energy than Pt [52]. Accordingly, Monte Carlo simulations predict the formation of Pd-enriched topmost surfaces [14]. Reaching that equilibrated morphology, however, depends strongly on synthesis factors such as the thermal treatment (temperature and atmosphere) and particle size [17]. We propose that the metal-containing species supported on alumina or aluminosilicate regions are more stable (less mobile) than those supported on silica. Hence, during the thermal treatments following impregnation and drying the segregation of Pd is reduced.

Another factor that may hinder the segregation of Pd is the local enrichment of Pt in certain domains of the supports, as suggested by the EXAFS characterization. The analysis derived from the fitting procedure shows that the Pd:Pt ratio of the bimetallic particles decreases from 1.69 to 1.17 by increasing the alumina

content up to 55 wt.% in the support. In accordance with ref. [17] the relatively limited supply of Pd atoms in those Pt-rich regions suppresses the segregation. The regions with relatively high concentration of Pt atoms are assumed to form because of the preferential anchoring of PtO species onto pentacoordinated Al^{3+} aluminum sites as reported in ref. [53]. Considering that the concentration of those preferential anchoring sites has to be proportional to the alumina concentration and the Lewis acidity, it is highly possible that the ASA(55/45) material, with the highest concentration of alumina and the highest acidity has also the highest concentration of Pt-enriched regions.

Thus, overall the results of this work demonstrate that the interactions between the metal precursors and the support critically influence the structure of the Pt-Pd bimetallic particles.

5. Conclusions

For the present series of amorphous silica-alumina and silica supported bimetallic Pt-Pd catalysts the preparation of Pt-Pd catalysts did not affect the properties of the supports. The concentration of the support Lewis acid sites increased with the alumina concentration, whereas the concentration of Brønsted acid sites reached a maximum at 20 wt.% of alumina. The synthesis procedure led to metal particles with average diameters between 1.4 and 1.8 nm and a relatively broad size distribution. By means of CO adsorption, IR spectroscopy and EXAFS, the surface composition of the materials was identified to be Pd enriched. Fitting the EXAFS spectra strongly suggests that bimetallic particles with a Pt rich core and a Pd rich shell, coexist with monometallic Pd particles in the catalysts. The composition of the support influences the Pd/Pt ratio in the bimetallic clusters by increasing the proportion of surface Pt with increasing concentration of alumina. Hence, the Pt-Pd catalyst supported on ASA containing 55 wt.% of alumina showed the highest proportion of Pt on the surface. The formation of joint Pt-Pd particles led to electron transfer from Pd to Pt as indicated by XANES.

6. Acknowledgements

The authors would like to thank Prof. Breitkopf, TU Dresden for the helpful discussions. The staff of the beamline X1 at Hasylab DESY, Hamburg, Germany is thankfully acknowledged for their support during the XAS experiments.

7. References

[1] V. Ponec, G.C. Bond, Catalysis by Metals and Alloys, Stud. Surf. Sci. Catal. Vol. 95, Elsevier, Amsterdam, 1995, p. 734.

[2] J.K. Lee, H.K. Rhee, J. Catal. 177 (1998) 208.

[3] T. Matsui, M. Harada, K.K. Bando, M. Toba, Y. Yoshimura, J. Jpn. Petrol. Inst. 47 (2004) 222.

[4] B. Pawelec, R. Mariscal, R.M. Navarro, S. Van Bokhorst, S. Rojas, J.L.G. Fierro, Appl. Catal. A: Gen. 225 (2002) 223.

[5] G. Jacobs, F. Ghadiali, A. Pisanu, A. Borgna, W.E. Alvarez, D.E. Resasco, Appl. Catal. A: Gen. 188 (1999) 79.

[6] L.M. Sikhwivhilu, N.J. Coville, D. Naresh, K.V.R. Chary, V. Vishwanathan, Appl. Catal. A: Gen. 324 (2007) 52.

[7] L. Piccolo, C.R. Henry, J. Mol. Catal. A: Chem. 167 (2001) 181.

[8] A. Morlang, U. Neuhausen, K.V. Klementiev, F.W. Schütze, G. Miehe, H. Fuess, E.S. Lox, Appl.Catal. B: Environ. 60 (2005) 191.

[9] T. Rades, C. Pak, M. Polisset-Thfoin, R. Ryoo, J. Fraissard, Catal. Lett. 29 (1994) 91.

[10] C.M. Grill, M.L. McLaughlin, J.M. Stevenson, R.D. Gonzalez, J. Catal. 69 (1981) 454.

[11] T. Fujikawa, K. Tsuji, H. Mizuguchi, H. Godo, K. Idei, K. Usui, Catal. Lett. 63 (1999) 27.

[12] P.L. Hansen, A.M. Molenbroek, A.V. Ruban, J. Phys. Chem. B 101 (1997) 1861.

[13] F. Bernardi, M.C.M. Alves, A. Traverse, D.O. Silva, C.W. Scheeren, J. Dupont, J. Morais, J. Phys. Chem. C 113 (2009) 3909.

[14] H. Deng, W. Hu, X. Shu, L. Zhao, B. Zhang, Surf. Sci. 517 (2002) 177.

[15] J. L. Rousset, A. J. Renouprez, A. M. Cadrot, Phys. Rev.B 58 (1998) 2150.
[16] D. Cheng, S. Huang, W. Wang, Chem. Phys. 330 (2006) 423.
[17] L.C.A. van den Oetelaar, O.W. Nooij, S. Oerlemans, A.W. Denier van der Gon, H.H. Brongersma, L. Lefferts, A.G. Roosenbrand, J. A. R. van Veen, J. Phys. Chem. B 102 (1998) 3445.
[18] O.K. Ezekoye, A.R. Drews, H.-W. Jen, R.J. Kudla, R.W. McCabe, M. Sharma, J.Y. Howe, L.F. Allard, G.W. Graham, X.Q. Pan, J. Catal. 280 (2011) 125.
[19] Y. Yu, B. Fonfé, A. Jentys, G.L. Haller, C. Breitkopf, J.A.R van Veen, O.Y. Gutiérrez, J.A. Lercher, Part II, J. Catal., submitted for publication (2011).
[20] M.F. Williams, B. Fonfé, C. Sievers, A. Abraham, J.A. van Bokhoven, A. Jentys, J.A.R. van Veen, J.A. Lercher, J. Catal. 251 (2007) 485.
[21] K.V. Klementiev, *VIPER and XANDA for Windows, freeware*
[22] A.L. Ankudinov, B. Ravel, J.J. Rehr, S.D. Conradson, Phys. Rev. B 58 (1998) 7565.
[23] A.L. Ankudinov, J.J. Rehr, Phys. Rev. B 62 (2000) 2437.
[24] M.H. Lee, C.F. Cheng, V. Heine, J. Klinowski, Chem. Phys. Lett. 265 (1997) 673.
[25] S.M.C. Menezes, V.L. Camorim, Y.L. Lam, R.A.S. San Gil, A. Bailly, J.P. Amoureux, Appl. Catal. A: Gen. 207 (2001) 367.
[26] M.P.J. Peeters, A.P.M. Kentgens, Solid State Nucl. Magn. Reson. 9 (1997) 203.
[27] G. Crepeau, V. Montouillout, A. Vimont, L. Mariey, T. Cseri, F. Mauge, J. Phys. Chem. B 110 (2006) 15172.
[28] B.M. De Witte, P.J. Grobet, J.B. Uytterhoeven, J. Phys. Chem. 99 (1995) 6961.
[29] J.P. Gilson, G.C. Edwards, A.W. Peters, K. Rajagopalan, R.F. Wormsbecher, T.G. Roberie, M.P. Shatlock, J. Chem. Soc. Chem. Commun. 2 (1987) 91.
[30] G.J. Ray, A. Samoson, Zeolites 13 (1993) 410.
[31] H. Koller, E.L. Meijer, R.A. van Santen, Solid State Nucl. Magn. Reson. 9 (1997) 165.

[32] D. Freude, T. Fröhlich, H. Pfeifer, G. Scheler, Zeolites 3 (1983) 171.

[33] Y. Lei, J. Jelic, L.C. Nitsche, R. Meyer, J. Miller, Top Catal. 54 (2011) 334.

[34] J.M. Dominguez, M.J. Yacamán, J. Catal. 64 (1980) 223.

[35] S.N. Khanna, F. Cyrot-Lackmann, Y. Boudeville, J. Rousseau-Voilet, Surf. Sci. 106 (1981) 287.

[36] S.N. Khanna, J.P. Bucher, J. Buttet, Surf. Sci. 127 (1983) 165.

[37] T. Tanaka, T. Shishido, H. Hattori, K. Ebitani, S. Yoshida, Physica B 208 (1995) 645.

[38] M. Primet, L.C. De Menorval, J. Fraissard, T. Ito. J. Chem. Soc. Faraday Trans. 81 (1985) 2867.

[39] T. Rades, V.Y. Borovkov, V.B. Kazansky, M. Polisset-Thfoin, J. Fraissard, J. Phys. Chem. 100 (1996) 16238.

[40] W.M.H. Sachtler, Catal. Rev. Sci. Eng. 14 (1976) 193.

[41] G.H. Via, K.F. Drake, G. Meitzner, F.W. Lytle, J.H. Sinfelt, Catal. Lett. 5 (1990) 25.

[42] M.A. Vannice, S.Y. Wang, J. Phys. Chem. 85 (1981) 2543.

[43] A.G.T.M. Bastein, F.J.C.M. Toolenaar, V. Ponec, J. Catal. 90 (1984) 88.

[44] A. Jentys, M. Englisch, G.L. Haller, J.A. Lercher, Catal. Lett. 21 (1993) 303.

[45] M.F. Williams, B. Fonfé, C. Woltz, A. Jentys, J.A.R. van Veen, J.A. Lercher, J. Catal. 251 (2007) 497.

[46] Y. Yoshimura, M. Toba, T. Matsui, M. Harada, Y. Ichihashi, K.K. Bando, H. Yasuda, H. Ishihara, Y. Morita, T. Kameoka, Appl. Catal. A: Gen. 322 (2007) 152.

[47] N. Matsubayashi, H. Yasuda, M. Imamura, Y. Yoshimura, Catal. Today 45 (1998) 375.

[48] J.P. Brunelle, Pure Appl. Chem. 50 (1978) 1211.

[49] M. Schreier, J. Regalbuto, J. Ctal. 225 (2004) 190.

[50] J.A. Schwarz, C.T. Driscoll, A. K. Bhanot, J. Colloid Interface Sci. 97 (1984) 55.

[51] M. Kosmulski, J. Colloid Interface Sci. 337 (2009) 439.

[52] X.Z. Wu, R. Wang, S.F. Wang, Q.Y. Wei, J. Surf. Sci. 256 (2010) 6345.

[53] J.H. Kwak, J.Z. Hu, D.H. Mei, C.W. Yi, D.H. Kim, C.H.F. Peden, L.F. Allard, J. Szanyi, Science 325 (2009) 1670.

Chapter 3

Bimetallic Pt-Pd catalysts: Structure-activity correlations in the hydrogenation of tetralin

The catalytic hydrogenation of tetralin in the absence and presence of quinoline and dibenzothiophene was studied on bimetallic Pt-Pd catalysts supported on silica and amorphous silica-alumina (ASA). The proportion of Pt on the surface determined the activity given that the Pt-Pd catalyst with the highest proportion of surface Pt was the most active. In the absence of poisons the electronegativity of the support correlated with the hydrogenation. In the presence of quinoline the activity of the catalysts increased with the dispersion of the metal particles, whereas in the presence of dibenzothiophene, the acidity of the support determined the activity. The observed effects of the poisons indicated the presence of two kinds of adsorption sites, i.e., metal particles and Brønsted acid sites at the perimeter. The key contribution of acid sites for hydrogenation was confirmed by removing the Brønsted acid sites of the support. Reference Pt catalysts were more active than the Pt-Pd counterparts in poison-free feed. In the presence of poisons, the Pt catalysts were also more active than the bimetallic formulations with the remarkably exception of the bimetallic catalyst with the higher proportion of Pt on the surface. The bimetallic catalysts were more resistant to sulfur and nitrogen poisoning as well as to sintering. The poison resistance of bimetallic catalysts originates from the electron transference from Pt to Pd that yields weak adsorption of poisons on electron deficient Pt atoms.

1. Introduction

The growing need to convert heavier crude oils that are richer in heteroatoms than traditional crudes requires improved hydrotreating processes to meet the current and future fuel specifications. In this context, aromatic molecules have to be saturated to increase the quality of diesel fuels. However, the presence of sulfur and nitrogen containing compounds poisons the catalysts best suited for this task [1-3]. Therefore, multi-stage hydrotreating processes are typically applied for upgrading of diesel fuels [4,5]. In the first stage the concentration of nitrogen and sulfur containing species is lowered over transition metal sulfide catalysts, while in the second stage aromatic compounds are hydrogenated on noble metal based catalysts. However, the activity of the noble metal catalysts is drastically reduced by the presence of residual S- and N-containing compounds.
Two strategies are followed to improve the sulfur and nitrogen tolerance of the catalyst, i.e., using (i) acidic materials as supports [4,6-8] and (ii) noble metal alloys as active catalyst component [5,6,9,10]. The use of acidic carriers enhances the hydrogenation activity of the Pt or Pd catalysts in addition to improving the sulfur resistance [11-13]. The strong acidity of zeolite supports leads, however, to excessive cracking and to rapid deactivation by coke formation [14,15]. Amorphous silica-alumina (ASA) is, in contrast, a more promising support, because it possesses intermediate acidity, which can be tuned further by varying the silica-alumina ratio [16,17]. Thus, ASA-supported Pt catalysts have been systematically studied with the focus on the hydrogenation of tetralin using dibenzothiophene (DBT) and quinoline as model substances for S- and N-containing poisons [18-20]. Two types of active sites, i.e., metal sites alone and metal sites in combination with Brønsted acid sites at the perimeter of the metal clusters, were identified to be active for the hydrogenation of tetralin on Pt/ASA catalysts. Sulfur species, resulting from the hydrogenolysis of dibenzothiophene, selectively poison the metal sites blocking so the main hydrogenation pathway occurring on metal particles. However, the hydrogenation of tetralin persists with a lower rate on an active site consisting of acid sites and metal atoms at the perimeter of the metal particles. In this reaction route the

hydrocarbon molecules adsorb on the acid sites and react with hydrogen dissociated on the (partially) sulfur covered metal surface. Quinoline neutralizes the acid sites, largely reducing the positive effect of the Brønsted acid sites. Thus, using acid supports to enhance the performance of Pt catalysts requires materials with relatively weak acid sites, which allow competition between the reacting substrates and sulfur and nitrogen components.

The strategy of alloying showed for instance, that Pt-Pd catalysts supported on ASA (Si/Al=20) are more effective with regard to increasing the cetane number of real diesel feedstock compared to an industrial reference catalyst [21]. Positive effects of other bimetallic catalysts for hydrogenation reactions in the presence of sulfur were observed for a variety of oxide supports [22-25]. The improved tolerance of bimetallic Pt-Pd catalysts has been attributed to pronounced metal-metal and metal-support interactions. The electronic effects were claimed to originate from the formation of electron deficient Pt species in the bimetallic Pt-Pd particles [17]. Alternatively, it has been suggested that Pd contributes to the hydrogenation activity, while Pt catalyzes hydrogenolysis [24].

The general agreement is that the sulfur tolerance of bimetallic catalysts is influenced by the composition and structure of the Pd-Pt clusters as well as by the interaction of the bimetallic particles with the supports. However, the impact of sulfur and nitrogen compounds on the hydrogenation activity on the metal and the acid sites of Pt-Pd catalysts is not understood on a molecular level.

In the first part of this study, a series of Pt-Pd catalysts supported on ASA with varying silica to alumina ratios were synthesized and characterized in detail with respect to the bulk and surface characteristics of the metal clusters, i.e., metal distribution and electronic effects of alloying. The aim of this second part is to show how the hydrogenation of tetralin in the absence and the presence of S- and N-containing poisons, i.e., DBT and quinolone, is influenced by the varying acid site and metal surface concentrations. Combining the structural information about the catalysts obtained in part one with the kinetic results presented here allowed us to describe the roles of the metal and acid functionality as well as the effect of alloying.

2. Experimental

2.1. Catalyst Preparation

A series of Pt-Pd based catalysts (with a molar ratio of Pd:Pt = 3) supported on ASA and SiO_2 was prepared by the incipient wetness impregnation method. The ASA materials are denoted as ASA(5/95), ASA(20/80) and ASA(55/45), the numbers in brackets indicate the ratio of alumina/silica in weight percentage. Additionally, a monometallic Pt catalyst (0.8 wt.% of Pt) was synthesized on ASA with alumina to silica mass ratio of 38/62 to study the role of the Brønsted acidity. A portion of this catalyst was exchanged with Cs^+ to fully eliminate its Brønsted acidity. The detailed preparation procedure of ASA materials and of the bimetallic Pt-Pd catalysts are described elsewhere [18,26].

2.2. Catalytic measurements

The hydrogenation of tetralin was carried out in a set of 4 parallel trickle-bed reactors in continuous down-flow mode (Fig. 1). The catalyst samples (particle size 250-500 µm) were diluted with SiC (particle size < 250 µm) before loading into the glass-coated reactors to ensure an isothermal environment during the reaction. The catalysts were reduced in situ at 623 K in hydrogen for 2h before the reaction. The activity of the catalysts was studied at 533-593 K and 50 bar of hydrogen pressure. As the conversion of tetralin decreased in the presence of poisons, different weight hourly space velocities (WHSV) were used to maintain tetralin conversion levels in a comparable range, i.e., 539 h^{-1} for the clean feed, 271 h^{-1} for N-poisoned feed, 77 h^{-1} for S-poisoned feed and 32 h^{-1} for N- and S-poisoned feed. The WHSV was defined as the weight of feed per hour and per unit weight of catalyst. The change of the WHSV was achieved by varying the amount of catalyst and/or the flow rate keeping a constant molar ratio between H_2 and tetralin of 20. The poison-free feed consisted of 20 wt.% tetralin, 11.5 wt.% tetradecane as GC standard and 68.5 wt.% hexadecane as solvent. For the catalytic experiments applying quinoline and DBT in separate 400 ppm N and 100 ppm S were used, whereas in the experiments with simultaneous quinoline

and DBT addition, 20 ppm N and 100 ppm S were used. The activity of the catalysts is reported as mol of tetralin converted per hour per gram of catalyst ($mol_{tetralin} \cdot h^{-1} \cdot g_{Cat.}^{-1}$). Continuous deactivation was observed in all reactions in the first 20 h time on stream (TOS). Thus, all catalytic activities reported in this paper were measured at steady state after 24 h TOS.

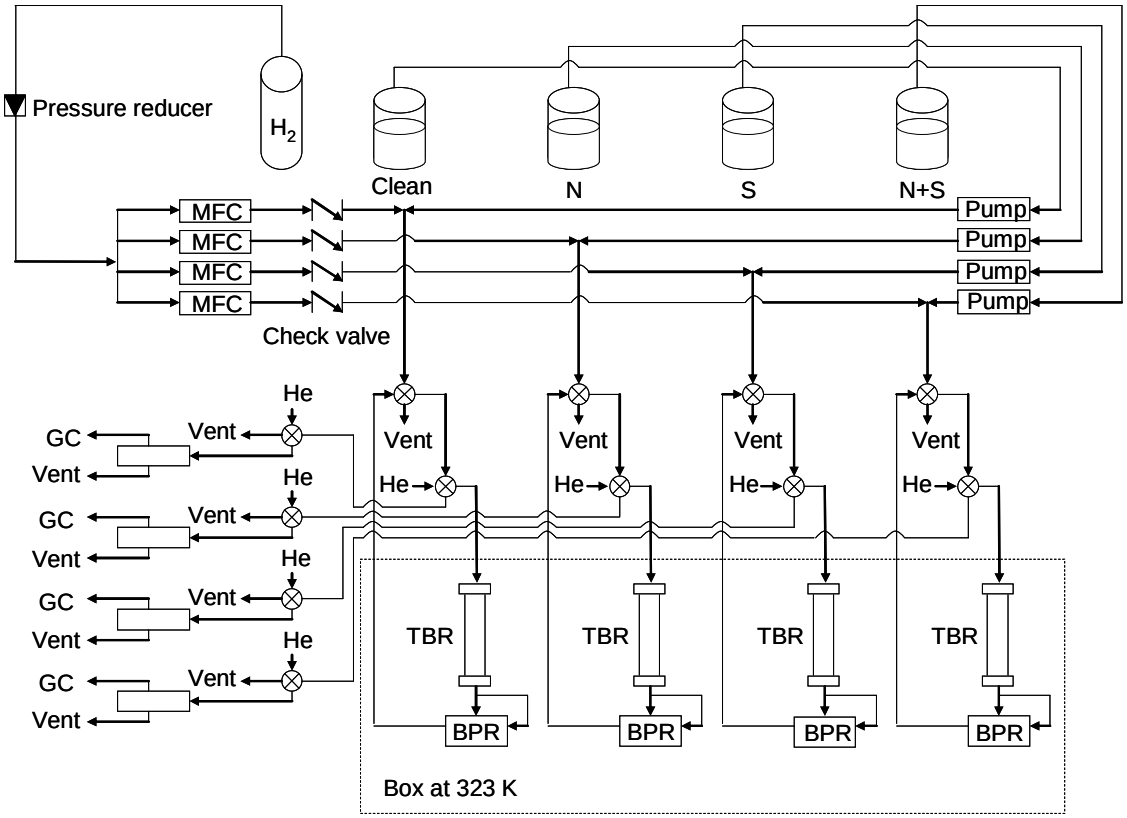

Figure 1. Schematic representation of the hydrogenation set-up; MFC=Mass flow controller; TBR = trickle bed reactor; BPR = back pressure regulator.

In order to verify the alloying effect on the sulfur resistance, the hydrogenation of tetralin was carried out on Pt/ASA(20/80) and Pt-Pd/ASA(20/80) in the presence of 100 and 500 ppm S. The reactions were carried out in the range of 533 to 593 K with a hydrogen pressure of 50 bar and a WHSV of 77.3 h-1.

The hydrogenation of toluene and isomerization of n-heptane were carried out on Pt/ASA(38/62) and Cs-Pt/ASA(38/62) to investigate the impact of the Cs^+-exchange on the metal and acid functions of the catalysts. For the former reaction, samples of 50 mg of the catalysts were loaded in the reactor and the hydrogenation pressure was kept at 1 bar. The reaction temperature was varied to obtain 40% conversion of toluene on the two catalysts. The isomerization of *n*-heptane to *iso*-heptane was carried out at 30 bar H_2, whereas the temperature was varied to obtain 40% *n*-heptane conversion.

In order to study the role of acid sites, the monometallic Pt/ASA(38/62) and Cs-Pt/ASA(38/62) catalysts were also tested in the hydrogenation of tetralin in the absence and the presence of quinoline and DBT at the same conditions used with the bimetallic catalysts.

2.3. Characterization of the catalysts after reaction by transmission electron microscopy

Transmission electron microscopy (TEM) was applied to investigate the metal particle size after reaction. The catalysts were washed in hexane, separated from the SiC by sieving and dried at 353 K. The samples were then ground and ultrasonically dispersed in ethanol. Drops of the dispersions were applied on copper grids with carbon film. A JEM-2010 Jeol transmission electron microscope operating at 120 kV was used.

3. Results

3.1. Characterization of the catalysts

The synthesis and characterization of the Pt-Pd/ASA catalysts here studied was described in detail in the first part of the work [26]. In order to complement the discussion, the activity of the Pt-Pd/ASA catalysts was compared to that of the Pt/ASA counterparts. The characterization of the series of Pt/ASA catalysts was reported in [20]. For a description of the effect of the Al_2O_3 and SiO_2 composition on the properties of the ASA material see Ref. [18].

3.2. Hydrogenation of tetralin on Pt-Pd catalysts in the absence of poisons

The catalytic hydrogenation of tetralin was studied between 533 and 593 K. The catalytic activities at steady state after 24 h TOS for different temperatures are compiled in Fig. 2a. The Pt-Pd/ASA(55/45) catalyst had the highest activity at all temperatures followed by Pt-Pd/ASA(5/95), Pt-Pd/ASA(20/80) and Pt-Pd/SiO_2. Accordingly, the apparent activation energies determined in the hydrogenation of tetralin in the absence of poisons were 54, 48, 46, and 36 kJ mol^{-1} for the catalysts supported on SiO_2, ASA(5/95), ASA(20/80), and ASA(55/45), respectively. The conversion of tetralin to decalin proceeded with high selectivity, side products from ring-opening or cracking reactions were not observed. The ratios of *cis- to trans*-decalin observed with the bimetallic catalysts were below 0.4 (see Fig. 2b), which is significantly lower compared to the monometallic Pt catalysts (higher than 1.0) and indicates a weaker adsorption of tetralin on the bimetallic particles.

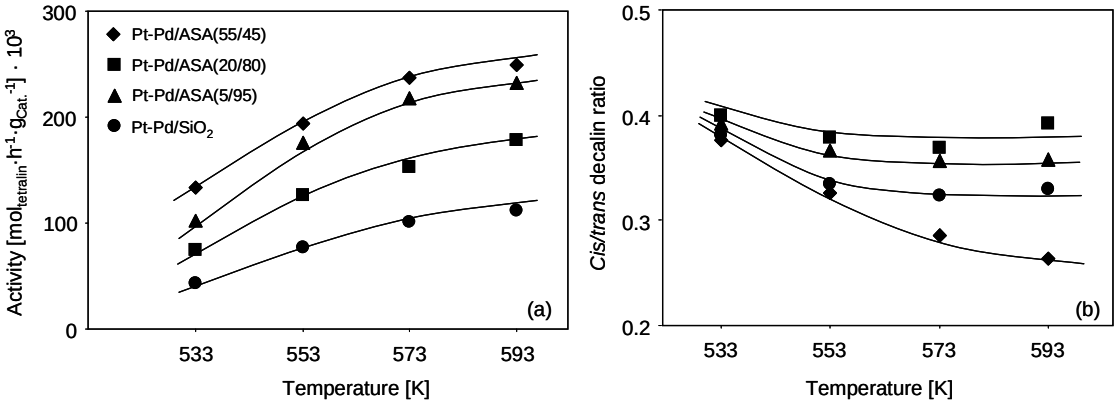

Figure 2. Activities of Pt-Pd catalysts (a) and c*is-/trans*-decalin ratios (b) observed at steady state for the hydrogenation of tetralin in the temperature range 533-593 K.

3.3. Hydrogenation of tetralin on Pt-Pd catalysts in the presence of quinoline

The rates of tetralin hydrogenation and the c*is-/trans*-decalin ratios in the presence of quinoline at steady-state are shown in Fig. 3. The Pt-Pd catalysts showed a significantly lower activity compared to the reactions conducted in the absence of quinoline. Pt-Pd/ASA(55/45) had the highest activity at all temperatures followed by the Pt-Pd/SiO_2, Pt-Pd/ASA(5/95) and Pt-Pd/ASA(20/80) catalysts. The apparent activation energies determined in the hydrogenation of tetralin in the presence of quinoline were 94, 84, 74, and 65 kJ mol^{-1} for the catalysts supported on SiO_2, ASA(5/95), ASA(20/80), and ASA(55/45), respectively. The *cis-/trans*-decalin ratios decreased with all catalysts with increasing temperature.

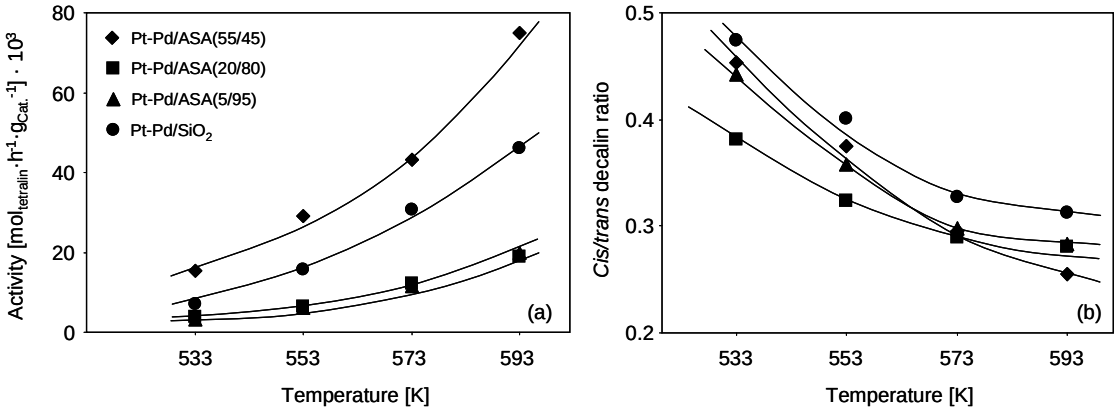

Figure 3. Activities of Pt-Pd catalysts (a) and c*is-/trans*-decalin ratios (b) observed at steady state for the hydrogenation of tetralin in presence of quinoline (400 ppm N) in the temperature range 533-593 K.

3.4. Hydrogenation of tetralin on Pt-Pd catalysts in the presence of DBT

The activities for the tetralin hydrogenation and the c*is-/trans*-decalin ratios in presence of DBT at steady-state are summarized in Fig. 4. In these conditions, the catalytic activities were drastically lower than in the absence of DBT. Pt-Pd/ASA(55/45) showed the highest activity. The apparent activation energies determined in the hydrogenation of tetralin in the presence of DBT were 70, 81,

86, and 89 kJ mol^{-1} for the catalysts supported on SiO_2, ASA(5/95), ASA(20/80), and ASA(55/45), respectively. The presence of sulfur induced a stronger dependence of the hydrogenation reaction rates on the temperature compared to the reactions performed in the presence of quinoline or in the absence of poisons, leading to a remarkable increase in the reaction rate between 573 and 593 K is (see Fig. 4a). The *cis*-/*trans*-decalin ratio (see Fig. 4b) decreased with temperature as in the case of the reactions performed in the presence of quinoline and were significantly lower compared with those obtained on monometallic Pt samples [20].

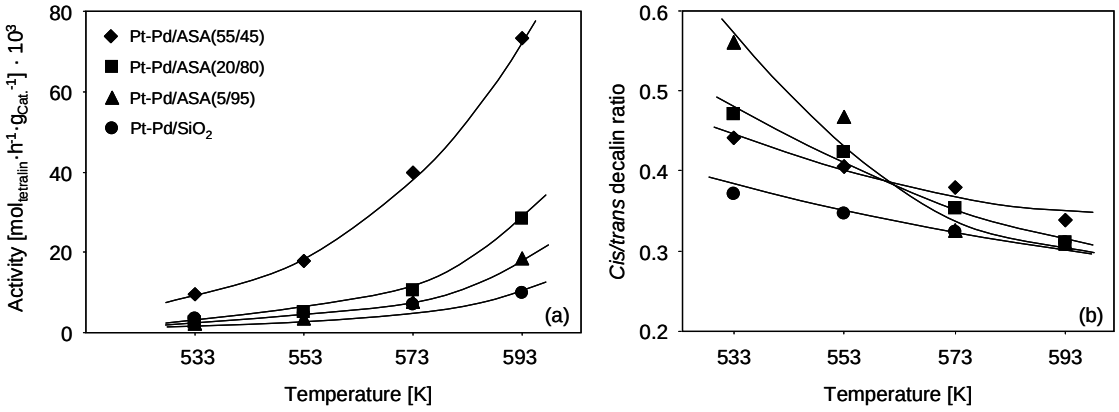

Figure 4. Activities of Pt-Pd catalysts (a) and c*is-/trans*-decalin ratios (b) observed at steady state for the hydrogenation of tetralin in presence of DBT (100 ppm S) in the temperature range 533-593 K.

3.5. Hydrogenation of tetralin on Pt-Pd catalysts in the presence of quinoline and DBT

The reaction rates of tetralin hydrogenation and c*is-/trans*-decalin ratios in the presence of N- and S-poisons are shown in Fig. 5. The catalytic activity drastically decreased compared to the reactions with poison-free, quinoline-, or DBT-containing feeds. The apparent activation energies determined in the hydrogenation of tetralin in the presence of DBT and quinoline were 75, 83, 81, and 83 kJ mol^{-1} for the catalysts supported on SiO_2, ASA(5/95), ASA(20/80), and

ASA(55/45), respectively. The observed *cis-/trans*-decalin ratios were generally below 0.4 and decreased with temperature with all catalysts.

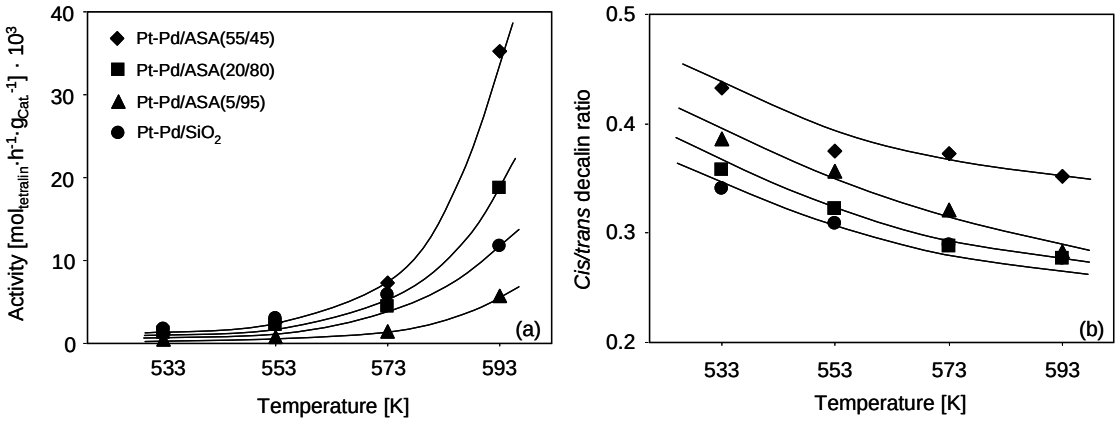

Figure 5. Activities of Pt-Pd catalysts (a) and c*is-/trans*-decalin ratios (b) observed at steady state for the hydrogenation of tetralin in presence of quinoline (20 ppm N) and DBT (100 ppm S) in the temperature range 533-593 K.

3.6. Impact of alloying with Pd on the resistance towards S-poisoning and metal particle sintering

The hydrogenation of tetralin in the presence of 100 and 500 ppm S on the monometallic Pt/ASA(20/80) and bimetallic Pt-Pd/ASA(20/80) catalyst was compared to evaluate the relative sulfur resistance of Pt and Pt-Pd catalysts. Figure 6 shows that the monometallic Pt catalyst has a higher hydrogenation activity than the bimetallic Pt-Pd/ASA(20/80) catalyst regardless of the sulfur concentration in the feed. However, it is remarkable that the increase of sulfur concentration influenced the activity of the bimetallic sample only slightly, while it led to a strong activity reduction for the Pt catalyst.

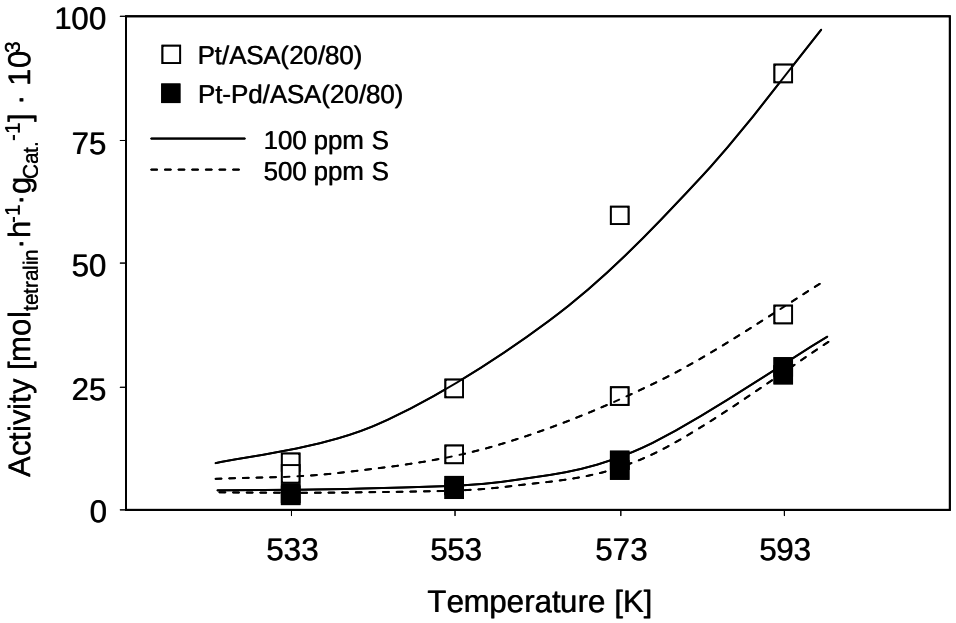

Figure 6. Comparison of different DBT poisoning levels on Pt/ASA(20/80) and Pt-Pd/ASA(20/80) catalyst for tetralin hydrogenation.

Samples of fresh and used Pt-Pd/ASA(5/95) were analyzed by transmission electron microscopy to explore sintering of metal particles during the reaction. Representative images of the catalyst used for the hydrogenation of the poison free, quinoline-, DBT- as well as the quinoline and DBT-containing feed are compiled in Figure 7. The average particle size for all used catalysts was 1.6 nm, which is the same average size determined for the as-synthesized catalyst. Note that the high stability of the bimetallic catalyst contrasts the lower stability of monometallic Pt catalysts, where the particle size increased from 0.8 to 1.3-1.6 nm during the reaction [20]. This is in line with the high stability found for bimetallic Pd-Pt particles supported on Y zeolites [27]. Consequently, we can conclude that the catalyst deactivation does not originate from sintering of the metal particles, as proposed elsewhere [28,29].

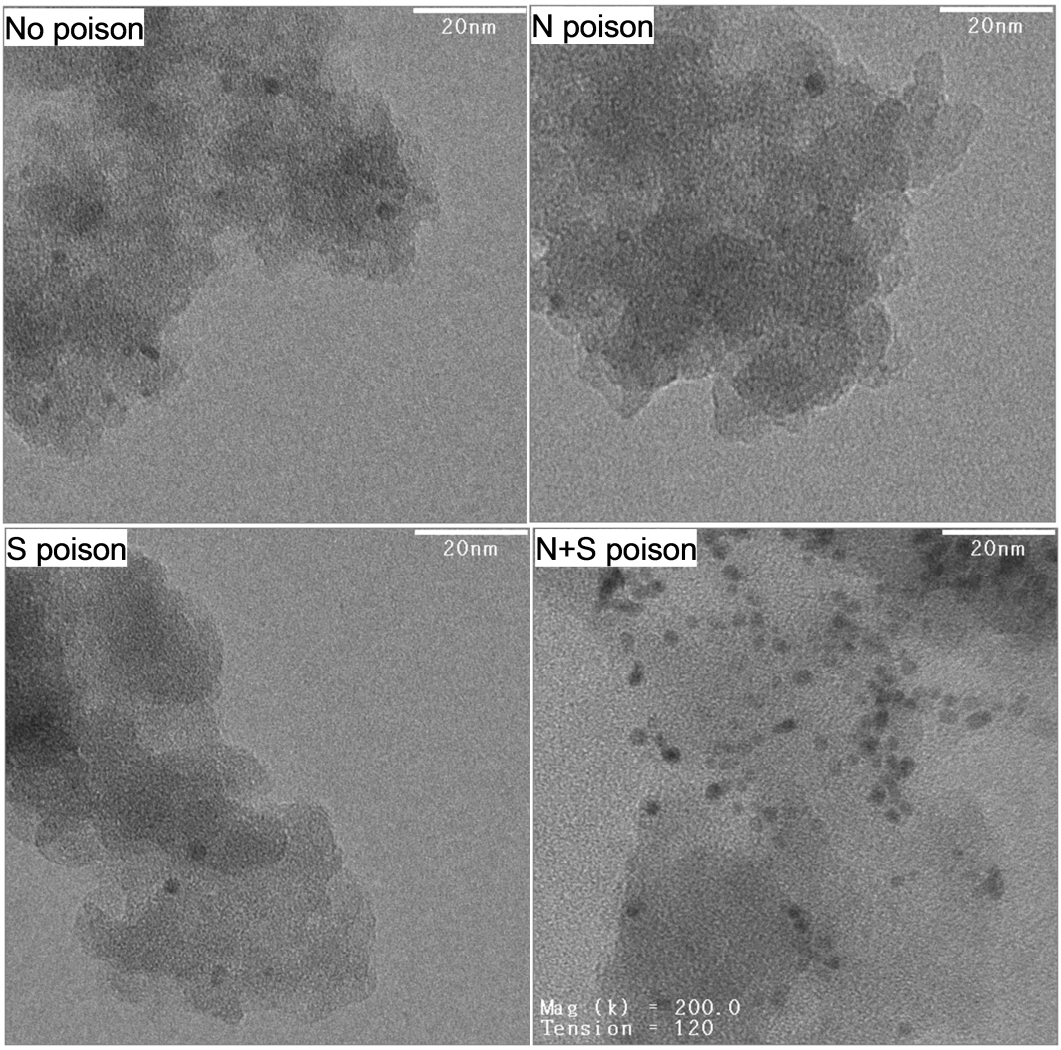

Figure 7. TEM micrographs of Pt-Pd/ASA(5/95) before and after the hydrogenation of tetralin in the absence and presence of quinoline and/or DBT.

3.7. Role of Brønsted acid sites

The role of Brønsted acid sites in the hydrogenation of aromatic compounds was studied by comparing the activity of monometallic Pt/ASA(38/62) and Cs-Pt/ASA(38/62) catalysts. In order to verify that the Pt particles were not affected by the ion exchange with Cs^+ the hydrogenation of toluene, a metal catalyzed reaction and *n*-heptane isomerization, which takes place on acid sites and on the metal were carried out on Pt/ASA(38/62) and on Cs-Pt/ASA(38/62). For the hydrogenation of toluene the temperature required for reaching 40% conversion

was almost the same, i.e., 337 K on Pt/ASA(38/62) and 332 K on Cs-Pt/ASA(38/62). In contrast, the temperature required to reach 40% conversion in the isomerization of *n*-heptane had to be increased from 626 K on Pt/ASA(38/62) to 692 K on Cs-Pt/ASA(38/62). Therefore, it can be concluded that the Pt particles were not affected by the ion exchange with Cs^+, while the acid sites were effectively removed and the activity remaining can be solely related to Pt.

The activity of Cs-Pt/ASA(38/62) and Pt/ASA(38/62) for hydrogenation of tetralin in the absence and presence of quinoline and/or DBT is shown in Fig. 8. In all cases, the activity of the Cs-modified catalyst was lower than that of the unmodified material and the difference became larger at higher temperatures. In the absence of poisons (Fig. 8a) the activity of Cs-Pt/ASA(38/62) was much lower than that observed for Pt/ASA(38/62). In the presence of quinoline (Fig. 8b) the activity decreased considerably compared to the poison-free feed, while the activity of the Cs-Pt/ASA(38/62) catalyst differed only slightly from the activity observed on Pt/ASA(38/62) at 533 and 553 K. In the presence of DBT (Fig. 8c) the activity of both catalysts decreased strongly and the differences in activity of both catalysts increased largely with temperature. In the presence of both poisons (Fig. 8d) the activity of the catalysts is negligible at 533 K and 553 K and at higher temperatures the activity of the Cs-exchanged catalyst remains much lower than that of Pt/ASA(38/62).

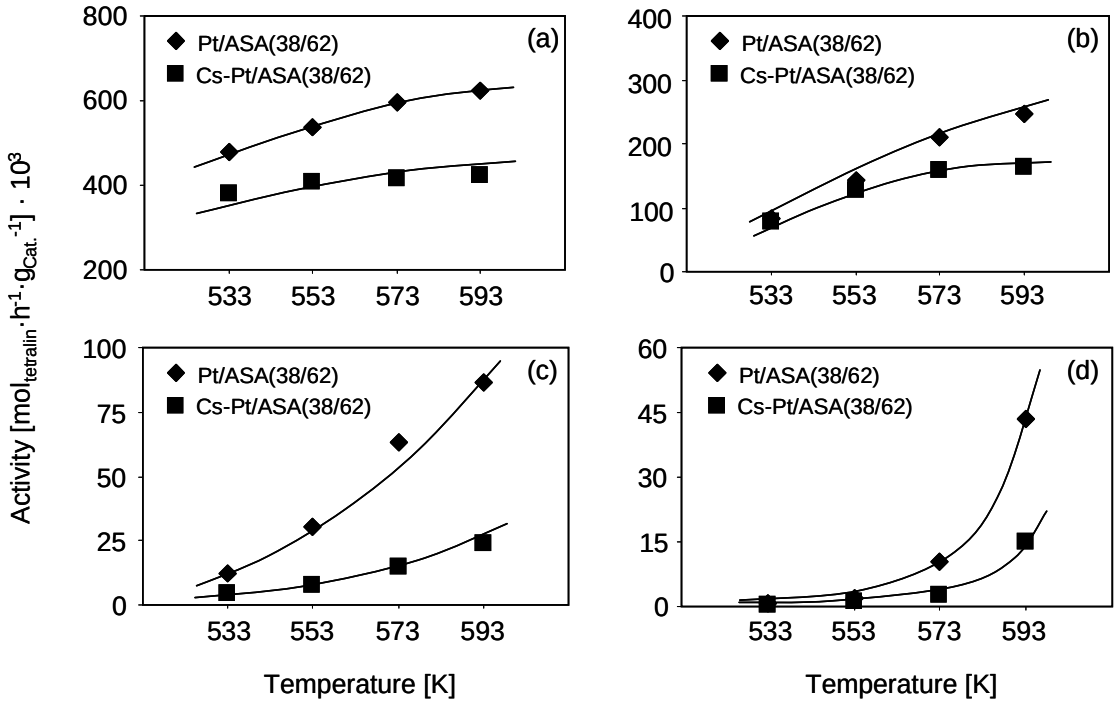

Figure 8. Comparison of the hydrogenation activities of Cs-Pt/ASA(38/62) and Pt/ASA(38/62) catalysts: (a) in absence of quinoline or DBT, (b) in presence of quinoline (20 ppm N), (c) in presence of DBT (100 ppm S) and (d) in presence of quinoline (20 ppm N)+ DBT (100 ppm S) in the temperature range 533-593 K.

4. Discussion

4.1. On the role of Brønsted acid sites in the hydrogenation of tetralin

Before commenting the results of the bimetallic Pt-Pd catalysts we would like to discuss the results obtained on Pt/ASA(38/62) and Cs-Pt/ASA(38/62) in order to emphasize the importance of Brønsted acid sites for the hydrogenation of tetralin. The differences observed in the catalytic behavior of both materials are attributed to the replacement of Brønsted acid sites by Cs^+ cations. This attribution assumes that the metal function was not affected by the Cs-exchange as concluded from the results of hydrogenation of toluene and isomerization of *n*-heptane.

In the absence of poisons, Cs-Pt/ASA(38/62) was less active than Pt/ASA(38/62) increasing the difference from 20 to 33% with increasing temperature in the range 533-593 K. The higher activity of Pt/ASA(38/62) is attributed to the participation of Brønsted acid sites in the reaction. The comparison of the rates shows that up to one third of the overall hydrogenation activity is related to molecules adsorbed on Brønsted sites at the perimeter of the Pt clusters.

In the presence of quinoline the activity of both catalysts decreases. However, the difference in activity between Pt/ASA(38/62) and Cs-Pt/ASA(38/62) is marginal at 533 and 553 K, i.e., only 5-10%. This nearly equal activity allows us to conclude that quinoline neutralizes the Brønsted acid sites in Pt/ASA(38/62), while it affects the metal particles in both catalysts through the same mechanism.

In contrast, in the presence of DBT, Pt/ASA(38/62) was clearly more active than Cs-Pt/ASA(38/62) showing a difference of around 70% over the whole temperature range. Thus, the absence of Brønsted acid sites in Cs-Pt/ASA(38/62) led to an activity which was only a third of that of Pt/ASA(38/62).

In the mixed-poison experiment, quinoline (20 ppm N) was added to the sulfur-containing feed. This small concentration of quinoline poisoned a surprisingly small fraction of Brønsted acid sites in Pt/ASA(38/62) decreasing the difference in activity between both catalysts to 50%.

In general, the activity difference between Pt/ASA(38/62) and Cs-Pt/ASA(38/62) increased with increasing temperature (the activity of the former catalyst was always higher). This tendency is attributed to lower coverage with sulfur compounds on metal particles as well as a lower concentration of basic nitrogen containing compounds on the Brønsted acid sites of Pt/ASA(38/62) as the temperature increased.

4.2. Hydrogenation of tetralin in the absence of poisons

The catalytic properties of monometallic Pt and Pd catalysts differ markedly. The different adsorption strengths of aromatic molecules on the metals led to different selectivities and causes the Pt-based catalysts to be more active than the Pd containing catalysts for the hydrogenation of benzene, toluene and naphthalene

[30-34]. All bimetallic Pt-Pd catalysts show intermediate activity and selectivity, which is usually rationalized as dilution of the more active Pt by Pd [35]. Interestingly, under reaction conditions in the presence of sulfur-containing compounds and with strongly acidic supports, the bimetallic Pt-Pd catalysts maintain higher activities than the corresponding monometallic catalyst [36, 37]. However, as we show in this work, alloying of Pt with Pd does not necessarily lead to catalysts with better catalytic performance.

Let us recall at this point the characteristics of the bimetallic catalysts as described in the first part of this work. A summary of the main properties of the bimetallic catalysts reported in Ref. [19, 26] is compiled in Table 1. The ASA supported Pt-Pd catalysts contain Pt-Pd and Pd nanoparticles with average diameter varying between 1.4 and 1.8 nm as determined by TEM. EXAFS analysis demonstrates that the Pt-Pd particles contain a Pt-enriched core and a Pd-enriched shell and have Pd/Pt molar ratios from 1.69 to 1.17. The presence of monometallic Pd particles is deduced from the mass balance, given that the overall Pd:Pt molar ratio in all catalysts was 3. Despite the Pd-rich surface, all bimetallic particles have a variable fraction of exposed Pt atoms available on the surface, decreasing in the order Pt-Pd/ASA(55/45) > Pt-Pd/SiO_2 > Pt-Pd/ASA(5/95) > Pt-Pd/ASA(20/80). The concentration of Brønsted acid sites increases in the sequence Pt-Pd/SiO_2 < Pt-Pd/ASA(55/45) < Pt-Pd/ASA(5/95) < Pt-Pd/ASA(20/80); the Lewis acid site concentration increases in the order Pt-Pd/SiO_2 < Pt-Pd/ASA(5/95) < Pt-Pd/ASA(20/80) < Pt-Pd/ASA(55/45). In the following, we discuss first the effect of alloying Pt-Pd on the hydrogenation activity of the catalysts in the poison-free feed to differentiate the decisive parameters for the activity in the presence of DBT and quinoline.

Table 1. Characterization of the supported Pt-Pd catalysts: chemical composition, Brønsted (BAS) and Lewis (LAS) acid sites concentration, size and proportion of surface Pt for the supported metal particles and intermediate Sanderson electronegativity of the supports (S_{int}) [19, 26].

Catalyst	Composition (wt.%)				Acidity (mmol g^{-1})		Particle size (nm)	Surface Pt (%)	S_{int}
	Pt	Pd	SiO_2	Al_2O_3	BAS	LAS			
Pt-Pd/ASA(55/45)	0.30	0.55	55.2	44.0	22	192	1.4	18.0	2.86
Pt-Pd/ASA(20/80	0.30	0.52	20.2	79.0	58	183	1.8	13.9	2.98
Pt-Pd/ASA(5/95)	0.29	0.50	5.4	93.8	45	156	1.6	14.0	3.04
Pt-Pd/SiO_2	0.30	0.52	0	99.2	0	0	1.4	14.5	3.05

The experimental activation energies (Ea_{exp}) determined for the series of bimetallic catalysts in the hydrogenation of tetralin in the absence of poisons are 54, 48, 46, and 36 kJ·mol^{-1} for the catalysts supported on SiO_2, ASA(5/95), ASA(20/80), and ASA(55/45), respectively. The values determined for the same reaction carried out with monometallic Pt catalysts are 57, 35, 40 and 47 kJ mol^{-1} for Pt/SiO_2, Pt/ASA(5/95), Pt/ASA(20/80), and Pt/ASA(55/45) [19]. Clearly, the Ea_{exp} values are in the same range; the trend, however, is different. While in the case of monometallic particles increasing concentrations of SiO_2 in the mixed oxide leads to an increasing activity of the platinum particles (the exception is the catalyst supported on SiO_2 as explained below), the more complex variation of the properties for the Pt-Pd catalysts used in this work suggests more than one influencing factor. The differences in the activation energies must be determined on the one side by the varying concentrations of Pd, which binds the aromatic molecules relatively weakly, and in the increasing strength of bonding by Pt (being influenced through alloying and through the support).

Pt-Pd/ASA(55/45) was the most active bimetallic catalyst, which is attributed to the high fraction of platinum on its surface. This is in line with the fact that the hydrogenation activity of Pt is higher than that of Pd in the absence of poisons [38, 39]. Accordingly, the experimental activation energy increases from 36 kJ

mol^{-1} for Pt-Pd/ASA(55/45) to 46 and 48 kJ mol^{-1} for Pt-Pd/ASA(20/80) and Pt-Pd/ASA(5/95), respectively i.e., by around 25%. This proportion corresponds to the decrease in Pt coverage from 18% to 14% comparing Pt-Pd/ASA(55/45) with the other bimetallic catalysts supported on ASA (28% of decrease). Hence accessible Pt surface atoms are the most important feature of the bimetallic catalysts for reaching high hydrogenation activity.

The relation between Ea_{exp} and the true activation energy (Ea) is given by the Temkin equation (1) where n_i is the reaction order in the reactant i and ΔH_i is the corresponding enthalpy of adsorption. In agreement with ref. [19] we assume that the variation of Ea_{exp} is related to changes in the heat of adsorption of tetralin.

$$Ea = Ea_{exp} - \sum n_i \Delta H_i \qquad (1)$$

As the reaction is first order in tetralin, the lowest Ea_{exp} for the Pt-Pd/ASA(55/45) catalyst suggests the strongest adsorption of tetralin, i.e., for the catalyst with the highest fraction of accessible Pt. Moreover, the Ea_{exp} for the catalysts supported on ASA(20/80) and ASA(5/95) are all lower than that of the SiO_2-supported catalyst suggesting that the presence of Lewis and Brønsted acid sites induces an important effect on the adsorption strength of tetralin [19].

The activity of the catalysts with low concentration of surface Pt in poison-free feed increases in the sequence Pt-Pd/SiO_2 < Pt-Pd/ASA(20/80) < Pt-Pd/ASA(5/95). The same dependence of the activity on the composition of the support was observed in the hydrogenation of tetralin on ASA-supported monometallic Pt catalysts [19]. Given that the proportion of surface Pt in those three bimetallic catalysts is rather similar (around 14%), it is proposed that the electronegativity of the support determines the activity of the catalyst. The adsorption of reactants on Pt becomes stronger with increasing electronegativity (intermediate Sanderson electronegativity) of the carrier. Thus, the activity of the catalyst increases with increasing SiO_2 content in the ASA support. However, the catalyst supported on SiO_2 is the least active, because the absence of LAS blocks any significant effect of the support electronegativity on the metal particles.

The different adsorption strength of tetralin on Pt and Pd leads to different intrinsic selectivities. Adsorption on Pt is stronger leading to high *cis*-decalin

selectivity, whereas the weaker adsorption on Pd causes the *trans*-decalin isomer to be preferred [39]. Weak interaction of the intermediate ($\Delta^{9,10}$–octalin) allows the desorption and re-adsorption forming adsorbed $\Delta^{1,9}$–octalin and eventually *trans*-decalin [40]. In the poison-free experiments, the *cis*-/*trans*-decalin ratio on all the bimetallic catalysts was below 0.4, as expected for a catalyst with abundant surface Pd. Interestingly, for the reaction in the absence of poisons, the *cis*- to *trans*-decalin ratio decreases steadily with increasing temperature on Pt-Pd/ASA(55/45), (with relatively high proportion of surface Pt), whereas on the rest of the catalysts the ratio decreased only to a very small degree and remained constant at higher temperatures (Figure 2). Note that conceptually the cis-/trans-ratio should decrease with temperature, as higher temperatures should lead to looser bound substrates, intermediates and transition states. The observations indicate, therefore, that only in the presence of a higher concentration of Pt higher temperature sensitivity exists. It is unclear at present as to why this is not reflected in a higher cis-/trans-decalin ratio at lower reaction temperatures (see the equal values of all catalysts in Fig 2). However, overall the observation is in agreement with the literature [39], reporting that on a monometallic Pd catalyst, the *cis*- to *trans*-decalin ratio is constant in a wide conversion range, whereas on a comparable Pt catalyst the ratio decreases steadily with conversion.

4.3. Hydrogenation of tetralin in the presence of poisons

The low *cis*- to *trans*-decalin ratio confirms the dilution of Pt in Pd because it is well below 1 (a value expected for hydrogenation on Pt). Also the increase in Ea_{exp} seems to be related to a decreasing proportion of surface Pt. Hence, at this point, the results imply that in the absence of poisons the bimetallic catalysts behave as a Pt catalyst diluted with Pd. In contrast, at reaction conditions inducing poisoning (DBT and quinoline present in the feed) the activity depends not only on the morphology of the bimetallic clusters and their interaction with the support, but also on the size of the metal particles, the concentration of acid sites and the feed composition.

As in the case of the poison-free feed, Pt-Pd/ASA(55/45) shows the highest activity in the presence of DBT, quinoline and in the presence of both poisons. This confirms that the proportion of surface Pt is the parameter with the largest influence on the hydrogenation activity. Let us focus now on the effect of quinoline and DBT on the activity of the other catalysts. In the presence of quinoline (Fig. 3), the activity follows the trend Pt-Pd/ASA(20/80) < Pt-Pd/ASA(5/95) < Pt-Pd/SiO_2, which correlates with the dispersion of the metal particles. The EXAFS and IR characterization of the bimetallic catalysts supported on ASA(20/80), ASA(5/95) and SiO_2, showed that the proportion of metal atoms on the surface is similar among these catalysts. Thus, the activity increases with the decrease in particle size, i.e., increasing dispersion of the metal. Special attention must be paid in the case of the catalysts Pt-Pd/ASA(20/80) and Pt-Pd/ASA(5/95). The activity of the former is only slightly higher than that of the latter because the particle size is also slightly larger in Pt-Pd/ASA(20/80). Given that both catalysts have almost identical proportion of surface Pt, their intrinsic activities are nearly the same.

The Ea_{exp} values observed in the presence of quinoline are much higher than those calculated in the series of reactions using clean feed. This is tentatively attributed to the competitive adsorption of quinoline (molecule of basic character and more electron rich than tetralin) decreasing the strength of adsorption of tetralin on the metal clusters [41]. The Ea_{exp} decreases in the same order as in the absence of poisons i.e., Pt-Pd/SiO_2 > Pt-Pd/ASA(20/80) > Pt-Pd/ASA(5/95) > Pt-Pd/ASA(55/45), suggesting that the hydrogenation activity depends largely on the adsorption of tetralin on the metal phase (in turn influenced by the metal surface proportion and electronegativity of the support).

In the presence of DBT, the activity of the catalysts with low proportion of surface Pt follows a different trend than in the presence of quinoline or of poison-free feed. The hydrogenation activity increases in the order Pt-Pd/SiO_2 < Pt-Pd/ASA(5/95) < Pt-Pd/ASA(20/80), which is in line with the increasing concentration of Brønsted acid sites on the catalysts. The measured activation energy in the presence of sulfur is higher than in the absence of poisons and the

presence of quinoline (except for the catalyst supported on silica). The high conversion of DBT suggests that DBT and products of its surface reactions adsorb on the stronger adsorbing metal sites (Pt for instance) permitting binding of tetralin only on relatively weaker sites. Considering that the -OH groups of the support must have the weakest adsorption strength, it is highly probable that tetralin interacts with the OH groups at the perimeter of the metal cluster during hydrogenation. With the metal surface interacting mostly with DBT, the adsorption of tetralin is limited to the Brønsted sites; hence, the support acidity becomes the determining factor for tetralin hydrogenation. While all evidence points to a different explanation, we do not think of it as a likely possibility. We cannot rigorously exclude that the strong adsorption of DBT on the metal surface drastically reduces the adsorption enthalpy of tetralin, thus increasing the Ea_{exp} that leads to the low reaction rates of tetralin hydrogenation.

In the simultaneous presence of DBT and quinoline, the hydrogenation activity is strongly reduced. The stronger adsorption of poisons on metal (DBT and reaction products of DBT) and acid sites (quinoline and reaction products of quinoline) hinders the hydrogenation of tetralin. Indeed, in all experiments the conversion rates of the DBT and quinoline are much higher than that of tetralin. The trends of the Ea_{exp} in the presence of sulfur (with and without quinoline) do not correlate with the parameters that are significant in other conditions, i.e., particle size, electronegativity of the support or proportion of surface Pt.

While in the presence of poisons the overall value for *cis*-/*trans*-decalin ratio decreases with temperature as to be conceptually expected, neither the overall values nor the changes induced by temperatures strictly reflect the surface concentration in Pt. Thus, the question arises as to what extent the variations of the *cis*-/*trans*-decalin ratio is influenced the surface concentration and to what extent this concentration changes as a function of the temperature. Unfortunately these questions cannot be addressed with the already quite extensive physicochemical data reported in Part I of this study and are subject to further studies with model catalysts.

The specific effects of the poisons are consistent with the model presented in ref. [20] suggesting that the adsorption of tetralin occurs on two different sites, i.e., on metal particles and on Brønsted and Lewis acid sites at the perimeter of the metal particles. Quinoline strongly adsorbs on the acid sites and, therefore, retards the hydrogenation pathway that involves adsorption at the perimeter of the metal particles. The metal-catalyzed hydrogenation route, however, remains active for the hydrogenation of tetralin and consequently, the fraction of accessible metal atoms is the decisive factor for the activity under these conditions. When DBT is added to feed the adsorption of substrate on the metal surface is blocked by strongly adsorbed sulfur containing molecules or sulfur on the metal (illustrated in Reaction (1)) and the activity is strongly reduced. The presence of DBT has a weaker influence than that of quinoline on the pathway involving acid sites. Thus, in the presence of DBT tetralin adsorbs on Brønsted acid sites at the perimeter of the metal cluster and reacts with hydrogen, which has been dissociated on the S-covered metal surface. Therefore, in the presence of quinoline the particle size is the determining factor for the activity, whereas in the presence of DBT, the acidity determines the rate of hydrogenation. The simultaneous addition of 20 ppm nitrogen and 100 ppm sulfur as quinoline and DBT to the feed results in very low activity, because for the metal particle and the Brønsted acid sites strongly adsorbing poisons compete with the substrate for adsorption sites. Thus, we conclude that the reaction pathway involving the Brønsted acid sites and metal particles is valid also for Pt-Pd -based catalysts.

With respect to the desulfurization of DBT we would like to note that direct desulfurization dominates, i.e., biphenyl and sulfur adsorbed on the metal as shown in Reaction (1) are formed in the most abundant reaction [42,43]. Subsequently, sulfur is removed by H_2 yielding H_2S and a free metal atom, via reaction (2) [44]. Note that Reactions (1) and (2) only illustrate the overall sulfur poisoning and surface regeneration of the metal, and do not intend to be mechanistically correct.

$$Me\text{-}C_{12}H_8S + H_2 \rightarrow Me\text{-}S + C_{12}H_{10} \qquad (1)$$

$$Me\text{-}S + H_2 \leftrightarrow H_2S + Me \qquad (2)$$

The increase in activity with temperature is more evident in the presence of DBT, suggesting that the extent of sulfur-poisoning strongly depends on the temperature. This is to be related to the decreasing concentration of adsorbed DBT with temperature (see the plot of DBT conversion versus temperature in Figure 9) as well as to the overall lower concentration of sulfur. At 573 K or above, the DBT conversion is well above 80% with all the catalysts indicating that the further increase would not increase the rate of sulfur formation on the metal surface, while the rate of sulfur removal will further increase. The net result is that the sulfur coverage of the surface decreases with temperature.

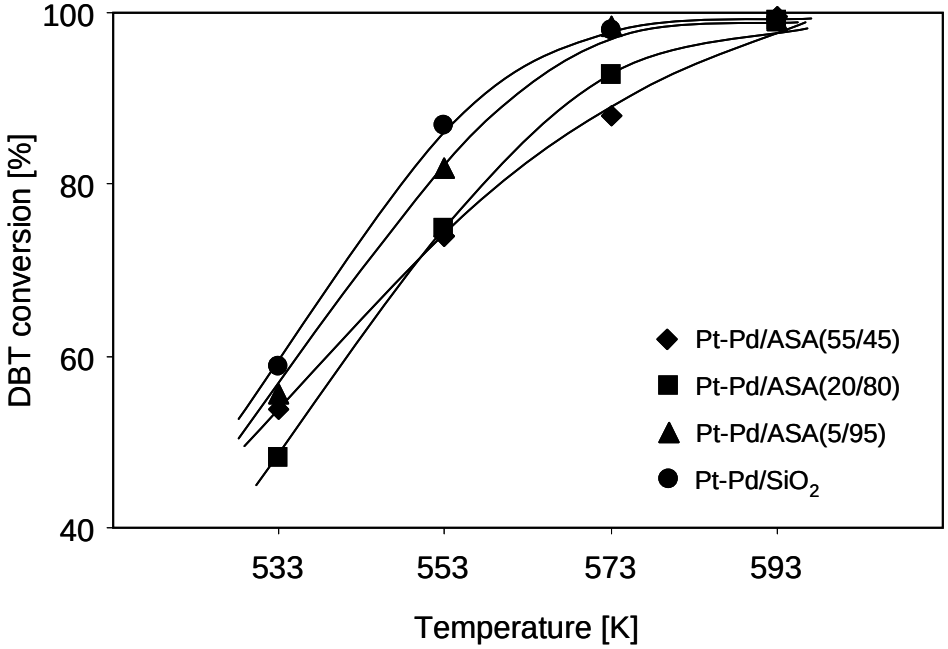

Figure 9. DBT conversion during the hydrogenation of tetralin in presence of DBT (100 ppm S) and quinoline (20 ppm N) in the temperature range 533-593 K over Pt-Pd catalysts.

4.4. Comparison of monometallic Pt and bimetallic Pt-Pd catalysts

The efficiency of bimetallic and monometallic Pt catalysts has to be compared to demonstrate the importance of optimizing the Pt-surface concentration. Hence, control experiments were performed on the Pt catalysts studied in Ref. [20]. All bimetallic Pt-Pd catalysts showed a significantly reduced activity compared to their monometallic Pt counterparts in the absence of poisons (Fig. 10). It has also been shown that the adsorption strength of tetralin is weaker on Pt-Pd/ASA than on Pt/ASA (deduced from the low *cis*-/*trans*-decalin ratio on Pt-Pd/ASA). Thus, the relatively low activity of Pd overcompensates the beneficial influence of the electronic interaction of Pt and Pd evidenced by the XANES analysis in [26] hindering any improvement of the hydrogenation activity. In the presence of DBT, the Pt-Pd catalysts still showed lower activities compared to the corresponding Pt samples except for the notable case of Pt-Pd/ASA(55/45) (see Fig. 11). The low activity of most of the bimetallic catalysts here studied contradicts the reports of high activity of bimetallic Pt-Pd catalyst in the presence of poisons [36,37]. The low activity of the bimetallic catalysts investigated here is attributed to the low concentration of Pt on the surface. The beneficial effect of alloying, is not completely compensated in the Pt-Pd/ASA(55/45) catalyst due to the higher proportion of surface Pt in the bimetallic clusters.

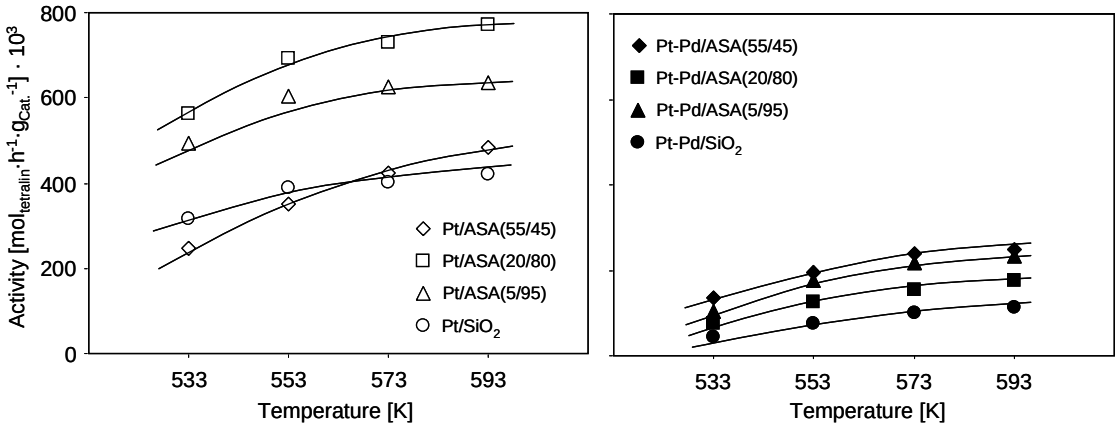

Figure 10. Activities of Pt and Pt-Pd catalysts at steady state for the hydrogenation of tetralin in the temperature range 533-593 K.

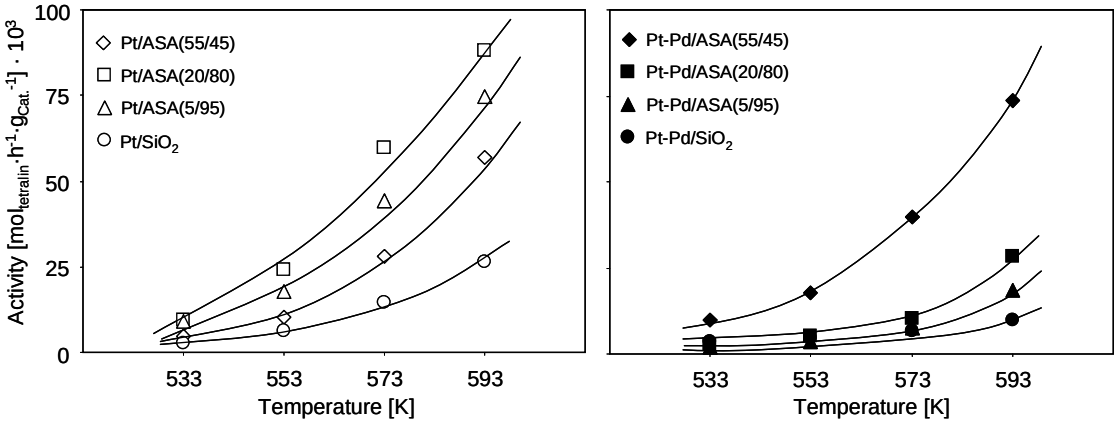

Figure 11. Activities of Pt and Pt-Pd catalysts at steady state for the hydrogenation of tetralin in presence of DBT (100 ppm S) in the temperature range 533-593 K.

The activity of Pt-Pd/ASA(55/45) in the presence of sulfur is higher than the activity of Pt/ASA(55/45). Considering that the concentration of exposed Pt in the bimetallic catalyst must be lower than in the monometallic catalyst, the higher activity must be attributed to an enhanced activity of Pt upon alloying with Pd. Specifically, the electron transference from Pt to Pd (exceeding the transfer to the support driven by electronegativity) reduces the strength of the metal-sulfur bond thereby accelerating the removal of surface sulfur via reaction (2) and shifting the equilibrium towards a more accessible metal surface [45]. While the electronic effect of alloying is similar in all bimetallic catalyst, the proportion of surface Pt in Pt-Pd/ASA(55/45) must be significant to allow the beneficial effect of alloying to overturn the negative effect of Pt dilution with Pd. This discussion does not imply that Pd lacks catalytic activity itself. However, for the catalysts target of this study, the activity of Pd must be significantly lower than that of Pt, because Pd enrichment in the surface leads to decreasing activities under all conditions. Therefore, we rule out that Pd atoms are the reason for the high activity of Pt-Pd/ASA(55/45) in the presence of DBT.

Direct evidence of the enhanced sulfur resistance of Pt alloyed with Pd is shown in Fig. 6. The activity of the Pt/ASA(20/80) catalyst decreases by 55%, whereas the activity of Pt-Pd/ASA(20/80) remains almost unaffected after increasing the sulfur content from 100 to 500 ppm. Let us emphasize that the main effect of alloying seems to be the weakening of the sulfur-metal bond so that sulfur is easier removed from the metal sites, or has a less favorable equilibrium as shown in Reaction (2). Moreover, some DFT calculations suggest that the enhanced sulfur tolerance of Pd-Pt alloys is related to an enhanced H_2 adsorption compared to that of sulfur compounds [46]. Thus, alloying increases the activation and the transfer rate of hydrogen to tetralin the acid sites at the perimeter of the metal clusters.

As a final remark we would like to emphasize that better Pt-Pd catalysts, i.e., ones with a higher surface Pt concentration, should exist and might be obtainable via different preparation procedures or tuning the properties of the support. This would also explain the differences in the reported properties of Pd-Pt catalysts for hydrotreating.

5. Conclusions

The catalytic hydrogenation of tetralin in the absence and presence of quinoline and dibenzothiophene was studied on bimetallic Pt-Pd (0.8 wt. % metal content, molar ratio Pd/Pt=3) catalysts supported on silica and amorphous silica-alumina (ASA). A complex interaction between the properties of the metal clusters and those of SiO_2 or ASA (Al_2O_3/SiO_2 wt.% ratio of 55/45, 20/80, and 5/95) determined the performance of the catalysts. The proportion of Pt on the surface was the most important parameter, because the Pt-Pd catalyst supported on ASA(55/45) with the highest proportion of surface Pt (18%) was the most active bimetallic formulation under all tested conditions. In the absence of poisons the electronegativity of the support correlated with the hydrogenation activity provided that it exhibits Lewis acidity. In the presence of quinoline the activity of the catalysts increased with the dispersion of the metal particles, whereas in the

presence of dibenzothiophene, the acidity of the support compensated for the sulfur poisoning of the metal phase.

The observed effects of the poisons indicated the presence of two kinds of adsorption sites for binding the reacting substrates, i.e., metal surface, and Brønsted acid sites at the perimeter of the metal particles. The key contribution of acid sites in the hydrogenation reaction was confirmed by exchanging the Brønsted acid sites of the support by Cs^+.

For comparison purposes, ASA-supported monometallic Pt catalysts (0.8 wt.%) were tested under the same reaction conditions. All the Pt catalysts were more active than the Pt-Pd counterparts in poison-free feed. In the presence of poisons, the Pt catalysts were also more active than the bimetallic formulations with the remarkable exception of Pt-Pd/ASA(55/45). The bimetallic catalysts, however, are more resistant to sulfur and nitrogen poisoning. It is concluded that the poison resistance of bimetallic catalysts originates from the electron transference from Pt to Pd that yields weak adsorption of poisons on electron deficient Pt atoms. However, the surface coverage of Pt must be maximized in order to compensate the dilution effect (Pt in Pd) that tends to decrease the hydrogenation activity.

6. Acknowledgments

The authors are grateful to the staff of the beamline X1 at Hasylab DESY, Hamburg, Germany for their kind help and continuous support during the experiments. Helpful discussions and editing of the manuscript by Prof. Breitkopf, TU Dresden, is thankfully acknowledged.

7. References

[1] G. Perot, Catal. Today 10 (1991) 447.

[2] T. Isoda, S. Nagao, X. Ma, Y. Korai, I. Michida, Appl. Catal. A 150 (1997) 1.

[3] M. Egorova, R. Prins, J. Catal. 224 (2004) 278.

[4] A. Stanislaus, B.H. Cooper, Catal. Rev. Sci. Eng. 36 (1994) 75.

[5] B.H. Cooper, B B.L. Donnis, Appl. Catal. A 137 (1996) 203.

[6] H. Yosuda, Y. Yoshimura, Catal. Lett. 46 (1997) 43.

[7] H. Yasuda, T. Sato, Y. Yoshimura, Am. Chem. Soc. Div. Petrol. Chem. Prepr. 42 (1997) 580.

[8] H. Yasuda, T. Sato, Y. Yoshimura, Catal. Today 50 (1999) 63.

[9] T.B. Lin, C.A. Jan, J.R. Chang, Ind. Eng. Chem. Res. 34 (1995) 4284.

[10] H. Jiang, H. Yang, R. Hawkins, Z. Ring, Catal. Today 125 (2007) 282.

[11] S.D. Lin, M.A. Vannice, J. Catal. 143 (1993) 563.

[12] S.D. Lin, M.A. Vannice, J. Catal. 143 (1993) 539.

[13] D. Poondi, M.A. Vannice, J. Catal. 161 (1996) 742.

[14] V. Fouche, P. Magnoux, M. Guisnet, Appl. Catal. 58 (1990) 189.

[15] O. Cairon, K. Thomas, A. Chambellan, T. Chevreau, Appl. Catal. A 238 (2003) 167.

[16] T. Fujikawa, K. Idei, T. Ebihara, H. Mizuguchi, K. Usui, Appl. Catal. A 192 (2000) 253.

[17] R.M. Navarro, B. Pawelec, J.M. Trejo, R. Mariscal, J.L.G. Fierro, J. Catal. 189 (2000) 184.

[18] M.F. Williams, B. Fonfé, C. Sievers, A. Abraham, J.A. van Bokhoven, A. Jentys, J.A.R. van Veen, J.A. Lercher, J. Catal. 251 (2007) 485.

[19] M.F. Williams, B. Fonfé, C. Woltz, A. Jentys, J.A.R. van Veen, J.A. Lercher, J. Catal. 251 (2007) 497.

[20] M.F. Williams, B. Fonfé, A. Jentys, C. Breitkopf, J.A.R. van Veen, J.A. Lercher, J. Phys. Chem. C 114 (2010) 14532.

[21] M. Jacquin, D.J. Jones, J. Roziere, A.J. Lopez, E. Rodriguez-Castellon, J.M.T. Menayo, M. Lenarda, L. Storaro, A. Vaccari, S. Albertazzi, J. Catal. 228 (2004) 447.

[22] Y. Yoshimura, M. Toba, T. Matsui, M. Harada, Y. Ichihashi, K.K. Bando, H. Yasuda, H. Ishihara, Y. Morita, T. Kameoka, Appl. Catal. A 322 (2007) 152.

[23] S. Albertazzi, G. Busca, E. Finocchio, R. Glockler, A. Vaccari, J. Catal. 223 (2004) 372.

[24] S. Albertazzi, E. Rodriguez-Castellon, M. Livi, A. Jimenez-Lopez, A. Vaccari, J. Catal. 228 (2004) 218.

[25] B. Pawelec, R. Mariscal, R.M. Navarro, S. van Bokhorst, S. Rojas, J.L.G. Fierro, Appl. Catal. A 225 (2002) 223.

[26] Y. Yu, B. Fonfé, A. Jentys, G.L. Haller, C. Breitkopf, J.A.R van Veen, O.Y. Gutiérrez, J.A. Lercher, Part I, J. Catal., submitted for publication (2011).

[27] C.C. Costa Augusto, J.L. Zotin, A. Da Costa Faro, Catal. Lett. 75 (2001) 37.

[28] T. Fujikawa, K. Idei, K. Ohki, H. Mizuguchi, K. Usui, Appl. Catal. A 205 (2001) 71.

[29] A. Infantes-Molina, J. Merida-Robles, E. Rodriguez-Castellon, J.L.G. Fierro, A. Jimenez-Lopez, Appl. Catal. B 73 (2007) 180.

[30] C. Song, A.D. Schmitz, Energy Fuels, 11 (1997) 656.

[31] J. Chupin, N.S. Gnep, S. Lacombe, M. Guisnet, Appl. Catal. A: Gen. 206 (2001) 43.

[32] T.T. Phuong, J. Massardier, P. Gallezot, J. Catal. 102 (1986) 456

[33] J.M. Orozco, G. Webb, Appl. Catal. 6 (1983) 67

[34] S.D. Lin, C. Song, Catal. Today 31 (1996) 93-104

[35] K. Thomas, C. Binet, T. Chevreau, D. Cornet, J.P. Gilson, J. Catal. 212 (2002) 63.

[36] A.D. Schmitz, G. Bowers, C. Song, Catal. Today 31 (1996) 45.

[37] S. Jongpatiwat, Z.R. Li, D.E. Resasco, W.E. Alvarez, E.L. Sughrue, G.W. Dodwell, Appl. Catal. A 262 (204) 241.

[38] H. Greenfield, N.Y. Ann, Acad. Sci. 214 (1973) 233.

[39] S. Dokjampa, T. Rirksomboon, S. Osuwan, S. Jongpatiwut, D.E. Resasco, Catal. Today 123 (2007) 218.

[40] A.W. Weitkamp, Adv. Catal. 18 (1968) 1.

[41] J.J. Rooney , J. Mol. Catal. (1985) 31 147.

[42] V.G. Baldovino-Medrano, S. Giraldo, A. Centeno, J. Mol. Cat. A 301 (2009) 127.

[43] V.G. Baldovino-Medrano, P. Eloy, E.M. Gaigneaux, S.A. Giraldo, A. Centeno, Cat. Today 150 (2010) 186.

[44] M. Guenin, M. Breysse, R. Frety, K. Tifouti, P. Marecot, J. Barbier, J. Catal. 105 (1987) 144.

[45] T. Matsui, M. Harada, K.K. Bando, M. Toba, Y. Yoshimura, Appl. Catal. A 290 (2005) 73.

[46] H. Jiang, H. Yang, R. Hawkins, Z. Ring, Catal. Today 125 (2007) 282.

Chapter 4

Bimetallic Pt-Pd catalysts: effect of synthesis parameter on the structure, hydrogenation activity and resistance towards poisons

A series of monometallic and bimetallic Pt-Pd catalysts (Pd:Pt molar ratio of 3) were prepared on amorphous silica alumina (silica:alumina weight ratio of 70:30) using different Pd precursors, i.e., $[Pd(NH_3)_4](NO_3)_2$ and $Pd(NO_3)_2$, whereas $[Pt(NH_3)_4](NO_3)_2$ was kept as the source of Pt. The analysis of the extended X-ray absorption fine structure and infrared spectroscopy of adsorbed CO indicate that the morphology and surface composition of the Pt-Pd particles depend on the metal precursor. X-ray absorption near edge structure provided evidence for the formation of electron deficient Pt atoms in the bimetallic Pt-Pd catalysts. The different reducibility of metal precursors, e.g. $[Pd(NH_3)_4]^{2+}$ and Pd^{2+}, was the main reason for forming Pt-Pd nanoparticles with varying segregation of Pd to the surface of bimetallic clusters. The catalysts were tested in the hydrogenation of tetralin in the absence and presence of quinoline and dibenzothiophene (DBT). Increasing proportion of electron deficient Pt on the surface of the bimetallic clusters increases the efficiency of the catalyst in the presence of poisons.

1. Introduction

Nowadays, fuels have to be produced from heavy oil given the depletion of conventional hydrocarbon sources. In response to this challenge, refineries have applied a two-stage process with different stage characteristics [1,2]. In the first stage most of the heteroatoms are removed from the feed on sulfide-based catalysts at severe temperatures and reaction conditions. The quality of the fuel is further improved in a subsequent hydrogenation step preferably under moderate conditions on noble metal-based catalysts. However, the poison resistance of noble metal systems is far from being optimized to be widely applied.

A large amount of research on noble metal catalysts has been performed to improve the resistance towards poisons. It is known that the acidity of the support plays an important role in the activity and sulfur tolerance of Pt or Pd catalysts [3-5]. Authors commonly infer that the contact between a strong acidic support and Pt or Pd clusters allows the withdrawal of electrons from the noble metal thereby creating electron-deficient metal particles [6,7]. The adsorption strength of sulfur on metal atoms is so weakened. As a result, the presence of sulfur does not impose a dramatic decrease in activity upon the hydrogenation of aromatic compounds [8-10]. The enhanced activity and sulfur tolerance by acid supports have been also explained by the presence of additional hydrogenation sites in the metal-support interfacial region that contribute to the overall rate of hydrogenation [11,12]. Alloying Pt and Pd is another strategy of improving the resistance towards sulfur poisoning [13]. Electronic effects are claimed to yield S-resistance catalysts on alloying. Consequently, considerable effort and research has been focused on solving the structure and understanding the electronic properties of bimetallic particles [13,14].

The selection of the metal precursor and thermal treatment used during the synthesis steps may be decisive for the activity of noble metal catalysts [15]. This also holds true for the properties and catalytic performance of bimetallic Pt-Pd clusters. Jung et al. [16] have studied the effect of several Pt precursors on the morphology and performance of Pt deposited on Pd/C for the oxygen reduction

reaction. The most selective deposition of Pt on the surface of Pd and highest activity was achieved using $Pt(NH_3)_4Cl_2$. Carrion et al. [17] reported the preparation of Pt-Pd nanoclusters on Zr-doped mesoporous silica using different precursors. Introducing both metals in the form of a binuclear Pd-Pt complex instead of as a mixture of metal salts enhanced the metal dispersion and selectivity of the catalysts for the hydrogenation of acetonitrile. Other studies also have proved that Pt-Pd catalysts prepared by different methods yield different alloying degree and catalytic behavior [18].

In our group, a series of Pt hydrogenation catalysts supported on amorphous alumina-silica (ASA) have been systematically investigated [19,20]. The effect of alloying Pt and Pd has been further examined for the hydrogenation of tetralin in the presence and absence of sulfur- and nitrogen-containing compounds [12,21]. It has been found that the bimetallic catalysts are less active than the Pt counterparts for the hydrogenation of tetralin in the absence of poisons. However, in the presence of poisons, the morphology of the bimetallic Pt-Pd nanocluster is a key factor for the hydrogenation activity and resistance towards poisons. A minimum proportion of surface Pt is needed in the bimetallic catalysts to observe the marked positive influence of alloying commonly reported in literature [22-24]. In turn, it is possible to tune the morphology of the bimetallic clusters by modifying the composition of the ASA support.

In the present work, we extend our investigations using a fixed support composition and several metal precursors to prepare ASA-supported Pt-Pd nanoclusters with different structure and surface composition. The hydrogenation activity of the catalysts was investigated in the presence of dibenzothiophene (DBT) and quinoline. By combining advanced physicochemical characterization techniques and the kinetic tests, the structure of the Pt-Pd nanoparticles and the corresponding hydrogenation activity and resistance towards poisons were correlated. Furthermore, the dependence of the final cluster structure on the precursor is explained in terms of different reducibility during the thermal treatments.

2. Experimental

2.1. Catalyst preparation

Three bimetallic Pt-Pd catalysts with the same metal loading (0.3 wt.% Pt and 0.5 wt.% Pd, molar ratio of Pd:Pt=3) supported on amorphous silica-alumina (Sasol, Germany) were synthesized by incipient wetness impregnation. The ASA carrier (SiO_2/Al_2O_3 weight ratio of 70/30) was impregnated with aqueous solution of $[Pt(NH_3)_4](NO_3)_2$ and $Pd(NO_3)_2$, catalyst Pt-Pd(1); $[Pt(NH_3)_4](NO_3)_2$ and $[Pd(NH_3)_4](NO_3)$, catalyst Pt-Pd(2); or $[Pt(NH_3)_4](NO_3)_2$ and $Pd(NO_3)_2$ changing the pH of the solution by adding NH_4OH, catalyst PtPd(3).

In order to gain insight into the synergetic effect of alloying in the Pt-Pd catalysts, several monometallic Pt and Pd catalysts supported on identical ASA material were also synthesized and kinetically tested. The monometallic catalysts are referred as 0.8Pt containing 0.8 wt.% Pt using $[Pt(NH_3)_4](NO_3)_2$ as precursor; 0.3Pt, with 0.3 wt.% Pt using $[Pt(NH_3)_4](NO_3)_2$ as precursor; 0.5Pd(1), with 0.5 wt.% Pd using $Pd(NO_3)_2$ as precursor; and 0.5Pd(2) with 0.5 wt.% Pd using $[Pd(NH_3)_4](NO_3)_2$ as precursor. All the catalysts were dried at 383 K for 12 h and treated in synthetic air at 673 K for 2 h and then reduced at 623 K in hydrogen for 2 h. A summary of all catalysts used is given in Table 1.

Table 1. List of catalysts prepared for this study. Metallic precursors and pH of the solutions used in the impregnation step.

Catalyst	Pt and Pd precursor(s)	pH value of precursor solutions
Pt-Pd(1)	$[Pt(NH_3)_4](NO_3)_2$, $Pd(NO_3)_2$	2.0
Pt-Pd(2)	$[Pt(NH_3)_4](NO_3)_2$, $[Pd(NH_3)_4](NO_3)$	7.7
Pt-Pd(3)	$[Pt(NH_3)_4](NO_3)_2$, $Pd(NO_3)_2$	2 to 7.7 [1]
0.8Pt	$[Pt(NH_3)_4](NO_3)_2$	6.7
0.3Pt	$[Pt(NH_3)_4](NO_3)_2$	6.8
0.5Pd(1)	$Pd(NO_3)_2$	2.0
0.5Pd(2)	$[Pd(NH_3)_4](NO_3)_2$	8.0

[1] The pH value was modified by adding NH_4OH to the precursor solution.

2.2. Metal content and textural properties

The Pt and Pd concentration of the catalysts was confirmed by atomic absorption spectroscopy (AAS) using an UNICAM 939 spectrometer. The specific surface area and average pore diameter of the catalysts were determined by N_2 adsorption-desorption measurements carried out at liquid nitrogen temperature using a PMI automated BET sorptometer. All samples were outgassed at 523 K for 20 h before the measurements. The specific surface area and the pore diameter were calculated applying the BET and BJH models, respectively.

2.3. Hydrogen chemisorption

The metal dispersion of the catalysts was measured by H_2 chemisorption. All the samples were activated in vacuum at 588 K for 1 h and then cooled to 298 K, after which successive doses of hydrogen were admitted. An isotherm of hydrogen adsorption (chemisorption together with physisorption) was measured over a pressure ranging from 1 kPa to 40 kPa. Afterwards, the samples were outgassed at 298 K for 1 h to remove the physisorbed H_2 and another adsorption isotherm was measured (physisorption). The concentration of hydrogen chemisorbed on the metal was calculated by subtracting the second isotherm from the first isotherm, and the metal dispersion was estimated from the chemisorbed hydrogen considering a stoichiometric metal:H ratio of 1.

2.4. Infrared spectroscopy

The IR spectra of adsorbed pyridine were measured to characterize the Lewis (LAS) and Brønsted (BAS) acid sites, while the spectra of adsorbed CO were used to characterize the properties of the metal surface. The spectra of pyridine were acquired using a Perkin Elmer 2000 spectrometer operating at a resolution of 4 cm^{-1}. Prior to the sorption experiments, the catalyst samples were activated in vacuum ($p = 10^{-6}$ mbar) at 723 K for 1 h. The activated samples were exposed to pyridine ($p_{(Py)} = 10^{-1}$ mbar) at 423 K for 0.5 h and the IR spectra were recorded after evacuation at 423 K for 1 h. The concentration of LAS and BAS were

quantified using the molar extinction coefficients of 0.965 cm μmol^{-1} and 0.726 cm μmol^{-1}, respectively.

The spectra of adsorbed CO were measured using a Bruker VERTEX 70 spectrometer with a resolution of 2 cm^{-1}. Samples of the catalysts were reduced in H_2 at 623 K for 1 h at a partial pressure of 0.5 bar followed by evacuation (p = 10^{-6} mbar) for 1 h to remove adsorbed hydrogen. The samples were cooled to 313 K and CO was adsorbed at p=0.5 mbar to record a spectrum. Subsequently the samples were evacuated for 15 minutes at 10^{-6} mbar and additional spectra were recorded.

2.5. Extended X-ray absorption fine structure

X-ray absorption spectra were collected at the beamline X1 at HASYLAB, DESY, Hamburg, Germany. The storage ring was operated at 4.5 GeV at an average current of 100 mA. The Si (311) double crystal monochromator was detuned to 60% of the maximum intensity to minimize the intensity of higher harmonics in the X-ray beam. Self-supporting wafers of the catalysts were first reduced with H_2 in situ at 623 K for 1 h and then flushed with He at 623 K for 0.5 h to remove adsorbed H_2. The X-ray absorption spectra were collected at the Pt L_{III} edge (11564 eV) and the Pd K edge (24365 eV) at 77 K. The position of the edge was calibrated using the spectra of a simultaneously measured Pt or Pd foil. For the extended X-ray absorption fine structure (EXAFS) and X-ray absorption near edge structure (XANES) analysis, the scattering background was subtracted using a polynomial function and all spectra were normalized to unity. The VIPER and XANDA programs were used for analyzing the data [25].

In the EXAFS analysis the oscillations were weighted with k^2 and Fourier transformed within the limits k = 2.0 – 11.0 $Å^{-1}$. The local environments of the Pt and Pd atoms were determined from the oscillation in k space using multiple-edge fitting with equal distances for Pt-Pd and Pd-Pt neighbors. The phase-shift and amplitude function for Pt-Pt, Pd-Pd, Pt-Pd and Pd-Pt were calculated assuming multiple scattering processes (FEFF Version 8.30) [26,27].

2.6. Temperature programmed reduction

Temperature programmed reduction (TPR) of catalysts pretreated with H_2S was applied to study the interaction of the catalysts with sulfur. 0.1 g of the catalysts were placed in a quarz reactor and mounted in a ceramic oven (Horst GmbH). The samples were treated in a flow of H_2S in He (1.25 vol.% H_2S in a total flow of 20 $ml \cdot min^{-1}$) heating with a rate of 10 $K \cdot min^{-1}$ up to 533 K and kept for 1 h. Then the H_2S/He mixture was replaced by 20 $ml \cdot min^{-1}$ of pure He and the temperature was kept at 533 K for another hour, and the reactor was cooled to room temperature in He flow. Subsequently, the TPR of the sulfided samples was performed with heating of 5 $K \cdot min^{-1}$ up to 1173 K in 10 $ml \cdot min^{-1}$ of H_2 flow. A mass spectrometer (Balzers QME 200) was used for screening the evolved gases within the whole procedure.

2.7. Catalytic measurements

The hydrogenation of tetralin on the Pt, Pd and Pt-Pd catalysts was carried out in a set of four parallel trickle-bed reactors in continuous down-flow mode, for detail see ref. [21]. The activity tests were performed at 533-593 K and 50 bar hydrogen pressure with a weight hourly space velocity (WHSV) of 3600 h^{-1} for clean feed, 400 h^{-1} for quinoline-containing feed, 300 h^{-1} for dibenzothiophene (DBT)-containing feed, and 60 h^{-1} for feed containing both quinoline and DBT. The WHSV is defined as the weight of feed flowing per hour per unit weight of catalyst. The change of the WHSV was achieved by varying the amount of catalyst and/or the flow rate keeping a constant molar ratio of H_2 to tetralin of 20. The poison-free feed consisted of 5 wt.% tetralin, 5 wt.% hexadecane as GC standard and 90 wt.% tetradecane as solvent. Catalytic experiments applying quinoline and DBT in separate tests used 400 ppm N and 100 ppm S, whereas the experiments with simultaneous quinoline and DBT addition used 20 ppm N and 100 ppm S. The activity of the catalysts was reported as mol of tetralin converted per hour per gram of catalyst ($mol_{tetralin} \cdot h^{-1} \cdot g_{Cat.}^{-1}$). A continuous deactivation was observed in all reactions in the first 20 h time on stream (TOS)

of the reaction. Thus, all catalytic activities reported in this paper were collected at steady state after 24 h TOS.

3. Results

3.1. Textural properties and chemical composition of the catalysts

The Pt and Pd concentration obtained from AAS, metal dispersion determined from H_2 chemisorption and textural properties of the catalysts are summarized in Table 2. The metal content was approximately 0.3 wt.% Pt and 0.5 wt.% Pd in the three bimetallic Pt-Pd catalysts. The specific surface area was 481 $m^2 \cdot g^{-1}$ for the ASA support. After impregnation of noble metals, all the surface areas of catalysts decreased; however, no correlation is found between the area of the catalyst and the metal precursor used for the preparation. The average pore diameters of the catalysts were only slightly smaller than that of the ASA support. In general, all catalysts exhibited high metal dispersion according to H_2 chemisoption results.

Table 2. Textural properties, chemical composition and metal dispersion of the catalysts.

Catalyst	Concentration (wt.%)		BET Surface area ($m^2.g^{-1}$)	Pore diameter (nm)	Dispersion (%)	Metal particle size[1] (nm)
	Pt	Pd				
ASA	-	-	481.0	7.4	-	
Pt-Pd(1)	0.29	0.52	430.1	7.3	82.4	1.37
Pt-Pd(2)	0.28	0.50	471.5	7.3	102.7	1.10
Pt-Pd(3)	0.29	0.49	450.6	7.1	98.2	1.15
0.8Pt	0.77	-	469.6	7.0	107.4	1.04
0.3Pt	0.28	-	466.2	7.2	86.6	1.29
0.5Pd(1)	-	0.49	461.7	7.4	74.6	1.51
0.5Pd(2)	-	0.50	447.1	7.3	81.5	1.39

[1] metal particle size calculated from H_2 chemisorption [28].

3.2. Acidic properties of the catalysts

The acid properties of the ASA support and the catalysts were characterized by pyridine adsorption/desorption followed by IR spectroscopy. The concentrations of Brønsted (BAS) and Lewis (LAS) acid sites, summarized in Table 3, were calculated from the quantitative evaluation of the corresponding spectra. After the incorporation of metals, the concentration of BAS and LAS decreased compared to that determined for the support. The decrease in acidity does not depend on the nature of the metal precursor.

Table 3. Brønsted acid sites (BAS) and Lewis acid sites (LAS) concentration calculated for the catalysts from pyridine adsorption/desorption followed by IR spectroscopy.

Catalyst	Acid site concentration ($\mu mol \cdot g^{-1}$)	
	BAS	LAS
ASA	56	526
Pt-Pd(1)	51	504
Pt-Pd(2)	54	462
Pt-Pd(3)	48	524
0.8Pt	41	387
0.3Pt	47	474
0.5Pd(1)	48	498
0.5Pd(2)	51	524

3.3. Characterization of the noble metal nanoparticles

The catalysts were further characterized by EXAFS, XANES and CO adsorption followed by IR spectroscopy. EXAFS was applied to characterize the morphology of metal nanoparticles of the Pt-Pd catalysts. The Fourier transforms of the EXAFS at Pt L_{III} edge and at Pd K edge for the reduced bimetallic Pt-Pd samples are shown in Fig. 1. Table 4 summarizes the structure parameters i.e.,

coordination numbers (CN) and interatomic distances (r) calculated from the analysis of the EXAFS oscillations in the k space. The interatomic distances for the Pt-Pt, Pt-Pd, Pd-Pd and Pd-Pt bonds showed a slight contraction typical for small metal nanoparticles [29]. For the analysis of the fitting CN values, recall that in a face-centered cubic arrangement (corresponding to the cubo-octahedral shape accepted for Pt and Pd nanoclusters [30-32]) the coordination number of the atoms in the surface is 6, whereas the coordination of the inner atoms is 12. Therefore, for the Pt-Pd nanoclusters in Pt-Pd(1) the sum of coordination numbers (CN_{Pt-Pt} + CN_{Pt-Pd}) of 11.23 and (CN_{Pd-Pd} + CN_{Pd-Pt}) of 6.63 indicates that the Pt atoms are preferably in the inner layers, whereas the main fraction of Pd is on the surface of the bimetallic particles. In contrast, the catalyst Pt-Pd(2), prepared with similar cations in the precursor salts has a more homogeneous distribution of Pt and Pd atoms in the bimetallic nanoclusters as suggested by the sum of coordination numbers i.e., (CN_{Pt-Pt} + CN_{Pt-Pd}) = 7.5 and (CN_{Pd-Pd} + CN_{Pd-Pt}) = 5.7. The catalyst Pt-Pd(3), prepared from precursors of different nature but added with NH_4OH shows coordination numbers similar to those obtained for Pt-Pd(1) being the difference between the CN of Pd and Pt smaller. Obtaining different structures of Pt-Pd nanoparticles is clearly related to the use of different precursors as it is discussed in detail later.

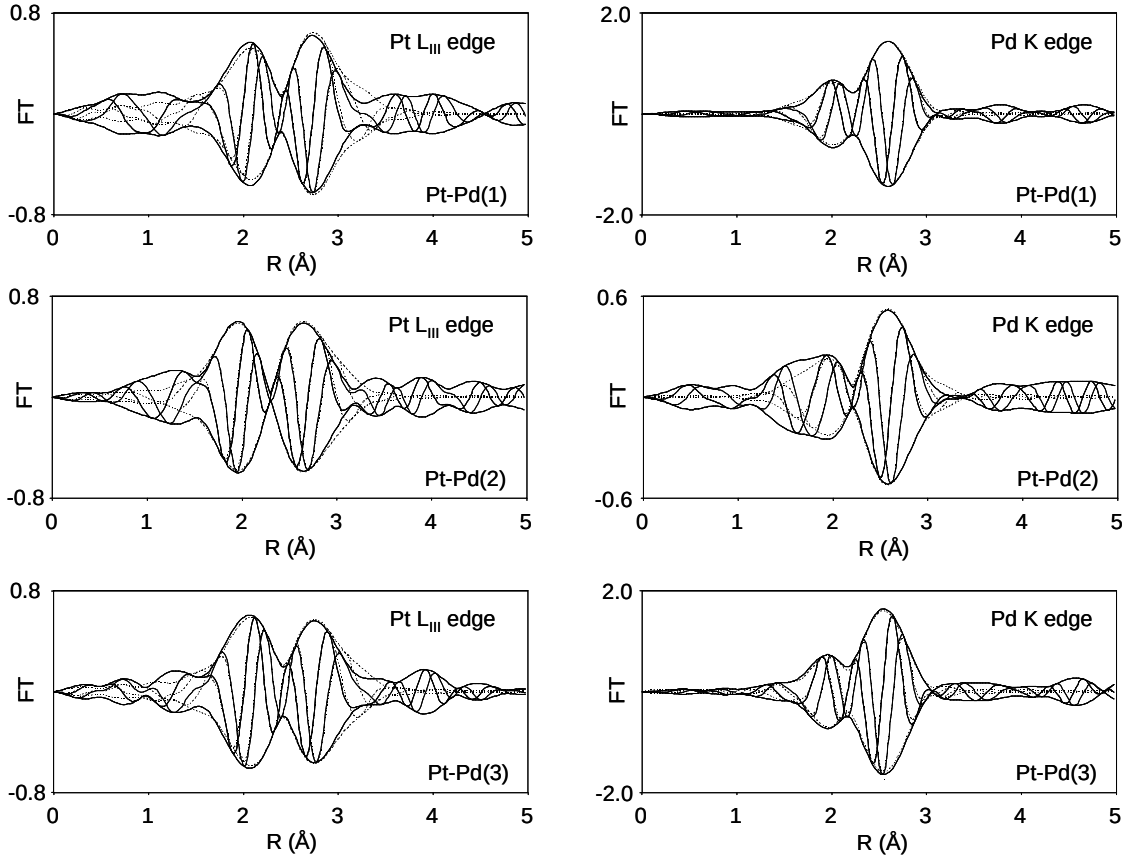

Figure 1. Fourier transforms (k^2 –weighted, Δk 2-11 $Å^{-1}$) of Pt-Pd(1), Pt-Pd(2) and Pt-Pd(3) at Pt L_{III} edge (11564 eV) and Pd K edge (24365 eV) after in situ treatment in H_2 at 623 K. Solid lines are original fourier transforms and dashed lines are the Pt-Pt, Pt-Pd fitted contributions for Pt L_{III} edge (11564 eV) and Pd-Pd, Pd-Pt fitted contributions for Pd K edge (24365 eV).

Table 4. Fitted values from the EXAFS spectra for the Pt-Pd catalysts: coordination number (CN), radial distance (r) and Pd:Pt ratio in the bimetallic clusters[1].

Catalyst	Edge	Pt-Pt		Pt-Pd		Pd-Pt		Pd-Pd		Pd:Pt ratio[1]
		CN	r (Å)	CN	r (Å)	CN	r (Å)	CN	r (Å)	
Pt-Pd(1)	Pt L_{III}	7.63	2.73	3.60	2.71					1.55
	Pd K					2.32	2.71	4.31	2.70	
Pt-Pd(2)	Pt L_{III}	3.62	2.68	3.88	2.63					1.34
	Pd K					2.90	2.63	2.80	2.70	
Pt-Pd(3)	Pt L_{III}	6.91	2.74	3.59	2.71					1.23
	Pd K					2.93	2.71	4.37	2.73	

[1] Pd:Pt ratio determined as CN_{Pt-Pd}:CN_{Pd-Pt}. This values correspond to the composition of the bimetallic cluster not to the overall Pd:Pt ratio of 3 as determined by atomic absorption spectroscopy.

The hole density in the $5d_{5/2}$ and $5d_{3/2}$ state is reflected in the white line intensity of the Pt L_{III} edge because both, $2p_{3/2}$ to $5d_{3/2}$ and $2p_{3/2}$ to $5d_{5/2}$ electronic transitions are allowed at the Pt L_{III} edge. Thus, the electronic effects of alloying Pt and Pd are evident in the X-ray absorption near edge structure (XANES) at the Pt L_{III} edge as shown in Figure 2. The increase of the white line height in the XANES at Pt L_{III} edge indicates a lower electron density of Pt in the bimetallic Pt-Pd nanoclusters compared to bulk Pt [33]. Correspondingly, a slight decrease of white line intensity at Pd K edge is observed in Figure 3, suggesting that the electron density was transferred from Pt to Pd in the Pt-Pd nanoclusters. The change in Pd K edge is not pronounced probably due to the nature of the electronic transition (from s to p orbitals). A more rigorous analysis of the XANES can be done by comparing the relative intensity of empty states at the Fermi level of the materials. This relative intensity is determined by subtracting the intensity of the absorption edge fitted by a sigmoidal function from the corresponding near-edge X-ray absorption fine structure [34]. The white line intensities above Pt

L_{III} edges and Pd K edge for Pt-Pd catalysts are summarized in Table 5. Pt-Pd(2) has the highest white intensity above Pt L_{III} edge, indicating that the Pt atoms in the Pt-Pd nanoclusters of Pt-Pd(2) are the most electron deficient among the catalysts studied. On the other hand, the white line intensity above Pd K edge of Pt-Pd(2) revealed the lowest value, which confirms the highest amount of electron density transfer from Pt to Pd atoms within the Pt-Pd cluster. Comparatively, the white line intensities above Pt L_{III} and Pd K edge showed that Pt-Pd(1), prepared by metal precursors with different cations, i.e., $[Pt(NH_3)_4]^{2+}$ and Pd^{2+}, has less intense electron transference from Pt to Pd than Pt-Pd(2) (prepared from $[Pt(NH_3)_4]^{2+}$ and $[Pd(NH_3)_4]^{2+}$ cations). Adding NH_4OH to the precursor solution increases the Pt electron deficiency when cations of different nature are used as it can be observed for Pt-Pd(3).

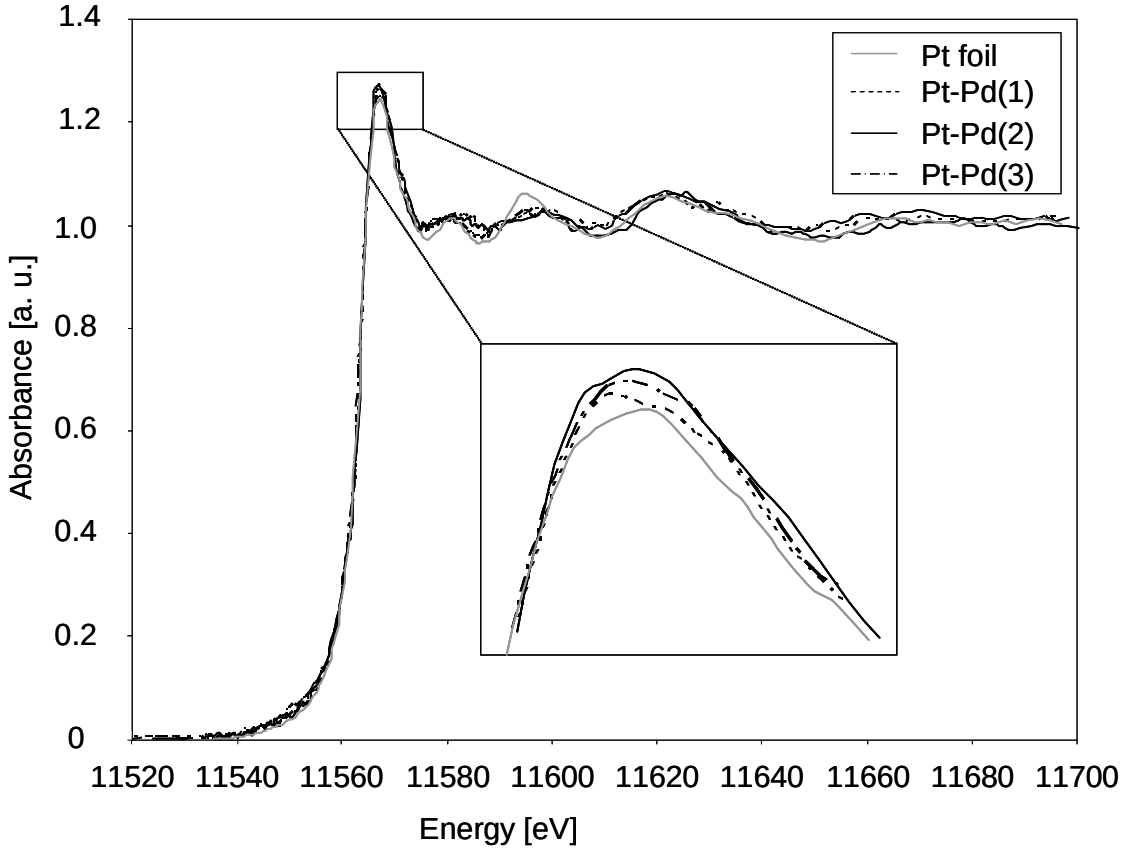

Figure 2. Normalized XANES at the Pt L_{III} edge in He at 623 K of Pt foil and Pt-Pd catalysts after in situ reduction in H_2 at 623 K.

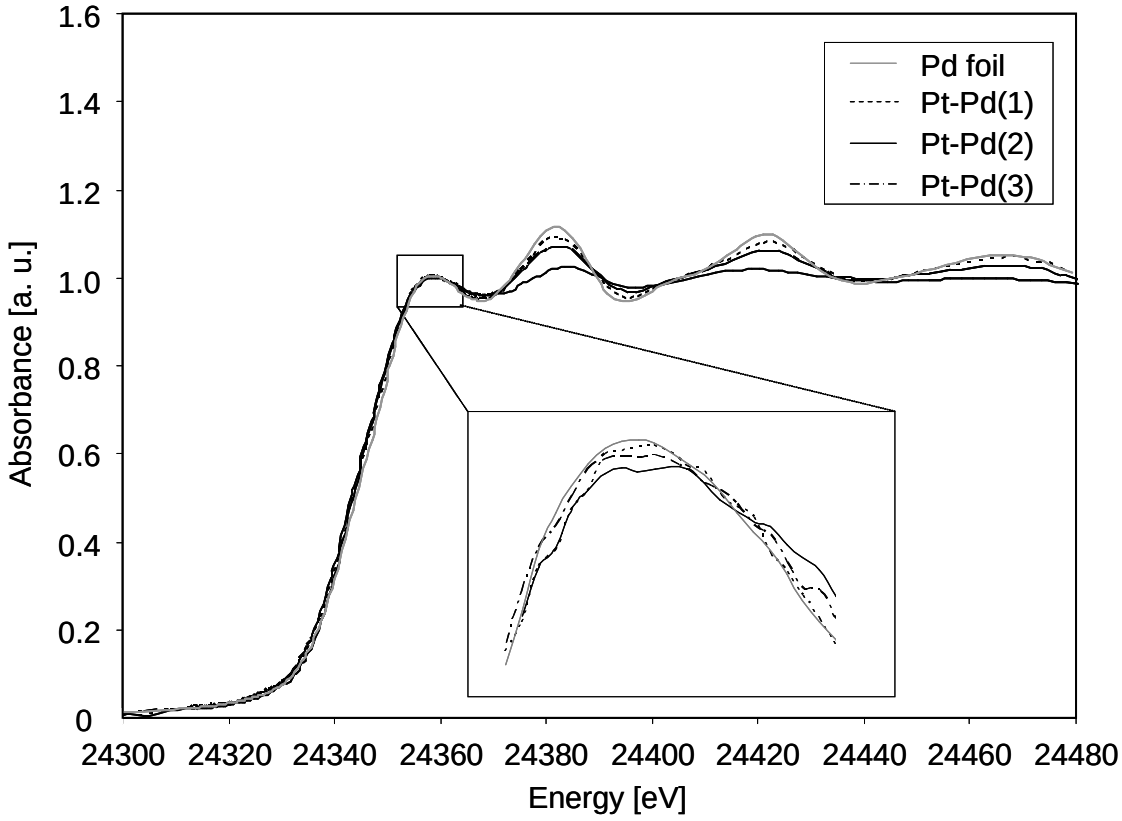

Figure 3. Normalized XANES at the Pd K edge in He at 623 K of Pd foil and Pt-Pd catalysts after in situ reduction in H_2 at 623 K.

Table 5. White line intensities above Pt L_{III} edge and Pd K edge for the Pt-Pd catalysts.

Catalyst	White line intensity (a. u.)	
	above Pt L_{III} edge	above Pd K edge
Pt-Pd(1)	1.48	0.84
Pt-Pd(2)	1.69	0.81
Pt-Pd(3)	1.55	0.83
Pt foil	1.27	-
Pd foil	-	0.88

The Pt-Pd nanoparticles were further characterized by CO adsorption IR experiments of the reduced samples (spectra presented in Fig. 4). Bands observed above 2050 cm^{-1} are assigned to linearly adsorbed CO on Pt and Pd [35]. In these bands, the signals of CO linearly bonded to Pt and to Pd overlap. After evacuation, the intensity of the bands decreased and the position of the maxima shifted to lower wave numbers. The decreasing intensity and maxima position shifting were attributed to a decrease of the CO surface coverage due to desorption of CO from Pd [36]. Thus the bands produced by adsorption of CO on Pt and Pd can be differentiated by comparing the spectra before and after evacuation.

Broad bands observed below 2000 cm^{-1} in the spectra of the bimetallic Pt-Pd materials were assigned to CO adsorbed in a bridged form on Pd atoms (the exact band position is shown in Figure 4) [37]. The bands at 1860-1920 cm^{-1} were assigned to Pd_2-CO complexes or CO adsorbed on a defect-rich terraces [35,38], whereas bands at frequencies between 1950 and 1990 cm^{-1} originated from dimeric $[Pd_2\text{-}CO]_2$ species or CO adsorbed on edges of aggregates [35,36]. Note that the bands assigned to dimeric $[Pd_2\text{-}CO]_2$ species can only be present if there are at least four adjacent Pd atoms on the cluster surface.

It is clear seen that the spectra of Pt-Pd(1) before evacuation has a band at 1980 cm^{-1} while there is nearly no CO adsorption at the same wavenumber for Pt-Pd(2). This qualitatively indicates a relative higher proportion of surface Pd in Pt-Pd(1) than in Pt-Pd(2). The bands in the region 1860-1920 cm^{-1} remained almost unchanged after evacuation probably due to the conversion of $[Pd_2\text{-}CO]_2$ to monomeric Pd_2-CO during the CO desorption.

The normalized integrated peak areas of linearly and bridged adsorbed CO at 0.5 mbar and after evacuation for 15 minutes are shown in Table 6. The Pt-Pd (2) catalyst had the highest ratio of linear to bridged adsorbed CO (1.78 and 1.34 before and after evacuation, respectively) and the highest intensity of linearly adsorbed CO (2060-2110 cm^{-1}) before and after evacuation. Both observations indicate the lowest concentration of surface Pd atoms, and consequently the highest concentration of Pt atoms on the Pt-Pd cluster surface. The Pt-Pd(1)

sample had the smallest value of linear to bridged adsorbed CO (1.36 after CO adsorption at 0.5 mbar and 1.12 after evacuation for 15 min), suggesting that the bimetallic cluster surface was Pd enriched compared with Pt-Pd(2). The linear to bridged adsorbed CO ratio of Pt-Pd(3) had medium valuesfor the linear to bridged adsorbed CO ratios compared to those of Pt-Pd(1) and Pt-Pd(2).

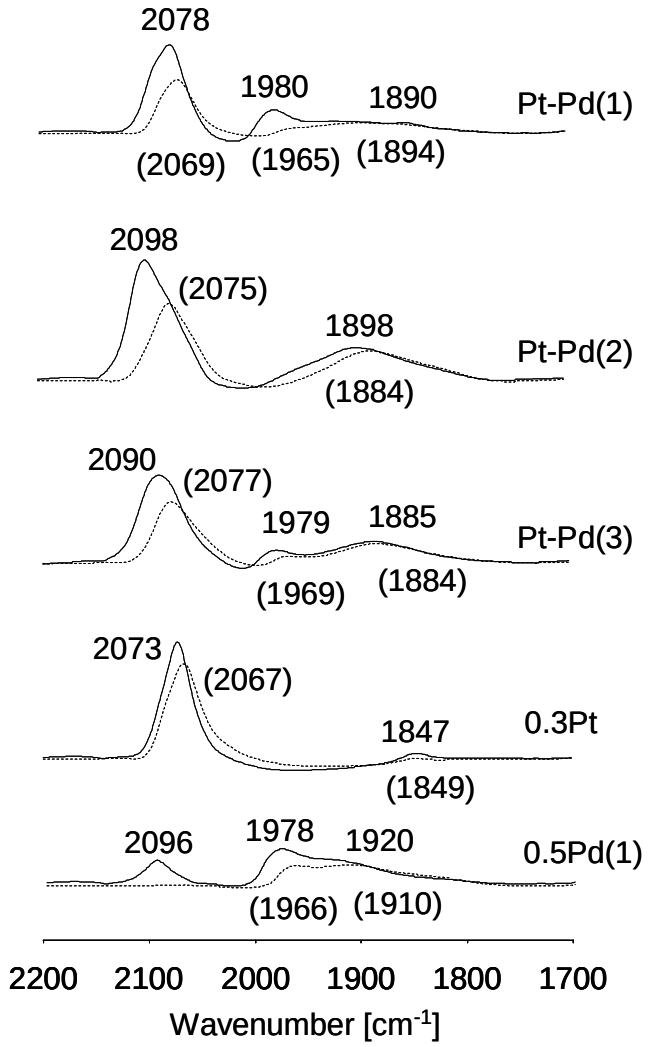

Figure 4. IR spectra of CO adsorbed on bimetallic Pt-Pd catalysts and monometallic Pt and Pd catalysts at T = 40 ºC, $p_{(CO)} = 5 \cdot 10^{-1}$ mbar (continuous lines) and after evacuation for 15 min (dashed lines, band values in brackets).

Table 6. Summary of weight normalized integrated peak areas of linearly and bridged adsorbed CO on the Pt-Pd catalysts at 0.5 mbar and after evacuation for 15 minutes at $5 \cdot 10^{-6}$ mbar (in brackets).

Catalyst	Linearly adsorbed CO (2060-2110 cm^{-1})	Bridged adsorbed CO (1840-1990 cm^{-1})	Ratio of linearly to bridged adsorbed CO
Pt-Pd(1)	929 (578)	682 (514)	1.36 (1.12)
Pt-Pd(2)	1310 (877)	737 (653)	1.78 (1.34)
Pt-Pd(3)	1059 (740)	662 (609)	1.60 (1.22)
0.3Pt	718 (714)	42 (13)	17.1 (54.9)
0.5Pd(1)	131 (23)	612 (529)	0.21 (0.04)

3.4. Temperature programmed reduction

The profiles of H_2S evolution during TPR of H_2S-pretreated catalysts are shown in Fig. 5. For the ASA support, two signals were observed, one with maximum at 507 K and another broad one starting from 650 K. Monometallic 0.8Pt and 0.3Pt samples showed 3 peaks at 506, 579, 692 K and at 505, 583, 695 K, respectively. Comparing those signals with the profile of the ASA support, the peaks in the ranges 500-510 K and 690-700 K were assigned to H_2S releasing from the support. The bands at 579 and 583 K were assigned to H_2S releasing from Pt. For monometallic 0.5Pd(2), the notably intensity of the signal at 478 K suggests that this peak was produced by H_2S released from sulfided Pd overlapping with the low-temperature signal from ASA support since they were generated at close temperatures. From the comparison of the TPR profiles of the monometallic catalyst it is concluded that the low temperature intense signal is associated with Pd, whereas the low-intensity signal produced at higher temperatures (just between the signals attributed to H_2S evolution from the support) is attributed to H_2S released from Pt. For the three bimetallic Pt-Pd catalysts, all signals shifted compared with those for ASA support or the monometallic counterparts. However, the characteristic shape and position of the peaks allow assigning all the peaks e.g., high intensity, low temperature signal for H_2S desorbing from Pd and broad

high temperature signals for H_2S released from the support. The peaks at 499, 486 and 487 K for Pt-Pd(1), Pt-Pd(2) and Pt-Pd(3), respectively have the contribution of H_2S desorbing from the support (relatively minor contribution) and from Pd. The shoulders at 561, 546 and 548 K are attributed to H_2S released from Pt given its low intensity and intermediate position.

It is expected the formation of metal sulfide covering the metal particles during the treatment in H_2S. Although, it is not possible to determine the thickness of the sulfide layer, the temperature of H_2S release reflects unequivocally the strength of the sulfur-metal bond. Thus, from the temperature shifts observed in the TPR experiments we can infer that the Pt-S bond cleavage is easier in the bimetallic catalysts than in the monometallic sample. Furthermore, the Pd-S bond seems to be strengthened although this effect is less noticeable. The shift of the H_2S release peak from the support to lower temperatures in the presence of metal particles strongly suggests the activation of H_2 in the metal and spillovering to the carrier.

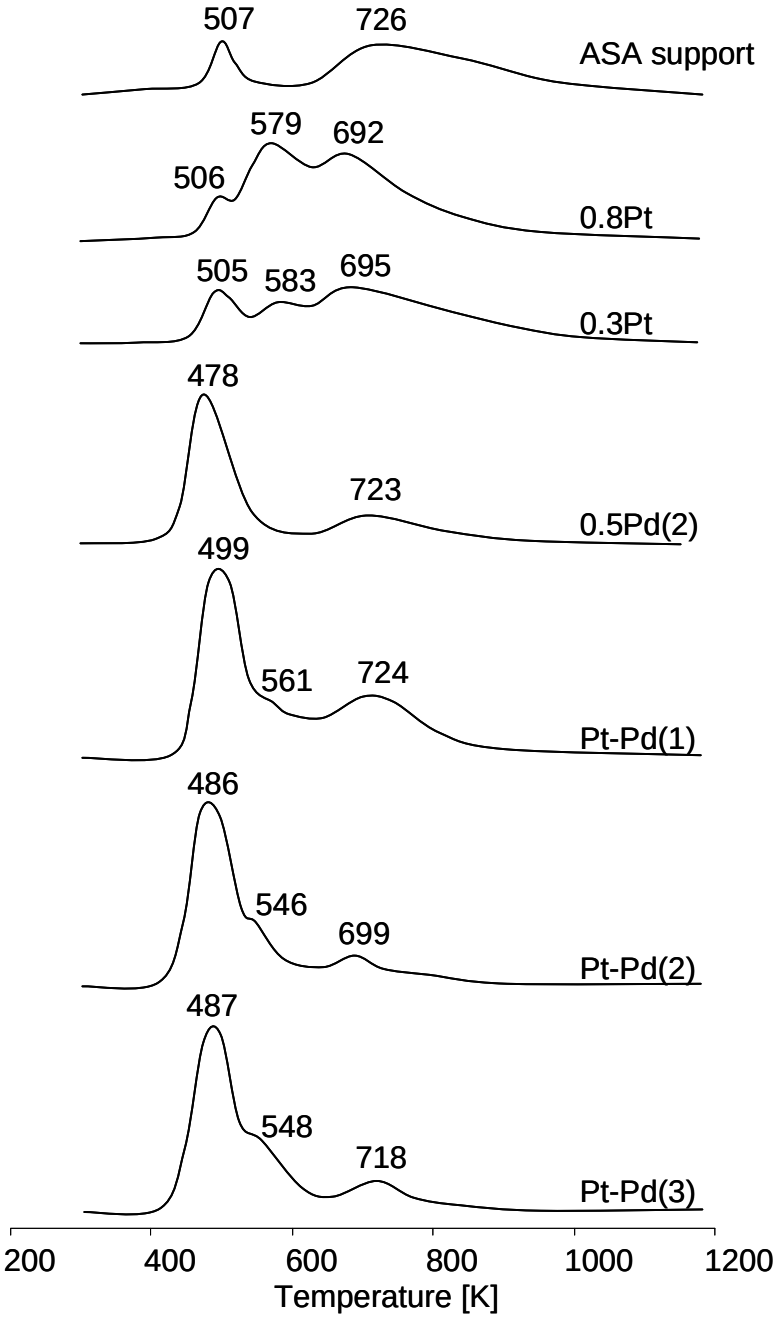

Figure 5. H_2S profiles during temperature programmed reduction of pre-sulfided ASA support and Pt, Pd, Pt-Pd catalysts.

3.5. Catalytic activity

The hydrogenation of tetralin in the absence of poisons was carried out in the temperature range of 533-593 K. The catalytic activities at steady-state after 24 h TOS for different temperatures are summarized in Fig. 6. The catalyst with 0.8 wt.% Pt on ASA exhibited the highest activity while the Pd catalysts were the least active in line with the fact that Pt is more active than Pd for hydrogenation of aromatics [39]. The activities of the bimetallic Pt-Pd catalysts follows the decreasing order Pt-Pd(2) > Pt-Pd(3) > Pt-Pd(1), which is in line with the decreasing content of surface Pt as suggested by the characterization results. Figure 7 shows the *cis*/*trans* decalin ratio over all catalysts. On monometallic Pt catalysts the highest selectivity to *cis*-decalin was observed, while the *trans*-decalin isomer was preferred on Pd catalysts. The c*is*- to *trans*-decalin ratios on bimetallic Pt-Pd catalysts were intermediate compared to the values obtained on Pt and Pd catalysts; with a marked preference, however, for trans-decalin.

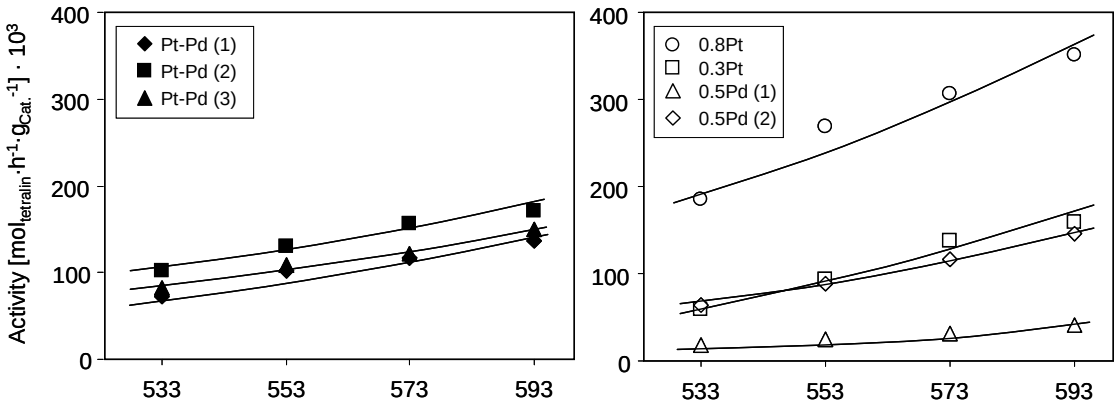

Figure 6. Activities at steady state for the hydrogenation of tetralin in the temperature range 533-593 K over Pt, Pd and Pt-Pd catalysts.

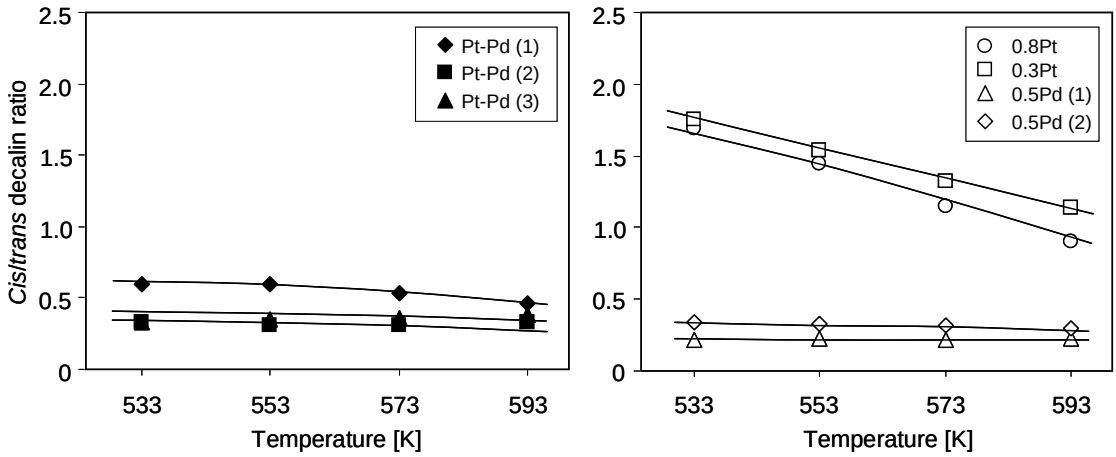

Figure 7. *Cis/trans* decalin ratios for the hydrogenation of tetralin in the temperature range 533-593 K over Pt, Pd and Pt-Pd catalysts.

The activities of the catalysts decreased when 400 ppm of nitrogen in form of quinoline was present in the reaction (see Fig. 8). The trend of activities was similar to that for poison-free feed the Pt catalysts being the most active; however, the difference between the activities of the different catalysts was smaller. The *cis-/trans*-decalin ratios (see Fig. 9) in the presence of quinoline followed the same trend observed when using poison-free feed. The monometallic Pt catalysts yielded to the highest cis-/trans-decalin ratios whereas the trans-decalin isomer is preferred on the rest of the catalysts, especially on monometallic Pd catalysts.

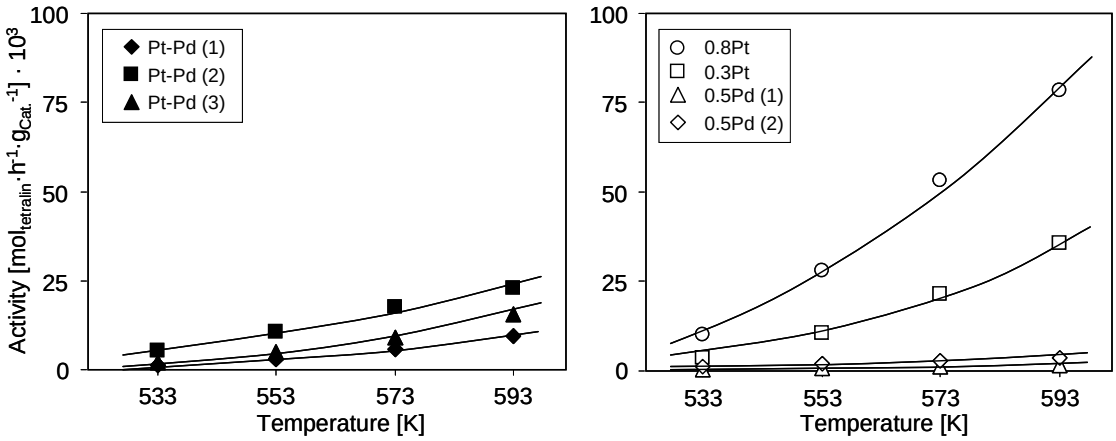

Figure 8. Activities at steady state for the hydrogenation of tetralin in the presence of quinoline (400 ppm N) in the temperature range 533-593 K over Pt, Pd and Pt-Pd catalysts.

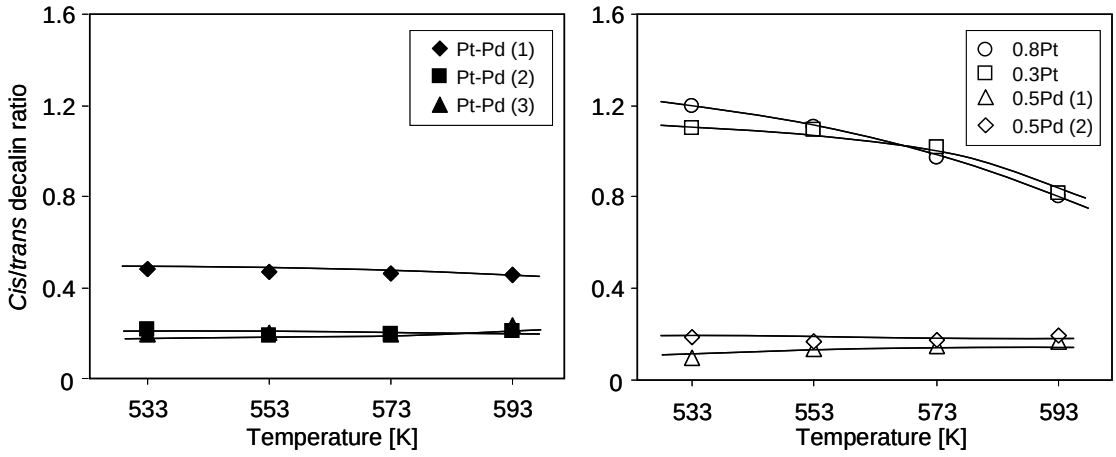

Figure 9. *Cis/trans* decalin ratios for the hydrogenation of tetralin in the presence of quinoline (400 ppm N) in the temperature range 533-593 K over Pt, Pd and Pt-Pd catalysts.

The activities for the hydrogenation of tetralin in the presence of DBT (100 ppm S) at steady-state are summarized in Fig. 10. In contrast to the activity trend observed for poison-free and N-containing feed, in the presence of sulfur the bimetallic Pt-Pd(2) catalyst becomes the most active catalyst, followed by Pt-Pd(3) > 0.8Pt > Pt-Pd(1) > 0.3Pt > 0.5Pd(2) > 0.5Pd(1). Interestingly, the activity of the monometallic catalysts was completely abated. The c*is*/*trans*-decalin ratios observed in the presence of DBT are shown in Fig. 11, the values are smaller than those observed using poison-feed feed. However, the trend is preserved, i.e., the monometallic Pt catalysts still showed the highest c*is*- to *trans*-decalin ratio.

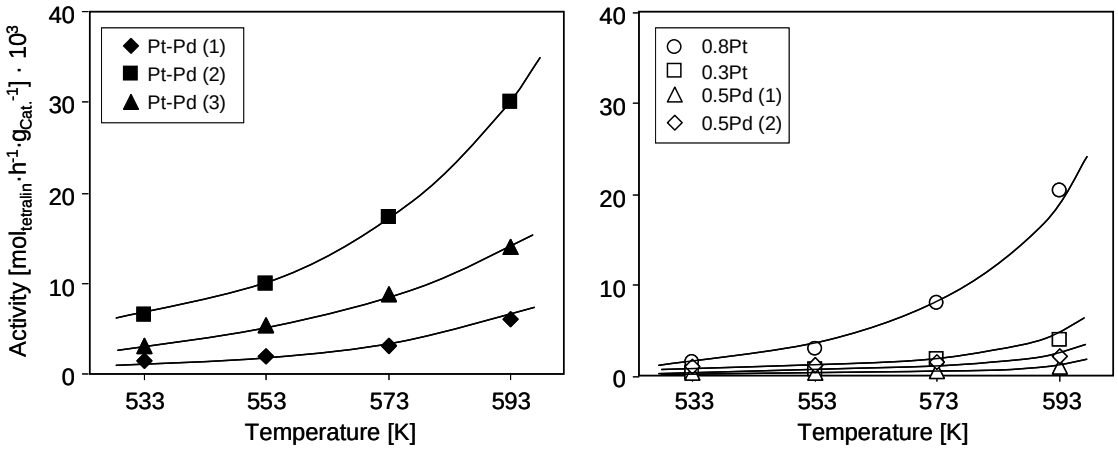

Figure 10. Activities at steady state for the hydrogenation of tetralin in the presence of DBT (100 ppm S) in the temperature range 533-593 K over Pt, Pd and Pt-Pd catalysts.

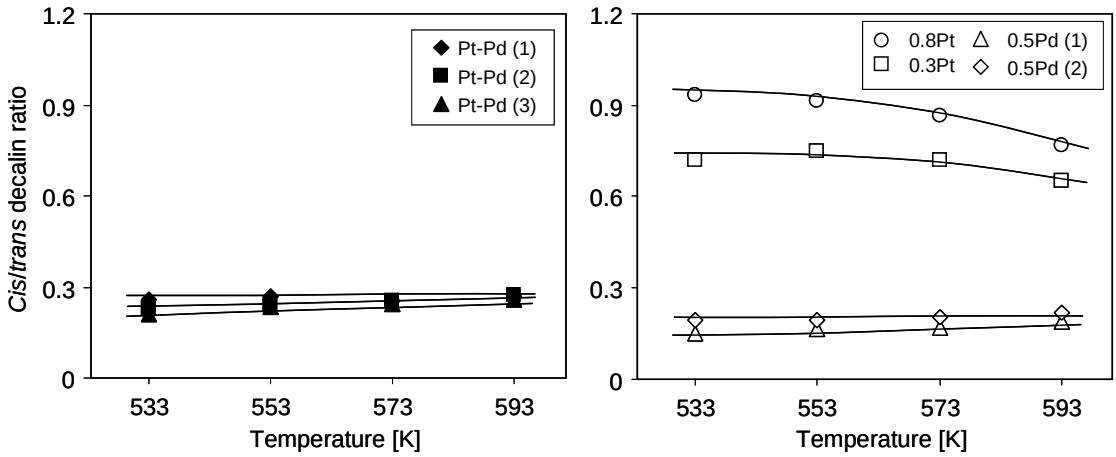

Figure 11. *Cis/trans* decalin ratios for the hydrogenation of tetralin in the presence of DBT (100 ppm S) in the temperature range 533-593 K over Pt, Pd and Pt-Pd catalysts.

The tetralin hydrogenation activities in the presence of both N- and S-poison are shown in Fig. 12. A dramatic decrease in activity was found compared to the reaction in absence of poisons. It is worth highlighting the significant increase in activity between 573 and 593 K. The Pt-Pd(2) catalyst has the best performance in tetralin hydrogenation in the presence of quinoline and DBT. For the rest of the catalysts the activity followed the decreasing trend Pt-Pd(3) > 0.8Pt > Pt-Pd(1) > 0.3Pt > 0.5Pd(2) > 0.5Pd(1). Interestingly, the presence of both poisons reduced the temperature dependence of the cis-/trans-decalin ratio as shown in Figure 13. The Pt samples yielded a cis-/trans-decalin ratio around 0.6, while the observed ratios are below 0.15 and 0.25 for Pd and Pt-Pd materials, respectively.

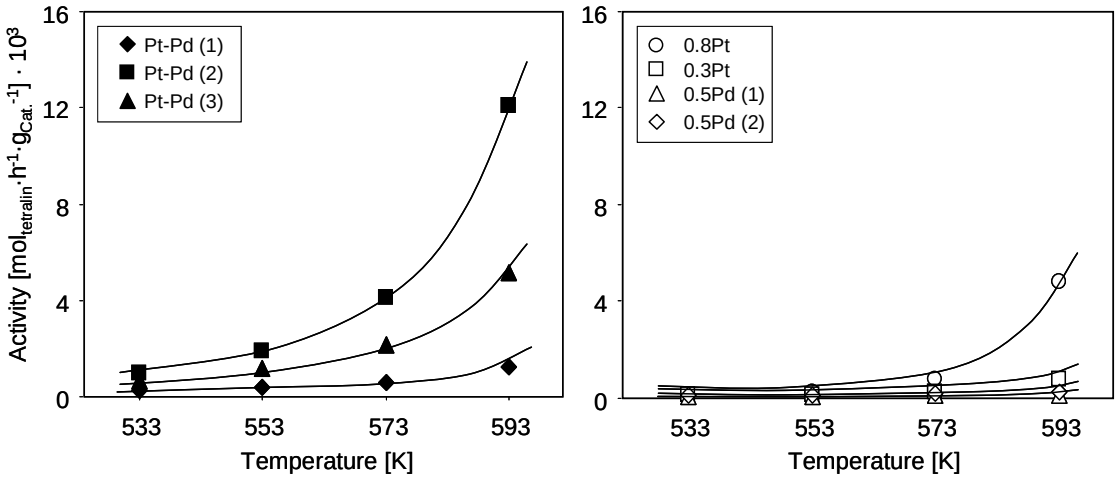

Figure 12. Activities at steady state for the hydrogenation of tetralin in the presence of quinoline (20 ppm N) and DBT (100 ppm S) in the temperature range 533-593 K over Pt, Pd and Pt-Pd catalysts.

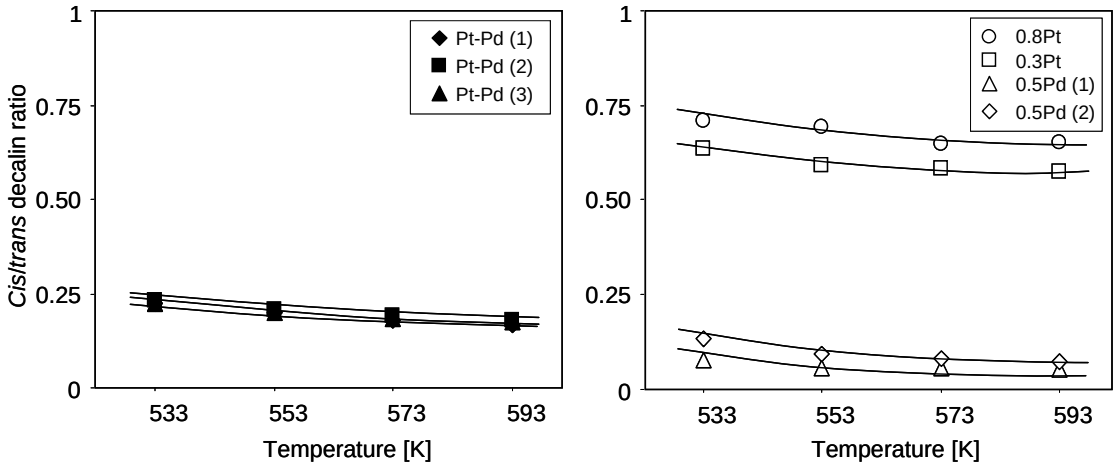

Figure 13. *Cis/trans* decalin ratios for the hydrogenation of tetralin in the presence of quinoline (20 ppm N) and DBT (100 ppm N) in the temperature range 533-593 K over Pt, Pd and Pt-Pd catalysts.

4. Discussion

4.1. Structure of the Pt-Pd nanoclusters

The large number of parameters involved in the synthesis of catalytic materials makes it difficult to describe the specific effect of each variable. However, some synthesis parameters are determining for the structure of the end active phases. For instance, the simple choice of the precursor may define the properties of the catalyst. In this study, it is shown that using different noble metal precursors and changing the pH of the impregnated solution greatly influences the structure of the Pt-Pd nanoclusters in the catalysts.

The bimetallic Pt-Pd catalysts reveal similar metal particle size (1.1-1.37 nm) than the monometallic Pt catalysts (1.04-1.29 nm). The metal particle size of Pd catalysts was larger than in the other formlations (1.39-1.51 nm). For all the bimetallic catalysts studied in this work the sum of the total coordination number of Pt (CN_{Pt-Pt} + CN_{Pt-Pd}) is higher than the coordination number of Pd (CN_{Pd-Pd} + CN_{Pd-Pt}). The difference indicates that Pd is located preferentially in the outer layers of the clusters because in a bimetallic nanocluster the total coordination numbers of the elements must be equal if the metals are homogeneously distributed. The difference in the coordination numbers greatly differs among the catalysts. Comparing the catalysts Pt-Pd(1) and Pt-Pd(2), it is clear that in the former, the proportion of surface Pd is higher than in the later as seen from the larger difference in total coordination numbers i.e., 11.23 - 6.63 and 7.5 - 5.7 for Pt-Pd(1) and Pt-Pd(2), respectively. For the catalyst Pt-Pd(3), the difference in coordination numbers is 10.5 – 7.3, which points to Pt and Pd distributions with an intermediate homogeneity compared to the other bimetallic catalysts.

The molar fractions of the elements (x_A and x_B) and the corresponding coordination numbers in a bimetallic cluster must fulfill the simple condition ($CN_{AB} \cdot x_A = CN_{BA} \cdot x_B$) [40]. Using this expression it is possible to obtain the mass balance expressed in Equation (1) for the bimetallic Pt-Pd clusters as was done in Ref. [14].

$$CN_{Pt-Pd} \cdot N_{Pt} = CN_{Pd-Pt} \cdot N_{Pd} \qquad (1)$$

Equation (1) can be used to calculate the molar ratio of Pd:Pt of the bimetallic Pt-Pd nanoclusters since CN_{Pt-Pd} and CN_{Pd-Pt} are known from the EXAFS fittings. The calculated Pd:Pt ratios are shown in Table 4, all the Pd:Pt ratios are smaller than 3, (the bulk molar ratio) indicating that besides the bimetallic Pt-Pd nanoclusters, a fraction of monometallic Pd nanoparticles has to be also present in the Pt-Pd catalyst. The Pt-Pd(1) catalyst has a Pd:Pt ratio of 1.55, which is higher than that of Pt-Pd(2) (Pd:Pt = 1.34). Thus the former catalyst has higher concentration of Pd in the Pt-Pd clusters. The catalyst Pt-Pd(3) had the lowest Pd:Pt ratio (1.28) indicating that the bimetallic clusters of this catalyst contain the highest proportion of Pt among the studied catalysts.

The study of CO adsorption IR spectroscopy confirms the results of EXAFS analysis. Table 6 shows the normalized integrated peak areas of linearly and bridged adsorbed CO at 0.5 mbar and after evacuation for 15 minutes. The Pt-Pd(2) catalyst had the highest ratio of linear to bridged adsorbed CO before and after evacuation, indicating the lowest concentration of surface Pd atoms among the three Pt-Pd samples. On the other hand, the Pt-Pd(1) sample had the smallest value of linear to bridged adsorbed CO, suggesting that the bimetallic cluster surface was Pd enriched compared with the other two Pt-Pd catalysts. The linear to bridged adsorbed CO ratio of Pt-Pd(3) was in-between the values of Pt-Pd(1) and Pt-Pd(2), implying that more Pt atom are present on the cluster surfaces when NH_4OH is added to the precursor solution. However, the highest proportion of Pt is reached when using Pt, Pd precursors with NH_3 ligands, i.e., $[Pt(NH_3)_4]^{2+}$, and $[Pd(NH_3)_4]^{2+}$.

It is possible to find values for the molar extinction coefficients of CO adsorbed on Pt or Pd [41,42]. Unfortunately, it is difficult to compare the values as they have been obtained following different methodologies and reported in different dimensions. To quantitatively estimate the Pd/Pt proportion on the surface we have determined the values for k_{Pt-L} and k_{Pd-L} from the H_2-chemisorption and IR characterization of the monometallic catalysts as follows.

The number of surface Pd and Pt atoms is obtained according to Equations (2) and (3) assuming that the concentration of adsorbed CO is given by the relation

nA_i/k_i. n is the number of metal atoms that each CO molecule "counts", A_i is the absorbance of CO adsorbed in a defined mode on Pt or Pd and k_i is the corresponding molar extinction coefficient.

$$\mathrm{Pd} = \frac{2A_{Pd-B}}{k_{Pd-B}} + \frac{A_{Pd-L}}{k_{Pd-L}} \qquad (2)$$

$$\mathrm{Pt} = \frac{2A_{Pt-B}K_{Pt}}{k_{Pt-B}} + \frac{A_{Pt-L}}{k_{Pt-L}} \qquad (3)$$

The absorbance values needed in Equations (2) and (3) are extracted from Table 6 considering that the absorbance of linearly adsorbed CO corresponds to the integrated peak area determined in the range 2060-2110 cm^{-1}, whereas the absorbance of CO adsorbed in the bridge mode corresponds to the area of the bands in the 1840-1990 cm^{-1} range. Assuming that the number of surface metals atoms is twice the monolayer of H_2 dissociatively chemisorbed, the numeric substitution of Equations (2) and (3) leads to Equations (4) and (5), respectively (the values are already normalized per gram of material).

$$35.0\ \mu\mathrm{mol} = \frac{2(612)}{k_{Pd-B}} + \frac{131}{k_{Pd-L}} \qquad (4)$$

$$13.3\ \mu\mathrm{mol} = \frac{2(42)}{k_{Pt-B}} + \frac{718}{k_{Pt-L}} \qquad (5)$$

Considering that ($k_{i\text{-}L}/k_{i\text{-}B}$)=2.5, according to [35], Equations (6) and (7) are obtained.

$$35.0\ \mu\mathrm{mol} = \frac{3060}{k_{Pd-L}} + \frac{131}{k_{Pd-L}} \qquad (6)$$

$$13.3\ \mu\mathrm{mol} = \frac{210}{k_{Pt-L}} + \frac{718}{k_{Pt-L}} \qquad (7)$$

After solving simultaneously Equations (6) and (7), the values 91.2 and 69.8 $cm^{-1}\cdot\mu mol^{-1}$ are obtained for $k_{Pd\text{-}L}$ and $k_{Pt\text{-}L}$, respectively. Hence, the ($k_{Pt\text{-}L}/k_{Pd\text{-}L}$) ratio determined from the characterization of the monometallic catalysts is 0.76. Using this ratio and the integrated areas of the spectra of bimetallic catalysts (Table 4) in Equation (8), it is possible to estimate the Pt and Pd proportion in the surface [14]. The (Pd/Pt) surface ratios corresponding to the Pt-Pd(1), Pt-Pd(2), Pt-Pd(3) are 3.8, 3.2 and 3.5, respectively, showing that Pt-Pd(2) has the highest Pt proportion on the Pt-Pd nanocluster surfaces.

$$\frac{\mathrm{Pd}}{\mathrm{Pt}} = \frac{k_{Pt-L}}{k_{Pd-L}} \frac{5A_{Pd-B}+A_{Pd-L}}{A_{Pt-L}} \qquad (8)$$

Schematic models of Pt-Pd nanoparticles of the three Pt-Pd catalysts are present in Fig. 14. The coordination numbers of the models are in good agreement with the values of the EXAFS fitting in Table 4 except for CN_{Pd-Pd}, which is met only including the presence of some monometallic Pd clusters in the three catalysts. In the catalyst Pt-Pd(1) the Pt atoms concentrate in the core and are almost covered by a Pd-shell. The core-shell structure, however, is not perfect allowing few Pt to be exposed. The average bimetallic cluster in the Pt-Pd(2) catalyst is rather different. The Pd and Pt alternate almost randomly although Pd still tends to the outer layer. The Pt-Pd(3) catalyst has an intermediate morphology with Pd strongly segregating to the surface but preserving higher Pt exposure than in Pt-Pd(1).

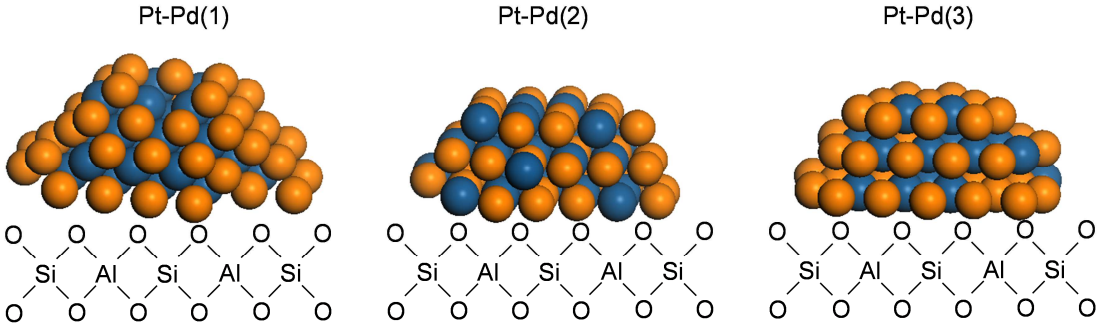

Figure 14. Model of Pt-Pd clusters of Pt-Pd(1), Pt-Pd(2) and Pt-Pd(3) catalysts.

4.2. Effect of the cations in the metal precursors on the morphology of the bimetallic clusters

The behavior of different cations during thermal treatments should be discussed first to account for an explanation of the change in structure of Pt-Pd nanoclusters by varying the metal precursors (e.g. $Pt(NH_3)_4]^{2+}$ with $[Pd(NH_3)_4]^{2+}$ or Pd^{2+}) and the pH of the precursor solution.

It has been reported that on silica and alumina, the autoreduction mechanism takes place involving surface oxygen [43-45]. Let us consider the $[Pt(NH_3)_4]^{2+}$ cation as example. This ammino complex may decompose to platinum oxide and then the ammonia released can reduce the oxide as illustrated in reactions (i)

and (ii) [44]. Another possible route for the formation of ammonia able to reduce cationic Pt is the formation of neutral platinous oxydiammine followed by the complete elimination of ammonia, reaction (iii) [45]. The autoreduction of noble metal salts with NH_3 ligands has also been observed on zeolites [46-49]. In this case, the mechanism of autoreductioon is claimed to involve the transference of protons to the support. The ASA support may either donate oxygen or accept protons. Thus, it is likely that both mechanisms occur.

$O^* + Pt(NH_3)_x \rightarrow PtO + xNH_3$ (i)

$3PtO + 2NH_3 \rightarrow 3\,Pt + 3H_2O + N_2$ (ii)

$[Pt(NH_3)_4]^{2+} + 2OH^* \rightarrow Pt(NH_3)_2O + H_2O + 2NH_3$ (iii)

If precursors of different nature, e.g. $[Pd(NH_3)_4]^{2+}$ and Pd^{2+} are used to synthesize Pt-Pd nanoclusters, they behave different during the thermal treatment in air and H_2. Starting the synthesis from metal precursors with the same NH_3 ligands ensures that the cations follow similar decomposition processes in each thermal treatment.

Let us comment in detail the case of the catalyst Pt-Pd(1), which was prepared from $[Pt(NH_3)_4](NO_3)_2$ and $Pd(NO_3)_2$ (see Table 1). The pH of the impregnation solution (pH = 2.0) is lower than the point of zero charge (PZC) of any of the possible oxide domain available for deposition, i.e., SiO_2 (PZC=2-3.5), Al_2O_3 (PZC=8-9), ASA (PZC=4-5), therefore, the support surface is positively charged [50,51]. Consequently, the incorporation of the cationic species $Pt(NH_3)_4^{2+}$ and Pd^{2+}) to the surface is likely to occur via an ion-exchange mechanism than via electrostatic adsorption [52]. Due to the stability of the platimun tetraamine complex and slow substitution of ammonia ligands, $Pt(NH_3)_{4-n}(H_2O)_n^{2+}$ cations are hardly formed, and the $Pt(NH_3)_4^{2+}$ complex adsorbs on the support surfaces without ligand exchange [53,54]. Hence free NH_3 in solution must not be available for the formation of $[Pd(NH_3)_x]^{2+}$ from Pd^{2+} cations in the precursor solution. During thermal treatment in air, the $[Pt(NH_3)_4]^{2+}$ ions decompose and Pt^0 nuclei are formed according to the autoreduction mechanisms described above. The Pd^{2+} ions would not be affected during the treatment in air and only reduced to Pd^0 during the treatment in H_2. During this reduction step, the Pd^0

atoms surround the already formed Pt nuclei, leading to Pt-Pd nanoparticles with a “Pt-core Pd-shell” structure.

When using the solution of $[Pt(NH_3)_4](NO_3)_2$ and $[Pd(NH_3)_4](NO_3)_2$ (Table 1) to prepare the Pt-Pd(2) catalyst, $[Pt(NH_3)_4]^{2+}$ and $[Pd(NH_3)_4]^{2+}$ complexes behave similarly during the preparation procedures [46]. The precursor solution had the pH value of 7.7, that is, higher than the PZC of ASA and SiO_2 but lower than the PZC of alumina. Thus, the ASA surface may exhibit a mixture of negatively and positively charged domains. On the former regions, $[Pt(NH_3)_4]^{2+}$ and $[Pd(NH_3)_4]^{2+}$ cations are adsorbed by means of electrostatic interactions [55]. On the positively charged Al_2O_3 domains, ion exchange has to be preferred over electrostatic adsorption. However, the proportion of Al_2O_3 domains must be low, since the ASA materials contains 30 wt.% Al_2O_3 and most of the Al cations are expected to be homogeneously dispersed in the material [56]. $[Pt(NH_3)_4]^{2+}$ and $[Pd(NH_3)_4]^{2+}$ cations may autoreduce at similar rate during the treatment in air and be completely reduced in H_2, forming Pt-Pd nanoclusters with more homogeneous distribution of Pt and Pd atoms in the clusters. Probably due to the high Pd to Pt ratio (Pd:Pt = 3), not all Pd alloyed with Pt and the formation of some monometallic Pd nanoparticles takes place.

The catalyst Pt-Pd(3), was prepared using the precursors $[Pt(NH_3)_4](NO_3)_2$ and $Pd(NO_3)_2$ as was done for the Pt-Pd(1) catalyst. The pH of the mixture, however, was changed to 7.7 by adding NH_4OH solution. According to the literature, Pd^{2+} cations react with NH_4^+ groups in ammonia solutions as shown in reaction (iv) [57]. Thus the preparation of aqueous solutions of $Pd(NO_3)_2$ and $[Pt(NH_3)_4](NO_3)_2$ in the presence of ammonia actually leads to a mixture of Pd^{2+}, $[Pd(NH_3)_n]^{2+}$ and $[Pt(NH_3)_4]^{2+}$. At pH of 7.7, these cations interact with the support in a similar way as described for the sample Pt-Pd(2), i.e., mostly through electrostatical adsorption. During thermal treatment in air, $[Pt(NH_3)_4]^{2+}$ and formed $[Pd(NH_3)_n]^{2+}$ ions would behave as was described for the case of the Pt-Pd(2) catalyst leading to bimetallic particles with higher homogeneity than the catalyst Pt-Pd(1). The incorporation of NH_3 groups may not be complete ($n<4$) and therefore, the reducibility of the $[Pd(NH_3)_n]^{2+}$ ion may not be identical to that of $[Pt(NH_3)_n]^{2+}$.

Hence, the distribution of Pt and Pd is then less homogenous than in the case of Pt-Pd(2).

$Pd^{2+} + nNH_4^+ \rightarrow [Pd(NH_3)_n]^{2+} + H^+, \qquad 0 \leq n \leq 4 \qquad (iv)$

In order to explore the different behavior of Pd^{2+}, $[Pd(NH_3)_4]^{2+}$ and $[Pt(NH_3)_4]^{2+}$ during thermal treatment in air, the 0.5Pd(1), 0.5Pd(2) and 0.8Pt catalyst precursors were investigated using CO adsorption IR spectroscopy. These materials were only dried after impregnation (without calcination in air or reduction in H_2) and activated in situ in 1 bar of O_2 at 673 K for 2 h prior to CO adsorption. After the first adsorption each sample was degassed for 15 min to measure a second spectrum. Figure 15 shows the CO adsorption IR spectra on 0.5Pd(1), 0.5Pd(2) and 0.8Pt. The 0.5Pd(1) only reveals an adsorption peak at 2155 cm^{-1}, which is assigned to linearly adsorbed CO on Pd^{2+} [58], indicating that only Pd^{2+} remained after thermal treatment in oxygen. On the other hand, some metallic Pd domains were formed on the 0.5Pd(2) catalyst, after thermal treatment in O_2, as is seen from the adsorption peaks at 2106 cm^{-1} (linearly adsorbed CO on Pd) and 1943 cm^{-1} (bridged adsorbed CO on Pd). The spectrum of CO adsorbed on 0.8Pt catalyst confirms the autoreduction phenomenon as the band at the wavenumber of 2060 cm^{-1} (CO linearly adsorbed on metallic Pt) appears. However, Pt^{2+} cations are still present as indicated by the band at 2130 cm^{-1} assigned to CO linearly adsorbed on Pt^{2+} [59].

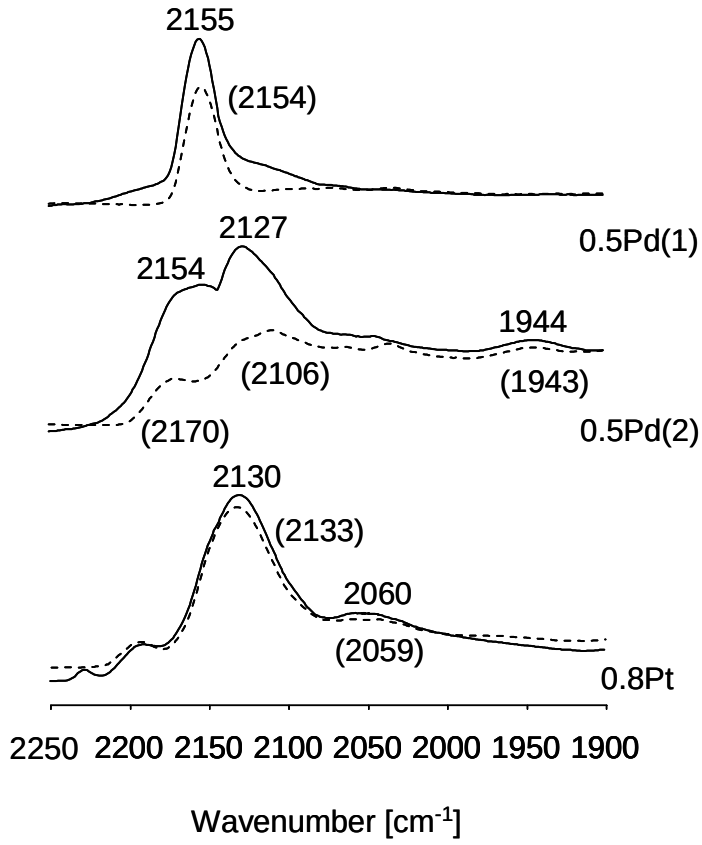

Figure 15. IR spectra of CO adsorbed on in situ treated (1 bar O_2, 673 K, 2 h) 0.5Pd(1), 0.5Pd(2) and 0.8Pt samples at T = 40 ºC, $p_{(CO)}$ = $5 \cdot 10^{-1}$ mbar (continuous lines) and after evacuation for 15 min (dashed lines, band values in brackets).

4.3. Electronic effect of alloying

The electron deficiency of Pt on alloying with Pd has been reported by several groups [22, 60, 61]. In this study, the XANES analysis at the Pt L_{III} edge showed a lower electron density of Pt atoms in the Pt-Pd clusters compared with Pt foil. According to the electron transference from Pt to Pd, the XANES spectra at Pd K edge evidenced the higher electronic density of Pd in the catalysts than in bulk Pd.

The densities of empty states are summarized in Table 5. The white line intensity at Pt L_{III} edge of sample Pt-Pd(2) is 1.69, i.e., larger than that of Pt-Pd(1) with a value of 1.48. This indicates that the Pt in the Pt-Pd nanoclusters of Pt-Pd(2) is more electron deficient than in the Pt atoms in Pt-Pd nanocluster of Pt-Pd(1). The catalyst Pt-Pd(3) exhibited the intensity at the Pt L_{III} edge of 1.55, i.e., an intermediate value compared to those of the other two bimetallic catalysts. According to our previous study [14], the electronic effects of the support can be excluded because the electronic transference promoted by the support acidity is compensated by the effect of alloying. This electron transfer takes place mainly between Pt and Pd atoms within the Pt-Pd clusters and the morphology of metal particles must be the parameter dominating the electronic exchange. The distribution of Pt and Pd atoms has the best homogeneity in the Pt-Pd nanoclusters of Pt-Pd(2) catalyst, implying that a large amount of Pt atoms are surrounded by Pd and the electron transfer to neighboring Pd atoms is eased. In contrast, the Pt-Pd nanoclusters in Pt-Pd(1) with a “Pt-core and Pd-shell” structure, has less Pd atoms next to Pt atoms, leading to a certain number of electron deficient Pt atoms, but much less than in the Pt-Pd(2) catalyst. Changing the pH value of the precursor solution with ammonia helps to obtain more homogeneous distributed Pt-Pd cluster than in Pt-Pd(1). Thus, the Pt atoms are in an intermediate electronic enviroment relative to the other two bimetallic catalysts.

4.4. On the poison-resistance of the bimetallic catalysts

It was established before that the proportion of Pt in the surface is of main importance for the activity of Pt-Pd catalysts. In this contribution we show that the concentration exposed Pt atoms is greatly influenced by the selection of the metal precursor. Now we discuss how the resistance to poisons is affected by tailoring the surface composition.

It has been proposed that the hydrogenation of tetralin takes place in noble metal catalysts supported on acidic materials trough two pathways: (1) on the metal sites and (2) after adsorbing on the Brønsted acid sites at the perimeter of the

metal clusters. In the absence of poisons, the reaction after adsorption on metal sites is the main pathway. It is worth to emphasize that the TPR experiments also suggest that in the presence of metal clusters the desorption of H_2S is eased. This is an additional evidence of spillover of activated hydrogen from the metal to the support. Either of the pathways can dominate in the presence of poisons due to the interplay of different poisoning mechanisms [21,62]. In this study, all catalysts are based on the same ASA material; hence, any effect of varying the support acidity is excluded. This allows us to correlate the hydrogenation activities in the absence and presence of N- and S-containing poisons only with the structure and surface composition of the metal clusters.

For hydrogenation of tetralin in poison-free conditions, 0.8Pt has the highest activity among all the catalysts (see Fig. 6), because Pt has higher hydrogenation activity compared to Pd. The dilution of Pt with Pd in the bimetallic catalyst leads to a decrease in activity following the trend: Pt-Pd(2) > Pt-Pd(3) > Pt-Pd(1). This is the same trend estimated for the relative abundance of surface Pt atoms in those catalysts. Following the same sequence, the apparent activation energy was 41, 30 and 33 $kJ \cdot mol^{-1}$ for Pt-Pd(1), Pt-Pd(2) and Pt-Pd(3), respectively. The calculated cis-/trans-decalin ratios are well in line with the known intrinsic activity of Pt and Pd. On the formed cis-decalin is preferred while on Pd the preferred product is the trans-decalin isomer.

When 400 ppm N in form of quinoline was added into the feed, the competitive adsorption decreases the activity of the catalysts. However, the acid sites of the materials are specially affected by neutralization and the hydrogenation on metal sites remains as the dominating path. Consequently the trend observed in the clean feed are preserved and the 0.8Pt catalyst still reveals the highest activity (Fig. 8). The trend in activity for the Pt-Pd catalysts still seems to depend on the relative amount of surface Pt atoms. However, the experimental activation energy became different (compared to those calculated for the poison free reactions), i.e., 95 $kJ \cdot mol^{-1}$ for Pt-Pd(1), 64 $kJ \cdot mol^{-1}$ for Pt-Pd(2) and 84 $kJ \cdot mol^{-1}$ for Pt-Pd(3). Given that quinoline blocks the acid sites at the perimeter of metal

clusters and may interact strongly with adsorbing sites on the metal, the overall adsorption strength of tetralin is diminished, increasing so the apparent activation energies. The cis/trans-decalin ratio decreases with the addition of quinoline. This is attributed to the lower strength of interaction of tetralin with the metal resulting from the competitive adsorption of quinoline and tetralin [12]. Alternatively, the electron donation of the aromatic system of quinoline to the metal would weaken the adsorption of olefin intermediates [63].

When DBT is present in the reaction, the desulfurization process leads to poisoning of the metal sites by adsorbed sulfur, which hinders the adsorption of aromatic molecules and causes very low activity. In this situation, the hydrogenation on adsorption on the Brønsted acid sites at the perimeter of the metal clusters is expected to become the most important pathway for hydrogenation. However, given that the Brønsted acidities of all materials are similar, the differences in performance of the catalysts must depend on the sulfur resistance of the metal sites and the reactivity of the sites located in the perimeter of the metal clusters. The hydrogenation activities followed the decreasing trend: Pt-Pd(2) > Pt-Pd(3) > 0.8Pt > Pt-Pd(1) > 0.3Pt > 0.5Pd(2) > 0.5Pd(1). The uncommon low activity of the Pt-Pd(1) catalyst in presence of sulfur (lower than that of the monometallic Pt catalyst) is explained by the low relative proportion of surface Pt although the Pt atoms in the Pt-Pd nanoparticles are more electron deficient than the Pt in monometallic Pt particles and thus, more resistant towards sulfur poisoning. The catalysts Pt-Pd(2) and Pt-Pd(3) perform better than 0.8Pt due to the higher proportion of Pt atoms on the surface of the Pt-Pd clusters. Moreover, the electronic transference to Pd eases desorption of sulfur (as H_2S), thus the metal sites are free to catalyze the hydrogenation of aromatic compounds. The bonding strength of Pt-S on the three bimetallic Pt-Pd catalysts can be differentiated from TPR experiments of the sulfided form of the catalysts. In Fig. 5, the signals at 561, 546 and 548 K were assigned to H_2S released from Pt of Pt-Pd nanoparticles. Pt-Pd(2) had the lowest temperature for H_2S release from the sulfided Pt, indicating the weakest Pt-S bonding among the three Pt-Pd catalysts.

The synergetic effect of alloying Pt and Pd is clearly observed by comparing the performance of bimetallic Pt-Pd catalysts with that of the monometallic Pt and Pd counterparts in the presence of sulfur. For instance, the sum of activities of 0.3Pt and 0.5Pd(2) in Fig. 10, is much smaller than the activity of Pt-Pd(2). This can only be explained by the electron transfer in the latter catalyst which leads to Pt atoms much more sulfur resistant than the Pt atoms in monometallic Pt catalyst. Studies of other groups confirm this conclusion [22,64,65].

When quinoline and DBT were co-feed in the reaction, the activity of tetralin hydrogenation is abated (Fig. 12). The synergetic effect in the catalyst Pt-Pd(2) is still observed. The significant increase in activity between 573 and 593 K is probably due to faster sulfur (H_2S) release from the metal surface as the temperature increases. Thus, metal sites are available again to hydrogenate aromatic molecules. Apparent activation energy of 71, 108 and 90 $kJ \cdot mol^{-1}$ was calculated for Pt-Pd(1), Pt-Pd(2) and Pt-Pd(3), respectively. It is interesting that the cis- to trans-decalin ratio does not change in a large extent with temperature.

5. Conclusion

A series of amorphous silica-alumina supported Pt, Pd and Pt-Pd catalysts were synthesized, characterized and tested in the hydrogenation of tetralin in the presence and absence of quinoline and dibenzothiophene (DBT). The catalysts have similar Lewis and Brønsted acid site concentration as measured by IR spectroscopy of adsorbed piridine. The general morphology of the bimetallic clusters was a Pt-rich core and a Pd-rich shell, as it is determined by extended X-ray absorption fine structure and IR spectroscopy of adsorbed CO. However, the particular morphology of Pt-Pd nanoparticles, i.e., the distribution of Pt and Pd in the clusters varies depending on the metal precursor used in the synthesis step. The mixture of Pd^{2+} and $[Pd(NH_3)_4]^{2+}$ cations leads to strong segregation of Pd to the surface. The presence of and $[Pt(NH_3)_4]^{2+}$ and $[Pd(NH_3)_4]^{2+}$ leads to nanoclusters with more homogenous metal distribution. The reducibility (decomposition mechanism) of the different metal precursors is the reason for

the formation of Pt-Pd nanoparticles with different distribution. The $[Pd(NH_3)_4]^{2+}$ and $[Pt(NH_3)_n]^{2+}$ groups are autoreduced during calcination in air, while Pd^{2+} is only reduced in H_2.

The X-ray absorption near edge structure indicates the formation of electron deficient Pt atoms in the bimetallic Pt-Pd nanoparticles. Homogeneous distribution of Pt and Pd atoms in Pt-Pd clusters increases the electronic transfer, thus increases the electron deficiency of Pt atoms. Temperature programmed reduction measurements of the pre-sulfided catalysts illustrated a weaker Pt-S bonding when Pt was alloyed with Pd. The activity of the catalysts for the poison free feed and poison-containing feed depends on the proportion of surface Pt in the catalyst. In the presence of DBT, the sulfur resistance of the electron poor Pt gives a higher activity to the bimetallic catalyst with the most homogeneous metal distribution than that of the pure Pt catalysts. Thus, in sulfur-poisoning conditions the synergy of alloying Pd and Pt is evident.

6. Acknowledgements

The authors would like to thank the staff of the beamline X1 at Hasylab DESY, Hamburg, Germany for their kind support during the XAS experiments.

7. References

[1] A. Stanislaus, B.H. Cooper, Catal. Rev. Sci. Eng. 36 (1994) 75.
[2] B.H. Cooper, B.B.L. Donnis, Appl. Catal. A : Gen. 137 (1996) 203.
[3] A. Corma, A. Martínez, V. Martínez-Soria, J. Catal. 169 (1997) 480.
[4] Y.W. Chen, C. Li, J. Chin. Inst. Chem. Eng. 28 (1997) 375.
[5] S.T. Homeyer, Z. Karpinski, W.M.H. Sachtler, J. Catal. 123 (1990) 60.
[6] R.A. Dalla Betta, M. Boudart, in Proc. 5th Int. Congr. on Catalysis (1973) North Holland.
[7] R.A. Dalla Betta, M. Boudart, P. Gallezot, R.S. Weber, J. Catal. 69 (1981) 514.

[8] M.T. Tri, J. Massardier, P. Gallezot, B. Imelik, Metal-support and Metal Additives Effects in Catalysis, ed. B. Imelik, et al. Vol. 11 (1982) 141 Amsterdam. Elsevier.

[9] F. Figueras, R. Gomez, M. Primet, ACS Adv. Chem. Ser. 121 (1973) 480.

[10] T.T. Phuong, J. Massardier, P. Gallezot, J. Catal. 102 (1986) 456.

[11] J. Wang, L.M. Huang, Q.Z. Li, Appl. Catal. A: Gen. 175 (1998) 191.

[12] M.F. Williams, B. Fonfé, A. Jentys, C. Breitkopf, J.A.R. van Veen, J.A. Lercher, J. Phys. Chem. C 114 (2010) 14532.

[13] Y. Yoshimura, M. Toba, T. Matsui, M. Harada, Y. Ichihashi, K.K. Bando, H. Yasuda, H. Ishihara, Y. Morita, T. Kameoka, Appl. Catal. A: Gen. 322 (2007) 152.

[14] Y. Yu, B. Fonfé, A. Jentys, G.L. Haller, C. Breitkopf, J.A.R van Veen, O.Y. Gutiérrez, J.A. Lercher, Part I.

[15] Z. Vít, H. Kmentová, L. Kaluža, D. Gulková, M. Boaro, Appl. Catal. B: accept, in press.

[16] D.H. Jung, S.J. Bae, S.J. Kim, K.S. Nahm, P. Kim, International Journal of hydrogen Energy, 36 (2011) 9115.

[17] M.C. Carrión, B.R. Manzano, F.A. Jalón, I. Fuentes-Perujo, P. Maireles-Torres, E. Rodríguez-Castellón, A. Jiménez-López, Appl. Catal. A: Gen. 288 (2005) 34.

[18] M. Bonarowska, Z. Karpiński, Catal. Tod. 137 (2008) 498.

[19] M.F. Williams, B. Fonfé, C. Sievers, A. Abraham, J.A. van Bokhoven, A. Jentys, J.A.R. van Veen, J.A. Lercher, J. Catal. 251 (2007) 485.

[20] M.F. Williams, B. Fonfé, C. Woltz, A. Jentys, J.A.R. van Veen, J.A. Lercher, J. Catal. 251 (2007) 497.

[21] Y. Yu, B. Fonfé, A. Jentys, G.L. Haller, C. Breitkopf, J.A.R van Veen, O.Y. Gutiérrez, J.A. Lercher, Part II.

[22] J.K. Lee, H.K. Rhee, J. Catal. 177 (1998) 208.

[23] T. Matsui, M. Harada, K.K. Bando, M. Toba, Y. Yoshimura, J. Jpn. Petrol. Inst. 47 (2004) 222.

[24] B. Pawelec, R. Mariscal, R.M. Navarro, S. Van Bokhorst, S. Rojas, J.L.G. Fierro, Appl. Catal. A: Gen. 225 (2002) 223

[25] K.V. Klementiev, *VIPER and XANDA for Windows, freeware*

[26] A.L. Ankudinov, B. Ravel, J.J. Rehr, S.D. Conradson, Phys. Rev. B 58 (1998) 7565.

[27] A.L. Ankudinov, J.J. Rehr, Phys. Rev. B 62 (2000) 2437.

[28] M. Choi, Z. Wu, E. Iglesia, J. Am. Chem. Soc. 132 (2010) 9129

[29] Y. Lei, J. Jelic, L.C. Nitsche, R. Meyer, J. Miller, Top Catal. 54 (2011) 334.

[30] J.M. Dominguez, M.J. Yacamán, J. Catal. 64 (1980) 223.

[31] S.N. Khanna, F. Cyrot-Lackmann, Y. Boudeville, J. Rousseau-Voilet, Surf. Sci. 106 (1981) 287.

[32]S.N. Khanna, J.P. Bucher, J. Buttet, Surf. Sci. 127 (1983) 165.

[33] T. Tanaka, T. Shishido, H. Hattori, K. Ebitani, S. Yoshida, Physica B 208 (1995) 645.

[34] A. Jentys, M. Englisch, G.L. Haller, J.A. Lercher, Catal. Lett. 21 (1993) 303.

[35] C.M. Grill, M.L. McLaughlin, J.M. Stevenson, R.D. Gonzalez, J. Catal. 69 (1981) 454.

[36] M. Primet, L.C. De Menorval, J. Fraissard, T. Ito. J. Chem. Soc. Faraday Trans. 81 (1985) 2867.

[37] T. Rades, V.Y. Borovkov, V.B. Kazansky, M. Polisset-Thfoin, J. Fraissard, J. Phys. Chem. 100 (1996) 16238.

[38] W.M.H. Sachtler, Catal. Rev. Sci. Eng. 14 (1976) 193.

[39] H. Greenfield, N.Y. Ann, Acad. Sci. 214 (1973) 233.

[40] G.H. Via, K.F. Drake, G. Meitzner, F.W. Lytle, J.H. Sinfelt, Catal. Lett. 5 (1990) 25.

[41] M.A. Vannice, S.Y. Wang, J. Phys. Chem. 85 (1981) 2543-2546.

[42] A.G.T.M. Bastein, F.J.C.M. Toolenaar, V. Ponec, J. Catal. 90 (1984) 88-95.

[43] A. Goguet, M. Aouine, F.J. Cadete Santos Aires, A. De Mallman, D. Schweich, J.P. Candy, J. Catal. 209 (2002) 135.

[44] A. Goguet, D. Schweich, J.P. Candy, J. Catal. 220 (2003) 280.

[45] A. Munoz-Paez, D. C. Koningsberger, J. Phys. Chem. 99 (1995) 4193.

[46] W.J. Reagan, A.W. Chester, G.T. Kerr, J. Catal. 69 (1981) 89.

[47] D. Exner, N. Jaeger, K, Möller, G. Schulz-Ekloff, J. Chem. Soc., Faraday Trans. 78 (1982) 3537.

[48] W.J. Reagan, A.W. Chester, G.T. Kerr, J. Catal. 69 (1981) 89.

[49] W.M.H. Sachtler, Z. Zhang, Adv. Catal. 39 (1993) 129.

[50] M. Kosmulski, J. Colloid Interface Sci. 337 (2009) 439.

[51] J.A. Schwarz, C.T. Driscoll, A. K. Bhanot, J. Colloid Interface Sci. 97 (1984) 55.

[52] M. Schreier, J. Regalbuto, J. Ctal. 225 (2004) 190.

[53] K.T. Kim, Y.G. Kim, J.S. Chung, Carbon 31 (1993) 1289.

[54] R.J. Cross, Adv. Inorg. Chem. 34 (1989) 219.

[55] D. Spielbauer, H. Zeilinger, H. Knözinger, Langmuir 9 (1993) 460.

[56] W. Daniell, U. Schubert, R. Glöckler, A. Meyer, K. Noweck, H. Knözinger, Appl. Catal. A : Gen. 196 (2000) 247.

[57] C. Contescu, M.I. Vass, Appl. Catal. 33 (1987) 259.

[58] D. Tessler, A. Rakai, F.B. Verduraz, J. Chem. Soc. Faraday Trans. 88 (1992) 741.

[59] E. Ivanova, M. Mihaylov, F.T. Starzyk, M. Daturi, K. Hadjiivanov, J. Mol. Catal. A: Chem. 274 (2007) 179.

[60] Y. Yoshimura, M. Toba, T. Matsui, M. Harada, Y. Ichihashi, K.K. Bando, H. Yasuda, H. Ishihara, Y. Morita, T. Kameoka, Appl. Catal. A: Gen. 322 (2007) 152.

[61] N. Matsubayashi, H. Yasuda, M. Imamura, Y. Yoshimura, Catal. Today 45 (1998) 375.

[62] M.F. Williams, B. Fonfé, A. Jentys, C. Breitkopf, J.A.R. van Veen, J.A. Lercher, J. Phys. Chem. C 114 (2010) 14532.

[63] J.J. Rooney, J. Mol. Catal. 31 (1985) 147.

[64] R.M. Navarro, B. Pawelec, J.M. Trejo, R. Mariscal, J.L.G. Fierro, J. Catal. 189 (2000) 184.

[65] M.A. Arribas, V. Fornés, A. Martínez, Studies in Surf. Sci. and Catal. 138 (2001) 231.

Chapter 5

Summary

1. Summary

In order to meet the strict legislation in diesel production, the aromatic content, nitrogen and sulfur concentration in diesel fuel has to be abated. By lowering the aromatic content and removing nitrogen and sulfur containing molecules in diesel fuel, the emission of particular matter, NO_x and SO_x is greatly depressed. Therefore, deep hydrotreating process, including hydrogenation, hydrodenitrogenation and hydrodesulfurization, must be applied for fuel production. Noble metal catalysts reveal excellent hydrogenation activity compared to conventional transition metal sulfides catalysts (e.g. Ni- or Co-promoted MoS_2 supported on γ-alumina). However, noble metal catalysts can be poisoned by small amount of sulfur or nitrogen containing molecules present in the feedstock. Numerous works have been focused on making the noble metal catalysts more resistant towards poisons. In general, two strategies are applied: (1) using acid support, such as zeolites or amorphous silica-alumina; (2) alloying different noble metals (e.g. Pt and Pd). The former strategy provides additional hydrogenation pathway at acid sites in the vicinity of the noble metal nanoparticles. On the other hand, alloying of Pt and Pd produces electron deficient Pt atoms due to electron transfer from Pt to Pd atoms within the Pt-Pd nanoclusters. The Pt-S bond is weaker when Pt is electron deficient, making S atoms easier to release from Pt surfaces and regenerating active metal sites for hydrogenation reactions.

The aim of this thesis is to gain the basis knowledge needed to design bimetallic Pt-Pd catalysts able to maintain high hydrogenation activity in the presence of poisoning compounds. To this end, Pt-Pd catalysts supported on amorphous silica alumina (ASA) are synthesized, characterized and tested in the hydrogenation of tetralin (model aromatic compound) in the absence and presence of poisons i.e., dibenzothiophene and quinoline (S- and N-containing compound respectively). Two strategies are followed to identify the parameters determining the hydrogenation activity and poison-resistance of the catalysts, i.e., to vary the carrier composition and the preparation procedure.

In chapter 2 and 3 of the work, Pt-Pd catalysts are synthesized using the respective tetrammonium complexes as noble metal precursors. The materials used as carriers are silica and ASA with Al_2O_3/SiO_2 wt.% ratio of 55/45, 20/80, and 5/95. According to the chemical analysis, the content of Pt and Pd is close to 0.3 and 0.5 wt.% respectively, keeping the Pd:Pt molar ratio of 3. The average particle size slightly varied from 1.4 to 1.8 nm (TEM). The analysis of the EXAFS and CO-adsorption IR spectroscopy reveal that the general morphology of the bimetallic clusters is Pt rich core and Pd-enriched surface. The Pt atoms in the bimetallic clusters are electron deficient due to electron transfer to Pd (XANES). Furthermore, monometallic Pd clusters coexist with those Pt-Pd particles. The Pd/Pt molar ratio in the bimetallic clusters decreased (from 1.69 to 1.17), while the proportion of surface Pt increased (from 13.9 to 18 %) with increasing alumina content in the support. The catalyst supported on ASA(55/45) exhibited the highest coverage of Pt.

A complex interaction between the properties of the metal clusters and supports determines the performance of the catalysts. However, the proportion of Pt on the surface is the most important parameter because the Pt-Pd catalyst supported on ASA(55/45) is the most active in all tested conditions. Under poison-free conditions the electronegativity of the support correlated with the hydrogenation activity provides that the support exhibits Lewis acidity. In the presence of quinoline the activity of the catalysts increases with the dispersion of the metal particles, whereas in the presence of dibenzothiophene, the acidity of the support compensates the sulfur poisoning of the metal phase. For comparison purposes, monometallic Pt (0.8 wt.%) catalysts are tested under the same reaction conditions. All the Pt catalysts are more active than the Pt-Pd counterparts in clean feed. In the presence of poisons, the Pt catalysts are more active than the bimetallic formulation with the remarkably exception of Pt-Pd/ASA(55/45).

In chapter 4, another series of bimetallic catalysts are synthesized on the same ASA material (30 and 70 wt.% of Al_2O_3 and SiO_2). The metal precursors used are tetramonium complexes (Pt or Pd) and nitrate (Pd). According to the

physicochemical characterization, Pt-Pd and Pd clusters with average size below 2 nm (H_2 chemisoprtion) are formed. The bulk Pd:Pt molar ratio is 3 (chemical analysis) whereas the molar ratio in the bimetallic clusters is 1.23-1.55 (EXAFS). The distribution of Pt in the bimetallic clusters varies depending on the metal precursor used in the synthesis. The most homogeneous distribution (i.e., the clusters least similar to the core-shell model) is obtained when the tetrammonium complexes of both metals are used during the impregnation step. In this case, the amonium ions ease the formation of metallic nuclei due to auto-reduction mechanisms. Given that the support is kept constant in this part of the work, the decomposition mechanism (reducibility) of the metal precursors is identified as the parameter determining the metal distribution in the bimetallic cluster. The homogeneous distribution of Pt and Pd atoms in Pt-Pd clusters increases the electronic transference from Pt to Pd.

The bimetallic catalyst prepared from tetrammonium complexes is the most active for the hydrogenation of tetralin in the absence and presence of dibenzothiophene and/or quinoline. Hence, providing invariability of the support properties, the morphology of the bimetallic nanoparticles (homogeneity and proportion of surface Pt) determines the hydrogenation activity. Comparing the activity of bimetallic Pt-Pd catalysts and the monometallic Pt or Pd counterparts, the synergy of alloying Pt and Pd is evident in the presence of sulfur poisons.

The conclusions of the whole work coincide in several facts of remarkable importance for the development of hydrogenation catalysts based in Pt-Pd alloys. (i) On bimetallic catalysts (as it has been demonstrated before for Pt catalysts) the hydrogenation of aromatic compounds occurs via adsorption on two sites i.e., metal surface and Brønsted acid sites at the perimeter of the meal clusters. Sulfur containing compounds poisons the metal phases whereas quinoline neutralizes the acidity of the support (Figure 1). (ii) Keeping the proportion of Pt atoms in the bimetallic clusters above certain critic threshold is essential to obtain catalysts with high hydrogenation activity in poisoning conditions. Several strategies can be followed to improve the coverage of the surface by Pt e.g., tuning the composition of the support and accelerating the reduction of the metal

precursor. (iii) The improved poison resistance of the bimetallic catalysts originates from electronic interactions. The electron transference from Pt to Pd decreases the adsorption strength of poisons on surface Pt atoms increasing so the active sites available for aromatic hydrogenation.

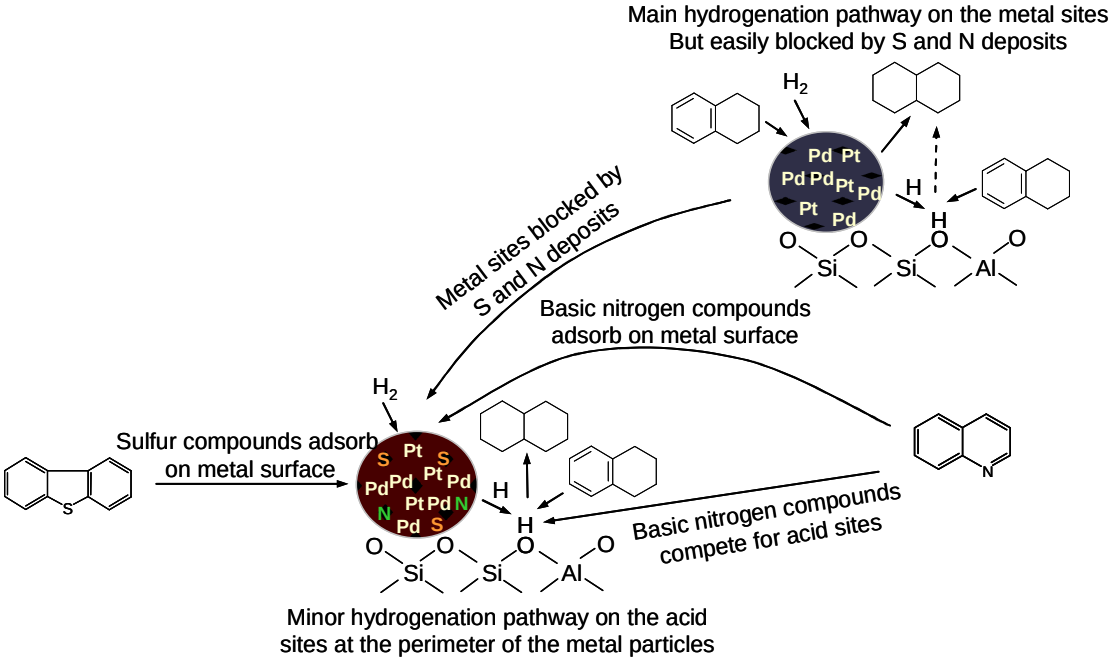

Figure 1. Schematic representation of the hydrogenation pathways on Pt-Pd catalysts in the absence and presence of Poisons.